OPTIMUM FM SYSTEM PERFORMANCE--AN INVESTIGATION EMPLOYING DIGITAL SIMULATION TECHNIQUES

by

TODD LEONARD RACHEL

B.S., Michigan State University
1965

SUBMITTED IN PARTIAL FULFILLMENT OF THE
REQUIREMENTS FOR THE DEGREE OF
MASTER OF SCIENCE
at the
MASSACHUSETTS INSTITUTE OF TECHNOLOGY
August, 1966

Signature of Author. . . . . .
Department of Electrical Engineering, August 10, 1966

Certified by . . . . . .
Thesis Supervisor

Accepted by. . . . . .
Chairman, Departmental Committee on Graduate Students

OPTIMUM FM SYSTEM PERFORMANCE--AN INVESTIGATION EMPLOYING DIGITAL SIMULATION TECHNIQUES

by

TODD LEONARD RACHEL

Submitted to the Department of Electrical Engineering on August 10, 1966, in partial fulfillment of the requirements for the degree of Master of Science.

ABSTRACT

The optimum phase-locked loop demodulator arises in a natural way from statistical detection theory when the received signal is an angle-modulated cosine function that is corrupted by additive independent white Gaussian noise. In particular, for a frequency-modulated signal the phase-locked loop can be revamped into a non-linear feedback system with the integrated message as an input.

The object of the thesis is to analyze the performance of the above explained non-linear system. The primary means of analysis is with the use of digital simulation techniques. Secondary methods include a quasi-linear analysis and a linear analysis. Only the simulation analysis provides complete coverage of the system performance for all input signal to noise power ratios. The other two methods only have validity over a limited range of signal to noise ratios.

For a means of comparison, the performance of a conventional receiver is also analyzed. Both simulation and analytical methods are employed to analyze the conventional receiver.

Finally, the performance of the two types of receivers are evaluated.

For a given message, the linear analysis predicted equal performance for both types of receivers.

For a one pole Butterworth message the quasi-linear analysis predicted an improvement in threshold for the phase-locked loop of about 6 db. For a two pole Butterworth message the theoretical improvement was predicted to be about 11 db.

For a one pole Butterworth message the simulation analysis indicated an improvement in threshold for the phase-locked loop of about 3 db. For the two pole Butterworth message the simulated improvement was about 6 db.

Thesis Supervisor: Harry L. Van Trees
Title: Associate Professor of Electrical Engineering

ACKNOWLEDGEMENTS

Two qualities mark Professor Harry Van Trees as being an outstanding thesis advisor. Those qualities are professional ability and human interest. When in conference, Dr. Van Trees would not only answer my questions fully but would ask some questions of his own to stimulate my thinking. In addition, his enthusiastic greeting and welcome smile always set the mood for a fruitful discussion. I thank you, Professor Van Trees.

Doctor Donald Snyder spent many laborious hours helping me understand the many details of digital simulations. Only with his assistance could I have finished this task.

My wife, Jean, has served me tirelessly for the past five years of my formal education. During anxious periods she always had effective words of encouragement. Whenever something good occurred, she always had plenty of praise. Also, I found that the unlimited confidence that she had in me was a powerful motivating force. Thus let it be known that Jean has been a vital instrument in my completion of this thesis.

TABLE OF CONTENTS

CHAPTER 1

HISTORY AND INTRODUCTION

1.0 INTRODUCTION

The text of this thesis is primarily devoted to the demodulation of a frequency modulated sinusoidal carrier which has been corrupted by additive white noise from the transmission media. Prior to delving into the demodulation scheme it seems appropriate that we first review briefly the fundamental ideas of frequency modulation.

Frequency modulation is a particular type of non-linear modulation. The modulator varies the argument of a sinusoidal function according to

$$S[t,a(t)] = \sqrt{2P} \sin [\omega_c t + \phi(t)] \qquad (1)$$

Here the constant $\sqrt{2P}$ is the amplitude of the modulated carrier and P is the power in the modulated carrier. If a(t) is defined as the analog message of interest, then for frequency modulation

$$\phi(t) = d_f \int_{-\infty}^{t} a(u)\, du \qquad (2)$$

A constant, d_f is included in (2) because, as we will see later, its presence strongly affects the performance of the demodulator. Intuitively, d_f controls the band width of the received signal and thus can be associated with the maximum frequency deviation of the received signal. In our system, however, since a(t) is a sample function from a Gaussian random process and hence a(t) can take on any value, then a "maximum frequency deviation" is a nebulous concept.

When the signal (frequency modulated carrier) is transmitted from one station to another it is invariably corrupted by noise. Throughout this text, the noise will be considered as additive white Gaussian noise defined as

$$n(t) = \text{additive white Gaussian noise.} \tag{3}$$

The characteristics of n(t) will be considered later.

Finally, combining (1), (2), and (3) we get the signal that is received at the demodulator

$$r(t) = S[t:a(t)] + n(t)$$

or

$$r(t) = \sqrt{2P}\ \sin\left[\omega_c t + d_f \int_{-\infty}^{t} a(u)\, du\right] + n(t). \tag{4}$$

1.1 TYPICAL F.M. DEMODULATORS

In section 1.0, it was observed that the information in the received signal is contained in the argument of the sine function. The purpose of the receiver then is to extract that message information from the argument of the received signal. Note that the message, is in fact, the instantaneous value of the frequency of the sine wave. Whatever the makeup of the receiver, its primary function is to determine the instantaneous frequency of the modulated carrier wave.

There has been a variety of receivers designed for this purpose. They vary in complexity and cost. Some appeal to one's intuition and others do not. Only a few of the many types of frequency demodulators will be discussed in the following paragraphs.

The receiver most commonly used for commercial use is called the conventional demodulator. In a conventional demodulator the received signal is usually clipped by a limiter so that only the time distribution of its axial crossings is preserved. The output of the limiter is then band pass filtered to suppress harmonics of the carrier and out-of-band noise. The result is applied to a discriminator. A discriminator is a device whose output wave has instantaneous amplitude values proportional to the instantaneous frequency of the input wave. Another filter is added after the discriminator to suppress noise at the output. Realizations of

conventional demodulators are clearly described in Schwartz,[1] Black,[2] and Armstrong.[3]

The advent of the conventional F.M. demodulator represents a successful first attempt to overcome many of the noise problems encountered in amplitude modulation systems. The price that is paid for improved output signal-to-noise ratio is increased bandwidth occupancy.

One important restriction on the performance of the conventional demodulator is the presence of a wide band intermediate filter at the output of the limiter. This filter passes the message satisfactorily but it also passes a lot of noise. If there was some way to further suppress the noise, the system performance would notably improve.

An improved receiver was presented by Chaffee.[4] His aim was to constrict the wide band intermediate filter used in the conventional demodulator. Chaffee's demodulator actually compresses the bandwidth of the received signal to permit the use of a narrow band intermediate filter. The idea is relatively simple. He used the output of the post discriminator filter to drive a voltage controlled oscillator. The frequency of the oscillator is centered around $\omega_c \pm \omega_{IF}$. When the output of the oscillator is mixed with the incoming signal the result is:

$$\sin \left\{\omega_{IF} t + \int_{-\infty}^{t} [a_i(u) - \hat{a}_i(u)]\, du\right\} \qquad (5)$$

where $a_i(t)$ is the instantaneous received message and $\hat{a}_i(t)$ is the estimate of $a_i(t)$. It can be easily seen from equation (5) that if the error is small the bandwidth of this signal is much less than the bandwidth of the received signal; thus allowing the narrow band filter.

Another method of achieving this narrow band effect is by using a phase-locked-loop. The essential parts of a phase-locked loop are shown in figure 1. Here the output of the low pass filter is the instantaneous frequency estimate of $r(t)$.

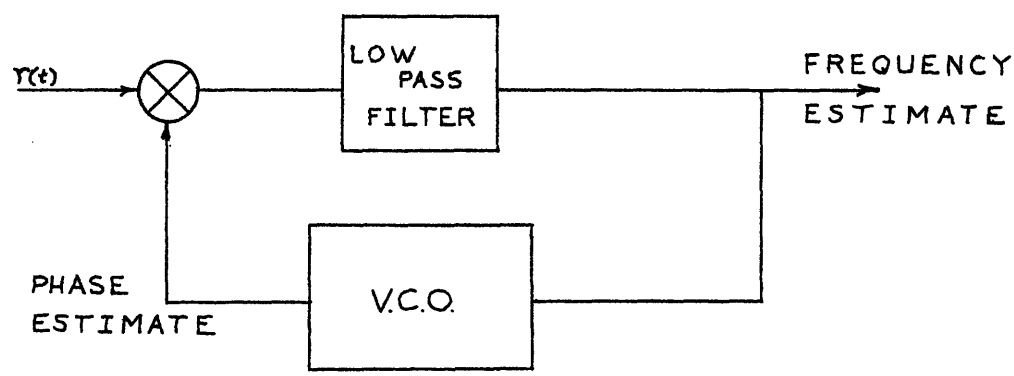

Figure 1

Phase-locked loop

The voltage controlled oscillator (VCO) physically provides an integrating action so that an instantaneous phase estimate is fed back to the input multiplier. The output of the multiplier is a low pass signal proportional to the

error in the phase estimate. This error signal is filtered and used to modify the frequency of the voltage controlled oscillator. Note that, the rate at which the oscillator frequency can change is governed by the loop filter. We can think of the output of the voltage controlled oscillator as "locked" in phase to the incoming signal—thus the name "phase-locked loop" is appropriate.

The phase-locked loop can be useful for synchronization purposes. The first wide-spread application of phase-locked loops was in synchronization circuits for color television. They are often used for synchronization in space communication systems. Also they can be used for demodulation purposes in almost any analog communication system.

1.2 THESIS PROSPECTUS

In this thesis we are going to study the performance of the optimum phase-locked loop analog demodulator. The results of this study will be realized primarily through the employment of digital simulation techniques. The simulation results will be verified analytically. To obtain a frame of reference we will examine the performance of an "optimum" conventional demodulator. The performance of the conventional receiver will also be analyzed by simulation and analytic methods.

The thesis will proceed in a straightforward manner. In chapter 2 we will derive our optimum, realizable, phase-locked loop demodulator directly from non-linear integral equations that arise from statistical detection theory. Chapter 3 will present a complete analytical analysis of the optimum demodulator and chapter 4 will present a digital simulation analysis. Chapters 5 and 6 will contain an analytic analysis and simulation analysis respectively of the "optimum" conventional receiver.

Each chapter will end with a short summary and discussion of the results in that chapter. Finally, chapter 7 will be devoted to a complete examination of all the results in all of the foregoing chapters.

CHAPTER 2

WAVEFORM ESTIMATION AND RECEIVER FORMULATION

2.0 INTRODUCTION

In this chapter we are going to derive an optimum receiver for the received waveform described by (4). For this case the received waveform is modulated by a sample function from a Gaussian random process and is corrupted by uncorrelated, additive white Gaussian noise. The receiver will process r(t) in an optimum fashion and give the best estimate of the original uncorrupted message, a(t).

General results will first be derived and then they will be applied to the specific case where we have a frequency modulated, stationary, Gaussian message and additive white Gaussian noise.

2.1 OPTIMUM WAVEFORM ESTIMATION (GENERAL)

As before the received signal is:

$$r(t) = S[t:x(t)] + n(t) \qquad t_o \leq t \leq t_1 \qquad (6)$$

where x(t) is a function of the message a(t) and S[t:x(t)] is a sine wave modulated by x(t). It may be phase or frequency modulation or even a combination of these.

A system that could generate such a signal r(t) is shown in figure 2. Note that for phase modulation the linear filter would be merely a straight wire but for frequency modulation it would be an integrator.

Our criterion for deriving the optimum receiver will be maximum a posteriori estimation (MAP).

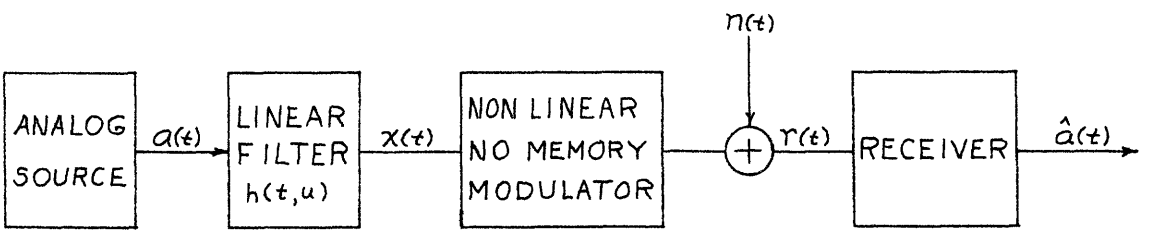

Figure 2

Analog com. system

The assumptions for the following results are:

(i) The function x(t) and the noise n(t) are sample functions from independent, continuous, zero-mean Gaussian processes with covariance functions $K_x(t,u)$ and $K_n(t,u)$ respectively. Note that if h(t,u) represents a straight wire; then $x(t) = a(t)$ and $K_x(t,u) = K_a(t,u)$.

(ii) The signal S[t:x(t)] has a derivative with respect to x(t).

After a fair amount of derivation, the MAP estimate for the function x(t) is:*

$$\hat{x}(t) = \int_{t_o}^{t_1} \frac{\partial S[z:\hat{x}(z)]}{\partial \hat{x}(z)} K_x(t,z)\, g(z)\, dz \qquad t_o \leq t \leq t_1 \qquad (7)$$

where, for white noise,

$$g(z) = \int_{t_o}^{t_1} Q_n(z,u)\{r(u) - S[u:x(u)]\}du \qquad t_o \leq t \leq t_1 \qquad (8)$$

and

$$Q_n(z,u) = \frac{2}{N_o} u_o(z,u) \qquad (9)$$

Equation (7) is the fundamental result from which the optimum receiver will be realized.

2.2 OPTIMUM RECEIVER INTERPRETATION

Assume:

i) $t_o = -\infty$, $t_1 = +\infty$ (10)

ii) $K_x(t,u) = K_x(t - u)$ (stationary) (11)

---

* Youla, Reference 6
Van Trees, Reference 7, Chapter 5

iii) $K_n(t,u) = \frac{N_o}{2} u_o(t - u)$

(white & stationary) (12)

Then from (9),

$$Q_n(t,u) = \frac{2}{N_o} u_o(t - u) \tag{13}$$

and from (8),

$$g(z) = \int_{-\infty}^{\infty} \frac{2}{N_o} u_o(z - u)\{r(u) - S[u:\hat{x}(u)]\}du \tag{14}$$

$$g(z) = \frac{2}{N_o} \{r(z) - S[z:\hat{x}(z)]\} . \tag{15}$$

Hence, substituting into equation (7) we obtain

$$\hat{x}(t) = \frac{2}{N_o} \int_{-\infty}^{\infty} K_x(t - z) \left[\frac{\partial S[z:\hat{x}(z)]}{\partial \hat{x}(z)} \{r(z) - S[z:x(z)]\}\right]dz \tag{16}$$

Now if we choose

$$r(t) = S[t:x(t)] + n(t) \tag{17}$$

$$r(t) = \sqrt{2P} \sin[\omega_c t + x(t)] + n(t) \tag{18}$$

then,

$$\frac{\partial S[t:x(t)]}{\partial x(t)} = \sqrt{2P} \cos [\omega_c t + x(t)] \tag{19}$$

Substituting into (16) gives

$$\hat{x}(t) = \frac{2}{N_o} \int_{-\infty}^{\infty} K_x(t-u) \left[\sqrt{2P} \cos\{\omega_c u + \hat{x}(u)\} \{ r(u) - \sqrt{2P} \cdot \sin [\omega_c u + x(u)] \} \right] du \quad (20)$$

Define

$$z_{\ell u} = \sqrt{2} \cos [\omega_c t + \hat{x}(t)] \{ r(t) - \sqrt{2P} \sin [\omega_c t + x(t)] \} \quad (21)$$

then;

$$\hat{x}(t) = \frac{2\sqrt{P}}{N_o} \int_{-\infty}^{\infty} K_x(t-u)\ z_{\ell u}(u)\ du \quad (22)$$

Equation (22) is the familiar convolution integral and can be considered as the input to a filter with an impulse response of $K_x(t - u)$. A block diagram realization of equations (21) and (22) is shown in figure 3. Note that $K_x(t - u)$ is an unrealizable impulse response because it is an even function of time. Also because it is inside the loop we cannot add delay to make it realizable.

If the loop shown in figure 3 was a linear system we could make the loop filter realizable and add an unrealizable post loop filter. We could then approximate the system of figure 3 arbitrarily closely by including delay in the post

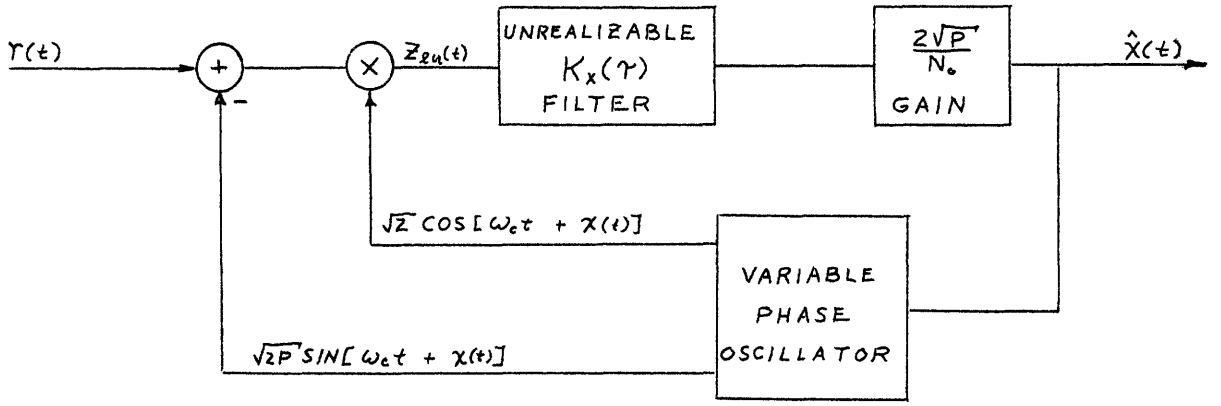

Figure 3

Realization of (21) and (22)

loop filter. With this fact in mind let us see if we can make the system in figure 3 approximately linear.

Observe that if the correlation function $K_x(\tau)$ is considered as the impulse response of a filter, then that filter would presumably have a pass band in the vicinity of the frequencies in x(t). Therefore, if the message is, for example, human speech then the filter would resemble a low pass filter.

Now remember

$$r(t) = \sqrt{2P}\sin[\omega_c t + x(t)] + n(t) \tag{23}$$

and, $$z_{\ell u}(t) = \sqrt{2}\cos[\omega_c t + \hat{x}(t)]\{\sqrt{2P}\sin[\omega_c t + x(t)] + n(t) - \sqrt{2P}\sin[\omega_c t + \hat{x}(t)]\} \tag{24}$$

Using trigonometric manipulation on equation (24) we obtain

$$z_{\ell u}(t) = \sqrt{P} \sin [x(t) - \hat{x}(t)] + \sqrt{2}\, n(t) \cos [\omega_c t + \hat{x}(t)]$$

$$+ \sqrt{P} \sin [2\omega_c t + x(t) + \hat{x}(t)]$$

$$- \sqrt{P} \sin [2\omega_c t + 2\hat{x}(t)] \qquad (25)$$

Now since we argued that $z_{\ell u}(t)$ is the input to a low pass filter, we may ignore the last two terms in (25) because the filter would not pass high frequencies like $2\omega_c$. Note also that the last term in (25) was contributed by the subtraction operation in figure 3. Hence we may erase that leg of the feedback path since it contributed nothing to our system. A new model of our system can be drawn as shown in figure 4. In figure 4 we have replaced the $K_x(\tau)$ filter and the gain term by a related low pass filter, $G(\omega)$.

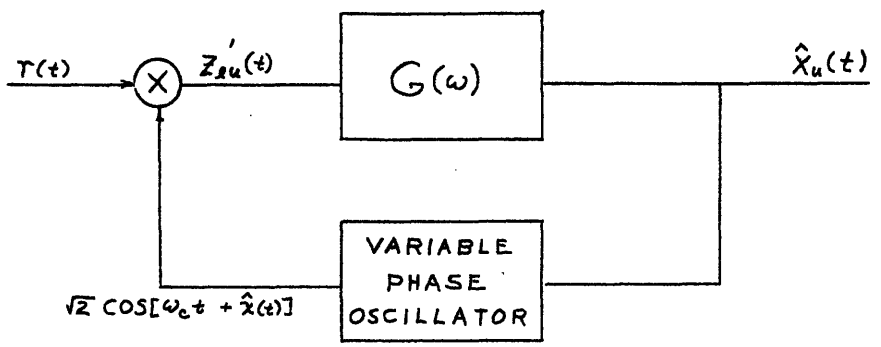

Figure 4

Phase-locked loop

This figure is familiar to us from chapter one. It is frequently called a phase-locked loop where the multiplier symbol, in practice, would be replaced by a phase detector. Note here that $z'_{\ell u}(t)$ consists of the first three terms of equation (25) and that the third term is of no consequence. Now consider the second term in equation (25).

We first decompose the noise n(t) into in-phase and quadrature components,

$$n(t) = \sqrt{2}\,[-n_1(t)\,\sin\,\omega_c t + n_2(t)\,\cos\,\omega_c t] \qquad (26)$$

where $n_1(t)$ and $n_2(t)$ are sample functions from independent low pass Gaussian processes with spectral density shown in figure 5. In this case W_n is considered large with respect to the signal band width but small compared to ω_c. If we denote the second term in (25) by $n^{(2)}(t)$ and use equation (26) we obtain,

$$n^{(2)}(t) = -\,n_1(t)\,\sin\,[-\,\hat{x}(t)] + n_2(t)\,\cos\,[-\,\hat{x}(t)]$$

$$+ \text{ double frequency terms} \qquad (27)$$

$$n^{(2)}(t) \simeq n_1(t)\,\sin\,[\hat{x}(t)] + n_2(t)\,\cos\,[\hat{x}(t)] \qquad (28)$$

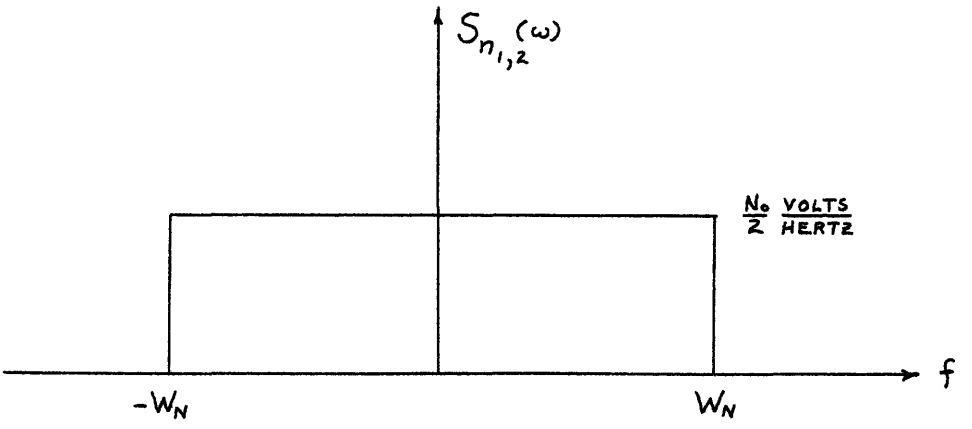

Figure 5

Noise Spectrum

Once again we can neglect the double frequency terms because they will never get through the low pass filter. Now if W_n is large compared to the bandwidth of sine $[\hat{x}(t)]$ we can make the approximation,

$$K_{n^{(2)}}(\tau) = K_{n_1}(\tau) = K_{n_2}(\tau) = \frac{N_o}{2} U_o(\tau). \quad * \qquad (29)$$

Hence we can combine the past several paragraphs of discussion to come up with a final approximation for $z_{\ell u}(t)$. For our system then,

$$z_{\ell u}(t) \simeq z_{\ell r}(t) \equiv \sqrt{P} \sin [x(t) - \hat{x}(t)] + n^{(2)}(t) \qquad (30)$$

---

* See appendix for proof.

The system of figure 4 now may be altered again to yield a model shown in figure 6.

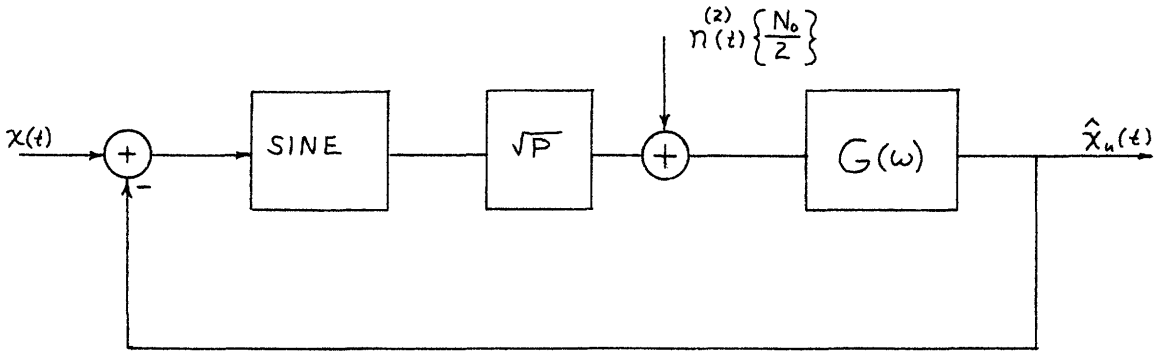

Figure 6

Nonlinear Realization of Equation (23)

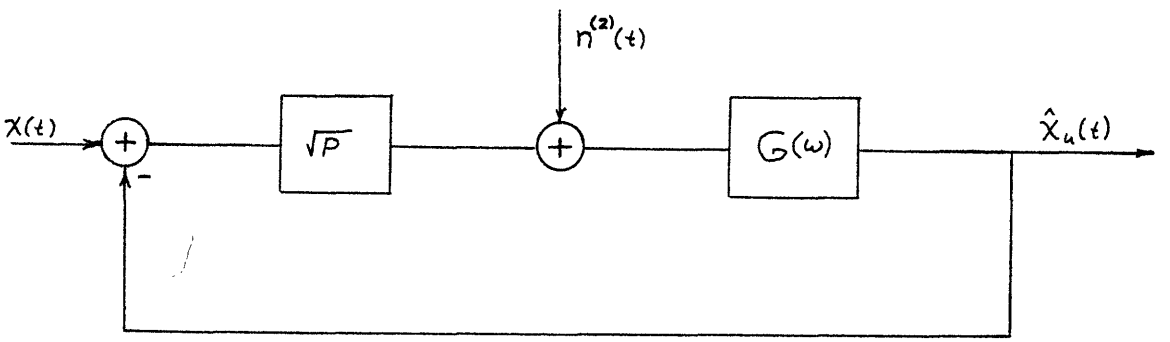

Figure 7

Linear Realization of Equation (22)

Note that this model is <u>still</u> a nonlinear system corrupted by additive white noise that is independent of the message. Remember that our goal was to make our system linear for the purpose of our in-loop filter. In figure 6,

if we define $e(t) = x(t) - \hat{x}(t)$ to be the error in the loop, then for small values of $e(t)$, the system is approximately linear. The linear model is shown in figure 7.

Now that we have achieved our objective (linear system), we can make $G(\omega)$ a realizable low pass filter and then add an unrealizable post loop filter to approximate the system shown in figure 3 arbitrarily closely. Our final linear and nonlinear models for an arbitrary message $x(t)$ are shown in figures 8 and 9 respectively.

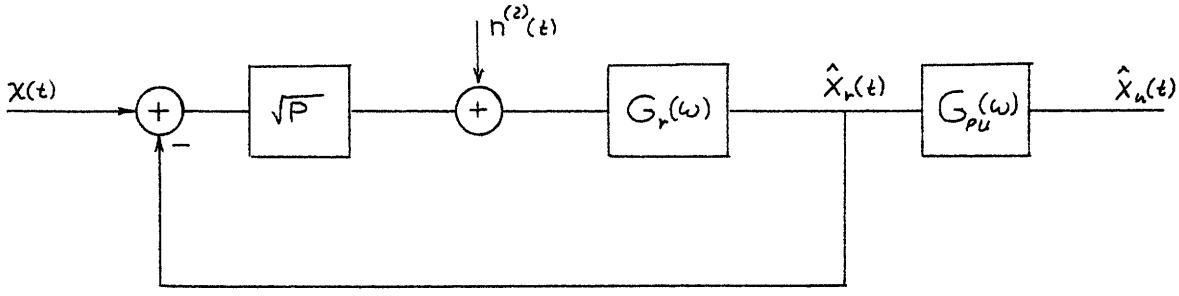

Figure 8

Final Linear Model for Arbitrary x(t)

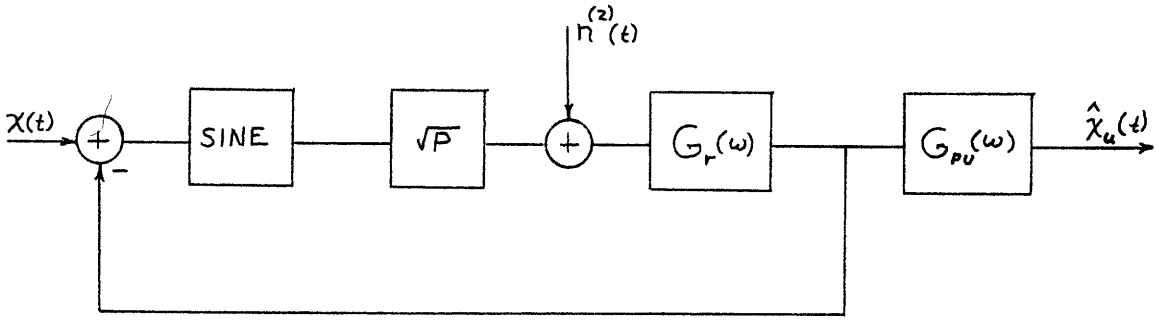

Figure 9

Final Nonlinear Model for Arbitrary x(t)

In figure 8, $G_r(\omega)$ is the realizable in loop filter that replaced the $G(\omega)$. $G_{pu}(\omega)$ is the post loop, unrealizable filter with delay so that we may approximate the system of figure 3 arbitrarily closely. Note also in figure 8 that the filters involved can be obtained easily by solving the Wiener filtering problem. *

2.3 OPTIMUM F.M. RECEIVER

We will now use the results of section 2.2 to find a model for the optimum demodulator. Recall that the received signal is, for a frequency modulated signal,

$$r(t) = \sqrt{2P}\, \sin[\omega_c t + x(t)] + n(t) \tag{31}$$

and

$$x(t) = d_f \int_{-\infty}^{\infty} a(u)\, du \tag{32}$$

Notice that the loop in the model of figure 8 will operate on $x(t)$. Since $x(t)$ is the phase of the received message, then the loop must be designed to minimize the error in the loop. In other words the loop must be designed so that $\hat{x}(t)$ is in some sense the optimum estimate of $x(t)$. We will be using Wiener filters in the receiver which means that $\hat{x}(t)$ will be the optimum estimate in the mean square sense.

---

* Reference 8

To solve the Wiener filtering problem, we use block diagram techniques to extract the additive noise so that it and the message are inputs to the loop as shown in figure 10.

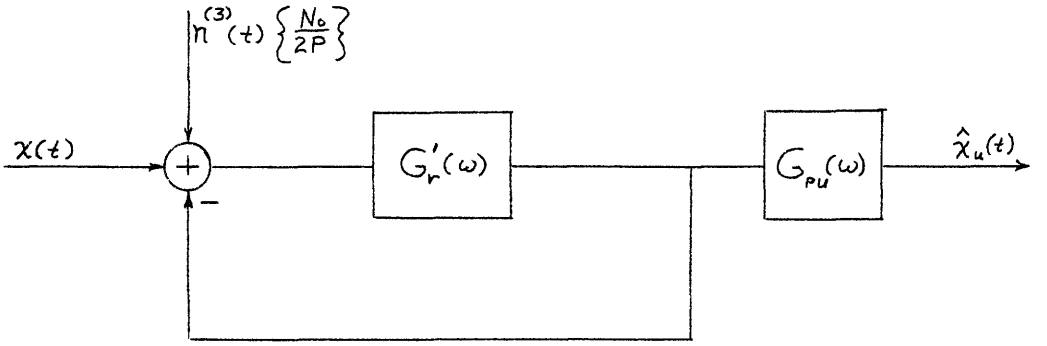

Figure 10

Revision of figure 8

Now it is easy to find the optimum $G_r'(\omega)$ that minimizes the mean square loop error. The next section will present some equations for finding this loop filter.

Our work is not yet finished. A realizable estimate of the message a(t) is actually the <u>desired</u> output of the receiver. Again we have a Wiener filtering problem but of a slightly different type. When the optimum <u>loop</u> filter was determined we found it by saying: "Find the optimum filter, $G_r'(\omega)$, such that when $x(t) + n^{(3)}(t)$ is the input we obtain $\hat{x}_r(t)$ as the output." Now to find the filter that will give $\hat{a}_r(t)$ we say: "Find the optimum filter, $H_{or}(\omega)$, such that when $x(t) + n^{(3)}(t)$ is the input we

obtain $\hat{a}_r(t)$ as the output." There is a distinct difference between the two filtering problems but both of them must be executed to realize the optimum system. Figure 11 shows the results of our filtering calculations.

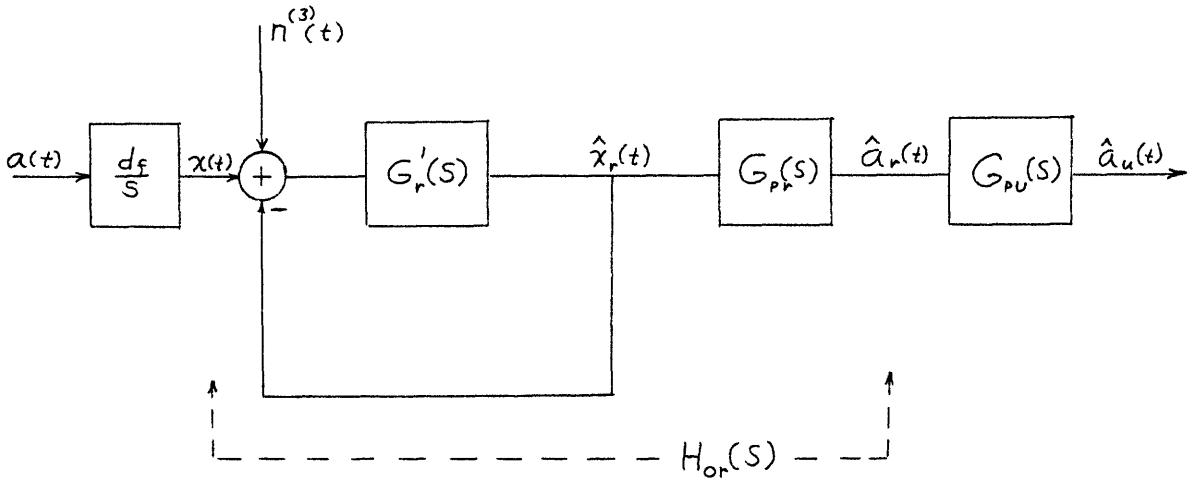

Figure 11

Notice in figure 11 we have maintained the integrity of the loop. This is necessary because eventually the sine nonlinearity will be put back into the forward path of the loop. The filter $G_{pr}(s)$ is an extra filter that is needed to make up the difference between the transfer function $[1 + G_r'(s)]^{-1} G_r'(s)$ and $H_{or}(s)$. The relation for finding $G_{pr}(s)$ is

$$G_{pr}(s) = \frac{[1 + G_r'(s)]}{G_r'(s)} H_{or}(s) \tag{33}$$

So far we have found the filters that will give the optimum realizable estimate of the message a(t). If it was so desired to obtain the optimum unrealizable estimate $\hat{a}_u(t)$ one would proceed in a similar fashion to the above argument and find the filter $G_{pu}(s)$. In the simulations of our optimum systems we will not use $G_{pu}(s)$ so it will be discarded at this point.

After we calculate all the filters for this linear case, we put them back into the nonlinear model of figure 9. The result is shown in figure 12. This is the final realizable, zero delay nonlinear model of our optimum receiver.

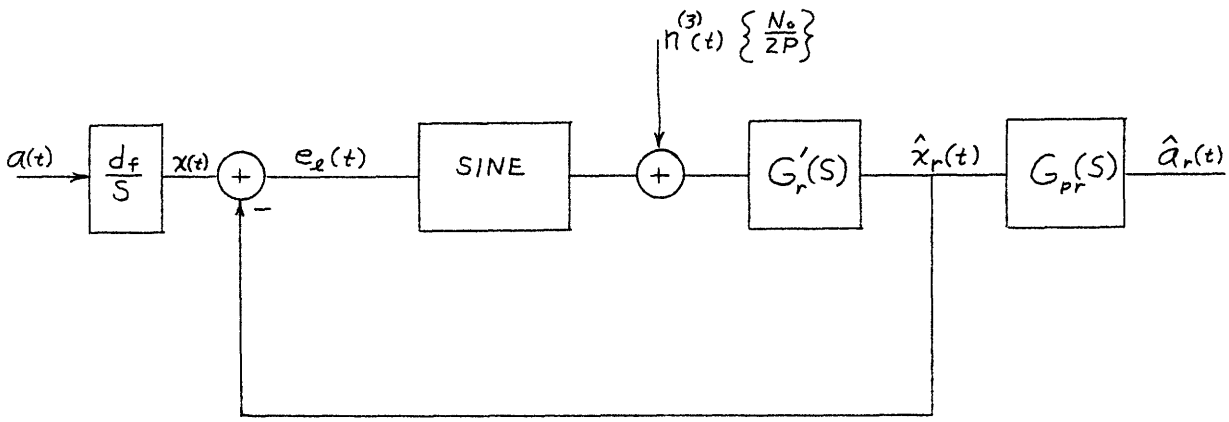

Figure 12

Nonlinear Model of Optimum F.M. Receiver

Note that in figure 12 the additive noise has changed. That is because after the noise was brought out past the $\sqrt{P}$, the $\sqrt{P}$ was absorbed into $G_r'(\omega)$. Therefore when we brought

the noise back into the loop we had no $\sqrt{P}$ to cross; i.e.,

$$n^{(3)}(t) = \frac{n^{(2)}(t)}{\sqrt{P}} \quad . \tag{34}$$

An equivalent version of figure 12 is shown in figure 13. Here a $d_f/j\omega$ term has been extracted from $G_r'(\omega)$ and placed in the feed back loop. When we do this the post loop filters will change slightly as indicated by the primed filter transfer functions shown in figure 13.

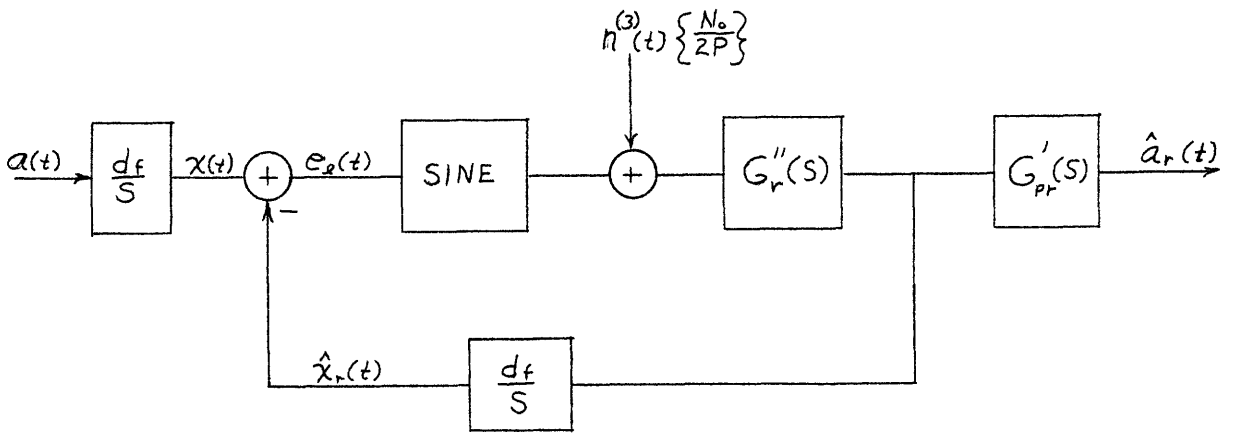

Figure 13

Equivalent Optimum Model

2.4 CONVENIENT EXPRESSIONS FOR WIENER FILTERS FOR FREQUENCY MODULATION CASE

In the final model of figure 13 note that the non-linearity is inside the loop. This fact dictates that when we make the linear approximation we must maintain

the integrity of the loop so that we can put the nonlinearity back in the proper place.

To obtain the loop filter one can first find the realizable Wiener filter $P(\omega)$ * to estimate the phase and then institute the familiar feedback formula

$$P(\omega) = \frac{G_r''(\omega)}{1 + G_r''(\omega)} \tag{35}$$

to find $G_r''(\omega)$.

Alternatively, the $G_r''(\omega)$ can be found directly by

$$G_r''(\omega) = \left[\frac{N_o}{2P}\right]^{-\frac{1}{2}} \left[S_x(\omega) + \frac{N_o}{2P}\right]^{+} - 1. \quad ** \tag{36}$$

In (36) the plus superscript indicates spectral factorization. To be specific it means that we are to separate the left half plane poles and zeros from the right half plane poles and zeros and include in (36) only the ones in the left half plane. Also this formula holds only when $n^{(3)}(t)$ is white Gaussian noise. The $S_x(\omega)$ is the power density spectrum of the function $x(t)$.

To find $H_{or}(\omega)$, the overall optimum linear filter for estimating $a(t)$ without delay we may use

---

* Reference 8.

** Reference 7, Chapters 6 and 7.

$$H_{or}(\omega) = J\omega\{S_n^{(3)}(\omega)\}^{\frac{1}{2}}\left[\{S_n^{(3)}(\omega)\}^{-\frac{1}{2}}\right.$$

$$\left. - \frac{J\omega + f(0)}{[S_a(\omega) + \frac{\omega^2}{d_f^2} S_n^{(3)}(\omega)]^+}\right] \qquad (37)$$

Equation (37) is also valid only when $S_n^{(3)}(\omega)$ is the spectral density of white noise, (typically $N_o/2P$), where,

$$f(0) = \int_{-\infty}^{\infty} \text{Log}\left[1 + \frac{d_f^2 S_a(\omega)}{\omega^2 [S_n^{(3)}(\omega)]}\right] \frac{d\omega}{2\pi} \quad * \qquad (38)$$

and simply represents a gain term. In general, this integral is best evaluated numerically. In a few cases, long hand results can be obtained.

As an alternative one can find f(0) by another method. Consider the linearized version of figure 12. The input to the loop is considered to be $x(t) + n^{(3)}(t)$. Now if the message a(t) has a spectral density $S_a(\omega)$, then the spectral density of x(t) is,

$$S_x(\omega) = \frac{d_f^2}{\omega^2} S_a(\omega) \qquad (39)$$

---

* Snyder, Reference 14

From previous results, we know that the spectral density of $n^{(3)}(t)$ is $S_n^{(3)}(\omega)$, or in our special case, $N_o/2P$. Using the frequency domain representation we write

$$1 + \frac{S_x(\omega)}{S_n^{(3)}(\omega)} = \frac{P(\omega)}{Q(\omega)} = \frac{P_\ell(\omega)\ P_r(-\omega)}{Q_\ell(\omega)\ Q_r(-\omega)} \tag{40}$$

Here both $P(\omega)$ and $Q(\omega)$ are even functions of frequency so that the left half plane zeros for both functions have a mirror image in the right half frequency plane. Hence both $P(\omega)$ and $Q(\omega)$ are factorable as shown in equation (40). If we consider the realizable part of $P(\omega)$ and $Q(\omega)$ which is $P_\ell(\omega)$ and $Q_\ell(\omega)$ and write,

$$P_\ell(\omega) = (J\omega)^M + a_1(J\omega)^{M-1} + a_2(J\omega)^{M-2} + \ldots + a_M \tag{41}$$

and,

$$Q_\ell(\omega) = (J\omega)^M + b_1(J\omega)^{M-1} + b_2(J\omega)^{M-2} + \ldots + b_M \tag{42}$$

then

$$f(0) = a_1 - b_1 \ .^{*} \tag{43}$$

---

* Reference 10.

CHAPTER 3

OPTIMUM F.M. SYSTEM PERFORMANCE (ANALYTICAL)

3.0 INTRODUCTION

Figure 13 of chapter 2 represents our model for the optimum demodulator. There remains the task of determining the performance of our optimum system. We have three alternatives for determining the performance. The first is to actually build the system in the laboratory. The second is to simulate the model in figure 13 using a computer and the third is to compute the performance analytically.

To physically build the system in the laboratory would be quite time consuming and would require a good facility for circuit design.

The second alternative seems somewhat more palatable. Computer simulation would be faster. Either an analog computer or a digital computer could be used for this purpose. Simulation techniques for both types have been well advanced in the past few years.

An analytical analysis of our model is also a reasonable approach. However, note that a complete analytical

analysis of a nonlinear system is in no sense trivial. For most messages, a(t), a complete analysis is not known. However, we can investigate the linear regions and get some idea as to where the system becomes nonlinear. Booton[11] advanced a technique for evaluating the performance of this system in the region where it is just beginning to become nonlinear.

In this thesis we will use two of the above methods to evaluate the performance of our demodulator. The first will be to analytically construct the performance using Booton's quasi-linearizing method and the second will be to simulate the model of figure 13 on a digital computer.

This chapter will be devoted to the analytical approach and the next chapter will explain the simulation techniques.

3.1 PERFORMANCE CRITERION

Before we can evaluate the performance of the demodulator we must establish some kind of framework from which we can judge how well the system is working. Remember from chapter one that the message that we are trying to reconstruct is a sample function from a random process, a(t). The output of the demodulator is an estimate of that random process, $\hat{a}_r(t)$. Hence we can define an error

$$e_a(t) = a(t) - \hat{a}_r(t). \tag{44}$$

Since both $a(t)$ and $\hat{a}_r(t)$ are random functions then so is $e_a(t)$. Therefore we can talk about the variance of the error $e_a(t)$ and it will be defined as

$$\sigma_f^2 = \mathrm{VAR}[e_a(t)]$$

The subscript "f" denotes frequency demodulation. Note that if the error is small, the variance of the error is correspondingly small and our demodulator is working well. On the other hand, if the error is large, then σ_f^2 is large. Thus if we consider the ratio $1/\sigma_f^2$, large values imply good demodulator performance and low values imply poor performance.

Another parameter which is important to this case is the carrier-to-noise power ratio in the message equivalent bandwidth.* In symbols

$$\mathrm{SNR} \equiv \Lambda \equiv \frac{P}{NB_{eq}} \quad \text{hertz}^{-1} \tag{45}$$

where P represents the carrier power and NB_{eq} represents the white noise power in the message equivalent bandwidth.

In receivers that employ a phase-locked loop there are two more parameters that give information about how well the system is performing. They are the phase error

---

* See appendix for explanation

variance, σ_x^2 and cycle skips.

The phase error variance is actually the variance of the loop error, $e_\ell(t)$ as shown in figure 13. Formally,

$$\sigma_x^2 = \text{VAR}[e_\ell(t)] = \text{VAR}[x(t) - \hat{x}_r(t)] \tag{46}$$

For small values of σ_x^2 the system of figure 13 is operating in the linear region of its performance characteristics. For large values of σ_x^2 interesting things happen and the performance degrades rapidly. By plotting $1/\sigma_x^2$ versus Λ we can obtain an additional insight as to what level of SNR our system begins to fail.

Consider figure 13, and recall that the sine operator is a modulo-2π device. When

$$e_\ell(t) = 2\pi + \varepsilon \tag{47}$$

the sine operator views this as

$$e_\ell(t) = \varepsilon \tag{48}$$

As a consequence of this, the actually large error of $2n\pi + \varepsilon$ is viewed by the loop as a small error. The result is that we get insufficient feedback from the loop and thus a larger error between $x(t)$ and $\hat{x}_r(t)$. This action of the loop is called cycle skipping and its occurrence implies degradation of receiver performance. Cycle skipping is therefore another measure by which we can judge the performance of our system.

3.2 ANALYSIS BY THE QUASI-LINEARIZATION TECHNIQUE

In figure 13 when $\sin [e_\ell(t)] \simeq e_\ell(t)$ the sine operator can be approximated by unity and the system is completely linear. When this is the case it is straightforward to compute the error variances. However, we know that $e_\ell(t)$ is not always small, especially for low SNR. When this is the case the nonlinear operator creates a drastic change in the performance curves.

Complete analytical analysis of the non-linear system is difficult. However, Booton[11] postulated that if the sine operator were replaced by an equivalent gain term, instead of unity, then the resultant quasi-linear system would perform more like the nonlinear system. A derivation of Booton's equivalent gain term is given in the following paragraphs.

If our system was linear and the input to the system was Gaussian with mean M_x and variance σ_x^2, then every variable in the system would be Gaussian with mean M_x and variance σ_x^2. * However, in general, nonlinear operations on an input function change the shape of its probability density function. Thus, in our system, when the amplitude of $x(t) - \hat{x}_r(t)$ is small, and the linear system approximation is valid, then $e_\ell(t)$ can be considered approximately

---

* Reference 17, Chapter 8.

Gaussian with zero mean and variance σ_x^2. With this approximation in mind we can proceed to find an "equivalent gain" to replace the sine operator.

The incremental gain of a sine operator for an input Y [or $e_\ell(t)$] is

$$\frac{d}{dY}\,[\sin\,(Y)] = \cos\,(Y) \tag{49}$$

Now since we have determined that Y is approximately Gaussian then the expected gain can be written as

$$\int_{-\infty}^{\infty} \frac{1}{\sqrt{2\pi}\,\sigma_x}\, e^{-\frac{Y^2}{2\sigma_x^2}}\, \cos\,(Y)\, dy = e^{-\frac{\sigma_x^2}{2}} \tag{50}$$

If we define

$$\nu \equiv e^{(\sigma_x^2)} \tag{51}$$

then

$$e^{-\frac{\sigma_x^2}{2}} = \frac{1}{\sqrt{\nu}} \tag{52}$$

By replacing the sine operator in figure 13 by its equivalent expected gain (52), we obtain the quasi-linear system shown in figure 14.

Given the quasi-linear model, it remains to compute σ_x^2 and σ_f^2 for a given SNR. Using block diagram reduction

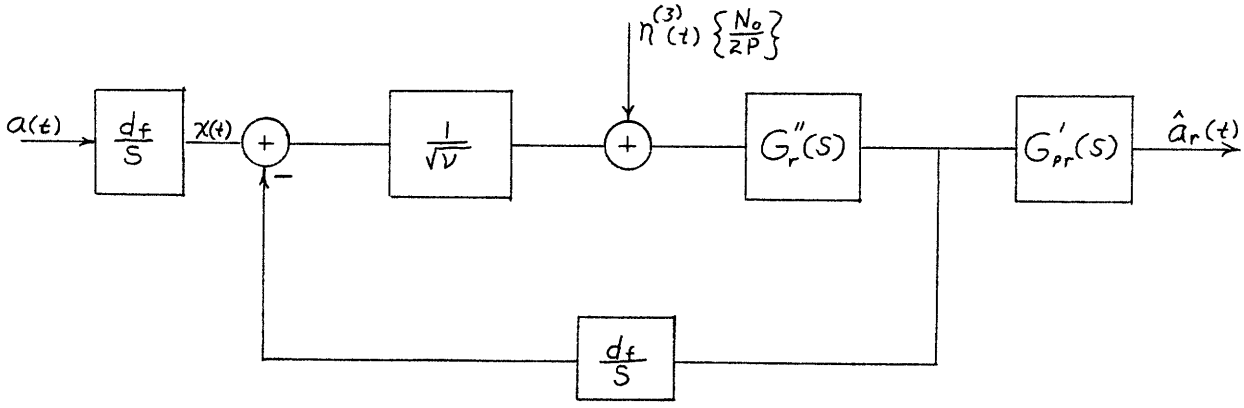

Figure 14
Quasi-linear model

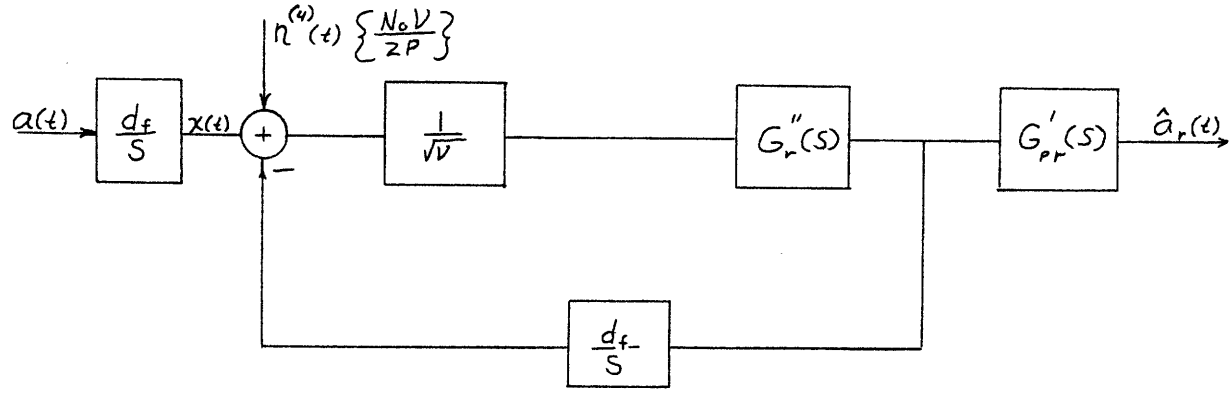

Figure 15

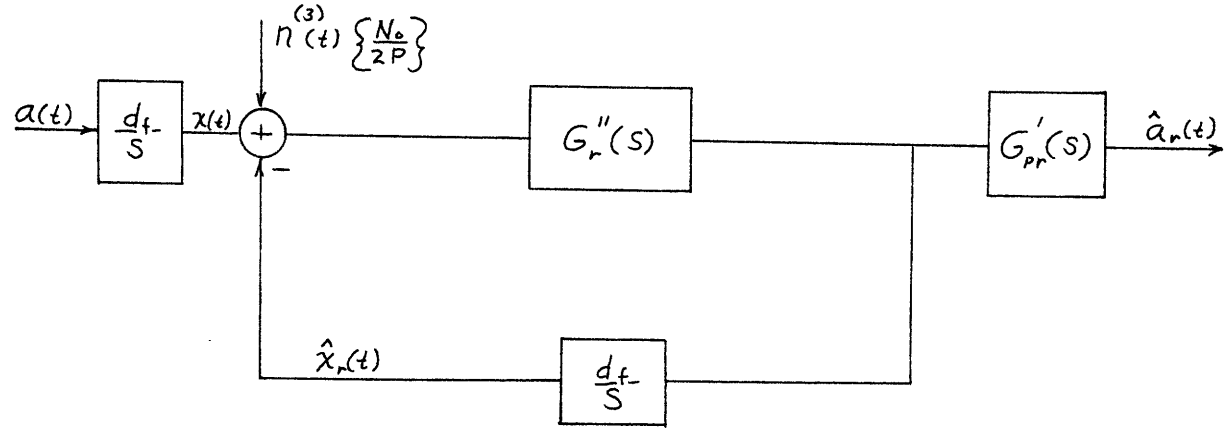

Figure 16
Complete, zero delay, linear, realizable model

we obtain figure 15 from figure 14. Now if,

$$a(t) \iff S_a(\omega) \tag{53}$$

then

$$x(t) \iff S_x(\omega) = \frac{d_f^2}{\omega^2} S_a(\omega) \tag{54}$$

and

$$S_n^{(4)}(\omega) = \frac{N_o}{2P} \nu \ . \tag{55}$$

In general the phase error is caused by two sources. There is an error due to distortion in the filters and there is an error due to the presence of additive noise in the system. If $H(\omega)$ is the system function that operates on the phase of the received signal [i.e. $x(t)$] then

$$\sigma_x^2 = \int_{-\infty}^{\infty} \{S_x(\omega) |1 - H(\omega)|^2 + S_n^{(4)}(\omega) |H(\omega)|^2\} \frac{d\omega}{2\pi} \tag{56}$$

For this case,

$$H(\omega) = \frac{\frac{d_f}{\sqrt{\nu}} \frac{G_r''(\omega)}{J\omega}}{1 + \frac{d_f}{\sqrt{\nu}} \frac{G_r''(\omega)}{J\ \omega}} \tag{57}$$

Likewise, if $\tilde{H}(\omega)$ represents the overall transfer function from $a(t)$ to $\hat{a}(t)$, then

$$\sigma_f^2 = \int_{-\infty}^{\infty} \{S_a(\omega)|1 - \tilde{H}(\omega)|^2 + S_n^{(4)}(\omega) \frac{\omega^2}{d_f^2}|\tilde{H}(\omega)|^2\} \frac{d\omega}{2\pi} , \quad (58)$$

where

$$\tilde{H}(\omega) = H(\omega) G''_{pr}(\omega) \quad (59)$$

For the purpose of investigating equation (56) and (58) we will use the Butterworth class of power spectral densities. This family is defined by the two sided spectra,

$$S_a(\omega:n) = \frac{\frac{2n}{k} \sin \frac{\pi}{2n}}{1 + (\omega/k)^{2n}} , \quad (60)$$

for all integers $n > 0$. The gain term in $S_a(\omega:n)$ is designed so that the variance of the spectra will be unity for all n.

$$\int_{-\infty}^{\infty} \frac{\frac{2n}{k} \sin \frac{\pi}{2n}}{1 + (\omega/k)^{2n}} \frac{d\omega}{2\pi} = 1 \quad (61)$$

Observe that we have a choice on how we are to proceed. We may choose to design the system filters for one of two cases. One case is shown in figure 15. Here the signal

that must be filtered is $x(t) + n^{(4)}(t)$. The other case is shown in figure 16 where the input to the loop is $x(t) + n^{(3)}(t)$. In either case the resultant filters will be arranged in the quasi-linear model as shown in figure 14.

In the body of this thesis, the system filters will be designed according to the system of figure 16. The other case will be considered in the appendix.

Example 1

Some details of the operations indicated in equations (56) and (58) will be carried out for the single pole Butterworth message $S_a(\omega:1)$. Only results will be presented for the higher order Butterworth messages.

Consider figure 15 when $a(t)$ is zero mean and Gaussian with power spectral density

$$S_a(\omega) = \frac{2}{\omega^2 + 1} \quad , \tag{62}$$

and the additive channel noise is zero mean and white with double sided power spectral density,

$$S_n(\omega) = \frac{N_o}{2} \tag{63}$$

Now using the symbols indicated in figure 15,

$$S_x(\omega) = \frac{d_f^2}{\omega^2} \frac{2}{\omega^2 + 1} , \tag{64}$$

and

$$S_n^{(4)}(\omega) = \frac{N_o}{2P} \nu . \tag{65}$$

Before we can proceed we must compute the in-loop and post-loop filters for our system. If we revert back to the completely linear model shown in figure 16, then the filters $G_r''(s)$ and $G_{pr}'(s)$ may be computed with equations (36) and (37).

The results are:

$$G_r''(s) = \frac{1}{d_f} \frac{(\gamma - 1)s + \delta}{s + 1} \tag{66}$$

and

$$G_{pr}'(s) = \frac{(\gamma - 1)}{2s + (\gamma + 1)} \tag{67}$$

where

$$\gamma = \sqrt{2\delta + 1} \tag{68}$$

$$\delta^2 = d_f^2 \Lambda \tag{69}$$

$$\Lambda = \frac{4P}{KN_o} \tag{70}$$

Substituting these results into equations (56) and (58), we obtain:

$$\sigma_x^2 = \frac{1}{2\pi J}\int_{J\infty}^{+J\infty} \frac{\frac{2\nu}{\Lambda}\{[(\gamma-1)s + \delta][-(\gamma-1)s + \delta]\} + 2d_f^2\nu}{\{\sqrt{\nu}\, s^2 + [\sqrt{\nu} + (\gamma-1)]s + \delta\}\{\sqrt{\nu}\, s^2 - [\sqrt{\nu} + (\gamma-1)]s + \delta\}} ds \; * \tag{71}$$

or

$$\sigma_x^2 = \frac{d_f^2 \nu^{\frac{3}{2}} + \frac{\nu d_f^2}{\delta}[(\gamma-1)^2 + \delta\nu^{\frac{1}{2}}]}{\delta\nu^{\frac{1}{2}}[\nu^{\frac{1}{2}} + (\gamma - 1)]} . \tag{72}$$

Similar computations with equations (58) and (59) yields,

$$\sigma_f^2 = \frac{2\nu^{\frac{1}{2}}\delta + (\gamma - 1)^2(\nu + 2)}{2\delta\nu + 2\delta\nu^{\frac{1}{2}}(\gamma - 1)} \tag{73}$$

Note that equation (72) is a rather complicated formula. It can be reduced to a transcendental equation involving only σ_x^2, d_f and Λ. By assuming values for σ_x^2

---

* A table of integrals of this kind are found in reference 12

we can compute the corresponding values for Λ. In this case for the one pole Butterworth message, equation (72) may be inverted to form a fourth order polynomial in Λ.

$$a_4\Lambda^{\frac{4}{2}} + a_3\Lambda^{\frac{3}{2}} + a_2\Lambda^{\frac{2}{2}} + a_1\Lambda^{\frac{1}{2}} + a_o = 0 \tag{74}$$

where

$$a_4 = 2d_f\sigma_x^2$$

$$a_3 = \sigma_x^2 - (\sigma_x^2 - \sigma_x^2\nu^{\frac{1}{2}})^2$$

$$a_2 = 8d_f\sigma_x^2\nu^{\frac{1}{2}} - 2(\sigma_x^2 - \sigma_x^2\nu^{\frac{1}{2}})(d_f\nu + 2\nu^{\frac{1}{2}}d_f + \nu d_f)$$

$$a_1 = 4\sigma_x^2\nu^{\frac{1}{2}} - 2(\sigma_x^2 - \nu^{\frac{1}{2}}\sigma_x^2)(2\nu^{\frac{1}{2}}) - (d_f\nu + 2\nu^{\frac{1}{2}}d_f + \nu d_f)$$

$$a_o = 8d_f\nu - 2(d_f\nu + 2\nu^{\frac{1}{2}}d_f + \nu d_f)(2\nu^{\frac{1}{2}})$$

Once (74) is solved for a set of σ_x^2 and Λ, then equation (73) can be solved for the mean square demodulation error. Plots of equations (72) and (73) are shown in figures (17) and (18).

When similar calculations are carried out for the second order Butterworth message the following results are obtained.

$$G''(s) = \frac{M}{d_f} \frac{s^2 + Ls + N}{s^2 + \sqrt{2}\, s + 1} \tag{75}$$

$$G'_{pr}(s) = \frac{1}{M} \frac{\tau_2 s + \tau_3}{s^2 + Ls + N} \tag{76}$$

$$\sigma_x^2 = \frac{\frac{2\sqrt{2}}{\gamma} M^2 \left[\left(\frac{MN}{\sqrt{\nu}}\right) \left(\frac{ML}{\sqrt{\nu}} + 1\right) + (L^2 - 2N) \frac{MN}{\sqrt{\nu}} + N^2 \left(\frac{M}{\sqrt{\nu}} + \sqrt{2}\right) \right] + 2\sqrt{2}\, d_f^2 \left[\frac{M}{\sqrt{\nu}} + \sqrt{2}\right]}{\frac{2MN}{\sqrt{\nu}} \left[- \frac{MN}{\sqrt{\nu}} + \left(\frac{ML}{\sqrt{\nu}} + 1\right) \left(\frac{M}{\sqrt{\nu}} + \sqrt{2}\right) \right]} \tag{77}$$

$$\sigma_f^2 = \frac{\frac{2\sqrt{2}}{\gamma} \left[\tau_2^2 \left(\frac{MN}{\sqrt{\nu}}\right) \left(\frac{ML}{\sqrt{\nu}} + 1\right) + \tau_3^2 \left(\frac{MN}{\sqrt{\nu}}\right) \right] + 2\sqrt{2} \left[\left(\frac{M}{\sqrt{\nu}}\right)^2 \left(\frac{M}{\sqrt{\nu}} + \sqrt{2}\right) + \frac{MN}{\sqrt{\nu}} \right]}{\frac{2MN}{\sqrt{\nu}} \left[- \frac{MN}{\sqrt{\nu}} + \left(\frac{ML}{\sqrt{\nu}} + 1\right) \left(\frac{M}{\sqrt{\nu}} + \sqrt{2}\right) \right]} \tag{78}$$

where

$$M = 2\gamma^{\frac{1}{6}} - \sqrt{2} \qquad \gamma = \Lambda d_f^2$$

$$L = (2\gamma^{\frac{1}{3}} - 1)/M \qquad \Lambda = \frac{4\sqrt{2}\, P}{N_o}$$

$$N = \gamma^{\frac{1}{2}}/M \qquad \nu = e^{\sigma_x^2}$$

$$\tau_2 = 2\delta^{\frac{1}{3}} - 2\sqrt{2}\gamma^{\frac{1}{6}} + 1$$

$$\tau_3 = \gamma^{\frac{1}{2}} - 2\gamma^{\frac{1}{6}} + \sqrt{2}$$

The results of equations (77) and (78) are plotted in figures (19) and (20) respectively.

Let us divert briefly from the quasi-linear analysis and consider the system when it's operating in its linear region only. That is to say,

$$\sin e_{\ell}(t) \simeq e_{\ell}(t) \tag{79}$$

or equivalently,

$$\sigma_x^2 \leq \sigma_{cr}^2 \tag{80}$$

where σ_{cr}^2 is just an arbitrary constant that implies (79). When $\sigma_x^2 \leq \sigma_{cr}^2$ we will say that our system is linear.

For a linear system with a message and white noise as its input, Yovits and Jackson[13] derived a useful closed form expression to compute the variance of the error. That expression is

$$\sigma_{opt}^2 = \int_{-\infty}^{\infty} N, \text{Log} \left[1 + \frac{S(\omega)}{N}\right] \frac{d\omega}{2\pi} \tag{81}$$

Now apply (81) to our special case, the variance of the loop error can be written as, (see figure 16)

$$\sigma_x^2 = \int_{-\infty}^{\infty} \frac{N_o}{2P} \text{Log} \left[\frac{\frac{N_o}{2P} + \frac{d_f^2}{\omega^2} S_a(\omega)}{\frac{N_o}{2P}} \right] \frac{d\omega}{2\pi} , \quad \sigma_x^2 \leq \sigma_{cr}^2 \tag{82}$$

Also, a convenient expression for the message error variance as given by Snyder[14] is,

$$\sigma_f^2 = \frac{1}{3d_f^2} \left(\frac{N_o}{2P}\right) f(0)^3 + F(0) \tag{83}$$

where

$$f(0) = \int_{-\infty}^{\infty} \text{Log} \left[1 + \frac{2P}{N_o} \frac{S_a(\omega)}{\frac{\omega^2}{d_f^2}} \right] \frac{d\omega}{2\pi}$$

and

$$F(0) = \frac{N_o}{d_f^2 \, 2P} \int_{-\infty}^{\infty} \omega^2 \text{Log} \left[1 + \frac{2P}{N_o} \frac{S_a(\omega)}{\frac{\omega^2}{d_f^2}} \right] \frac{d\omega}{2\pi} \quad . \tag{84}$$

Plots of the linear relations are given in figures 21, 22, and 23 for the Butterworth family, n = 1, 2, and 5. Notice that these curves are valid only when the system is approximately linear. The constraint $\sigma_x^2 \leq \sigma_{cr}^2$ must be true for the linear equations (82) and (83) to hold true.

3.3 DISCUSSION

The results of this chapter are all embodied in figures 17 through 23. Figures 17 through 20 indicate the performance of our optimum receiver during operation in the linear region. In addition they indicate where the system becomes nonlinear and hence where the performance begins to drop off rapidly. For the one and two pole cases, Booton's quasi-linear method shows that the systems become nonlinear when $\sigma_x^2 \simeq$ one radian^2. Comparing the one and two pole cases we see that the linear region performance is a whole order of magnitude better for the latter case. Also notice that for larger values of d_f, the threshold occurs at a considerably lower value of SNR. Booton's technique was not applied to the fifth order Butterworth case because of the complexity of the computations.

Figures 21 through 23 are the results using strictly a linear analysis. As would be expected, these linear analysis results do agree with the quasi-linear analysis results for large values of SNR.

$$\frac{1}{\sqrt{\nu}} = \text{EXP}\left[-\frac{1}{2}\sigma_x^2\right]$$

One pole message
First order phase-locked loop

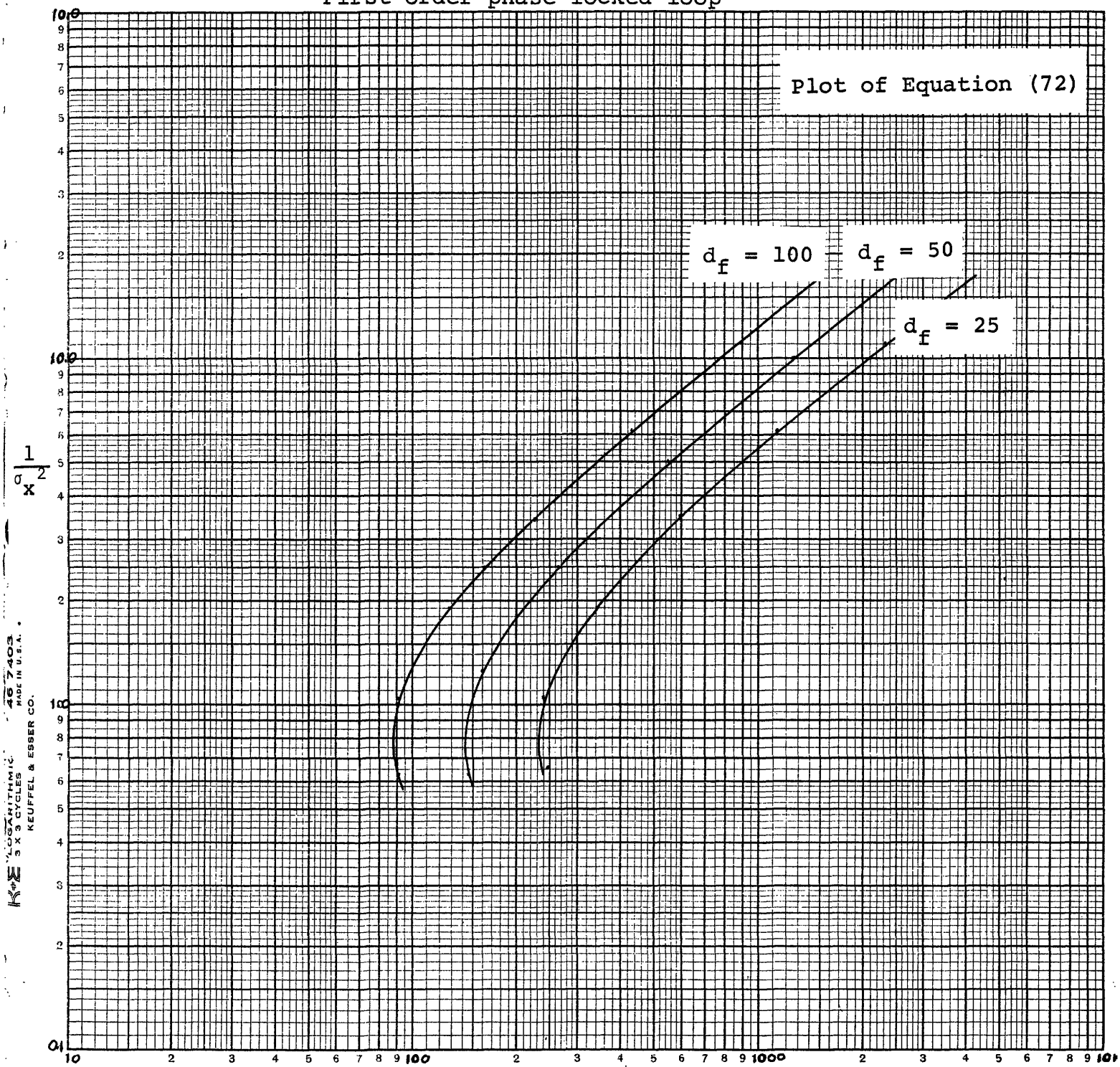

Figure 17

Booton Theoretical Performance for Figure 15

$$\text{GAIN} = \text{EXP}\left[-\frac{1}{2}\sigma_x^2\right] = \frac{1}{\sqrt{\nu}}$$

One pole message

First order phase-locked loop

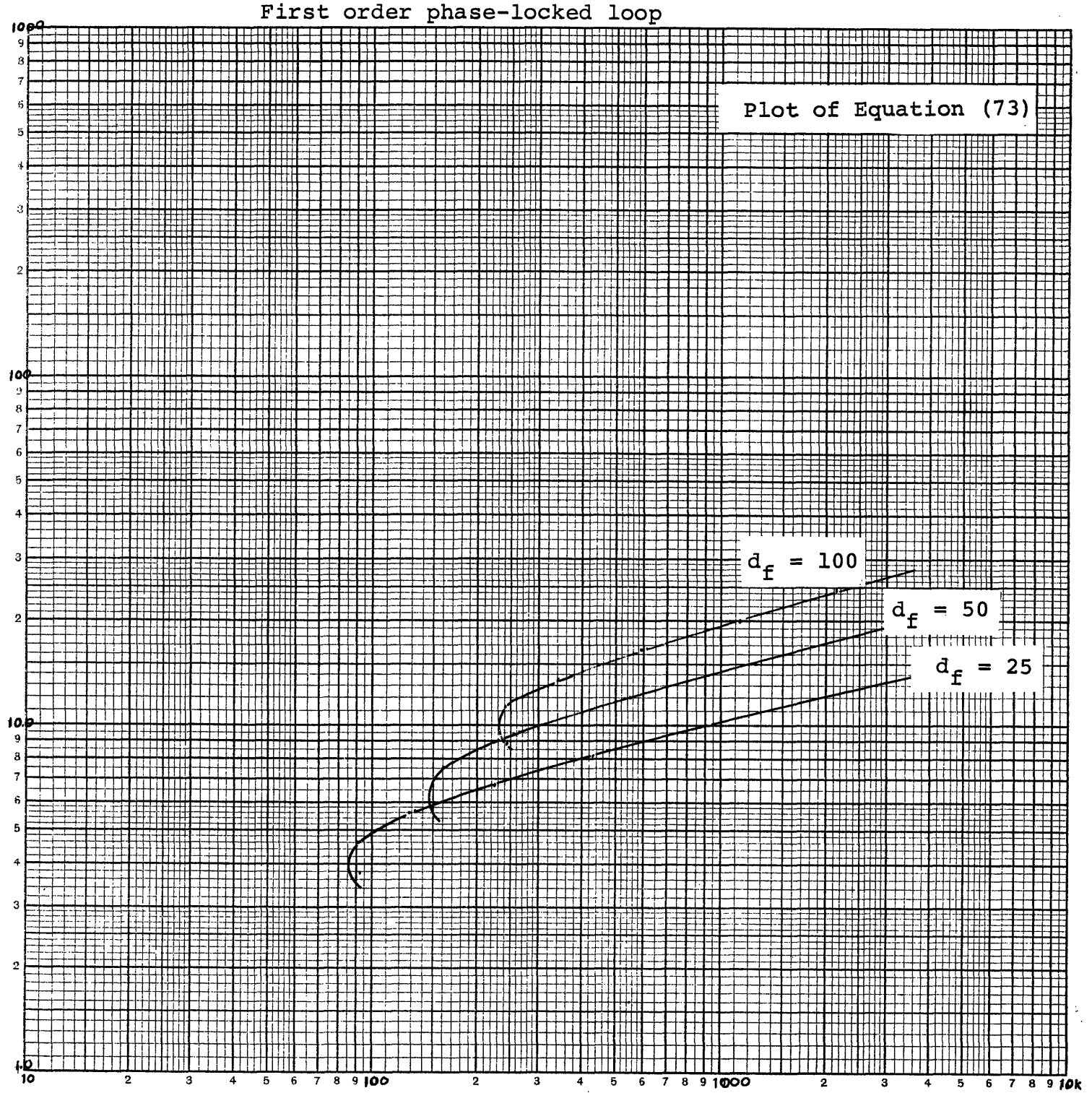

Figure 18

Booton Theoretical Performance for Figure 15

$$\frac{1}{\sqrt{\nu}} = \text{EXP}\left[-\frac{1}{2}\sigma_x^2\right]$$

Two pole message

Second order phase-locked loop

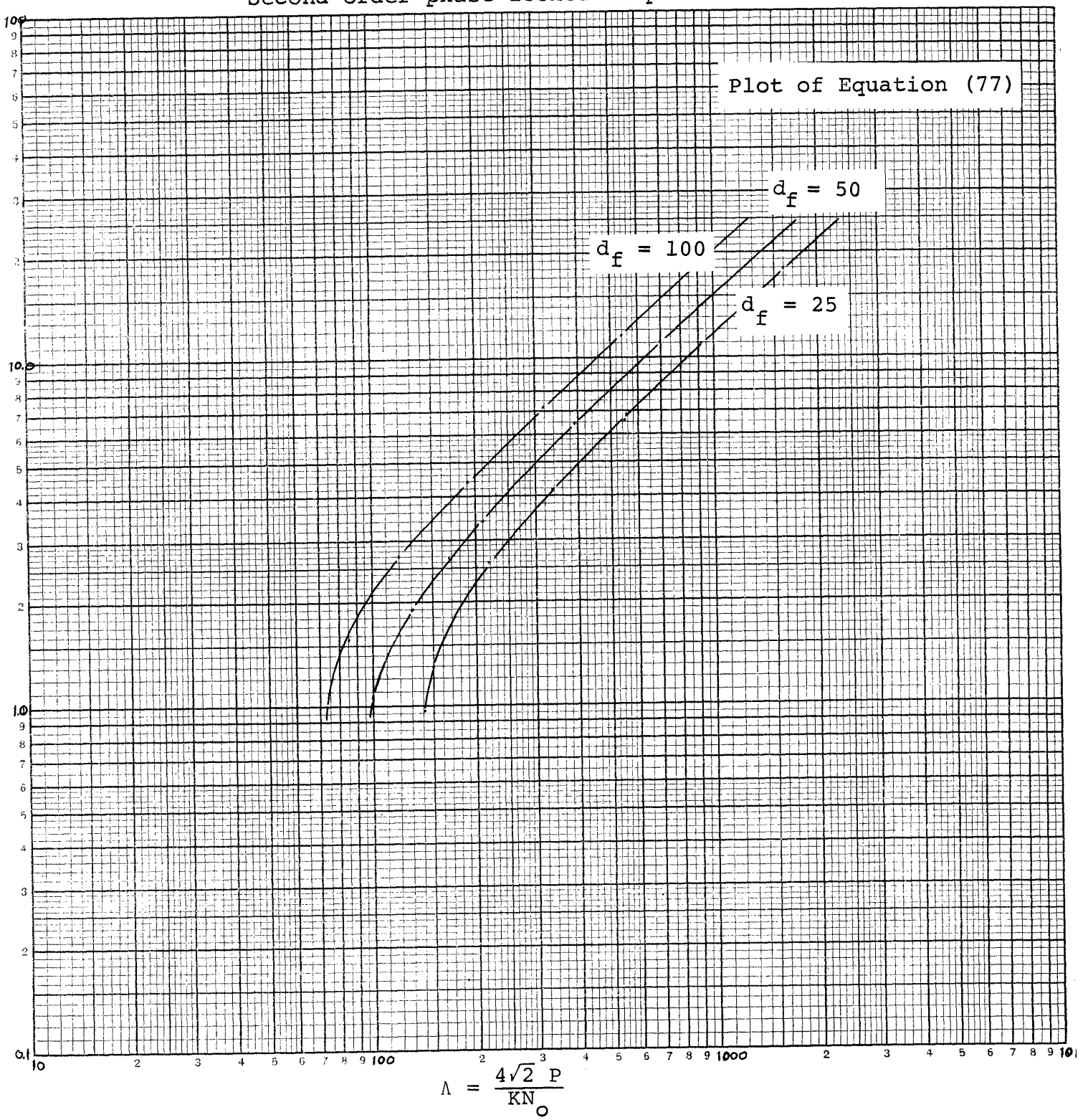

Figure 19

Booton Theoretical Performance for Figure 15

$$\frac{1}{\sqrt{\nu}} = \text{EXP}\left[-\frac{1}{2}\sigma_x{}^2\right]$$

Two pole message

Second order phase-locked loop

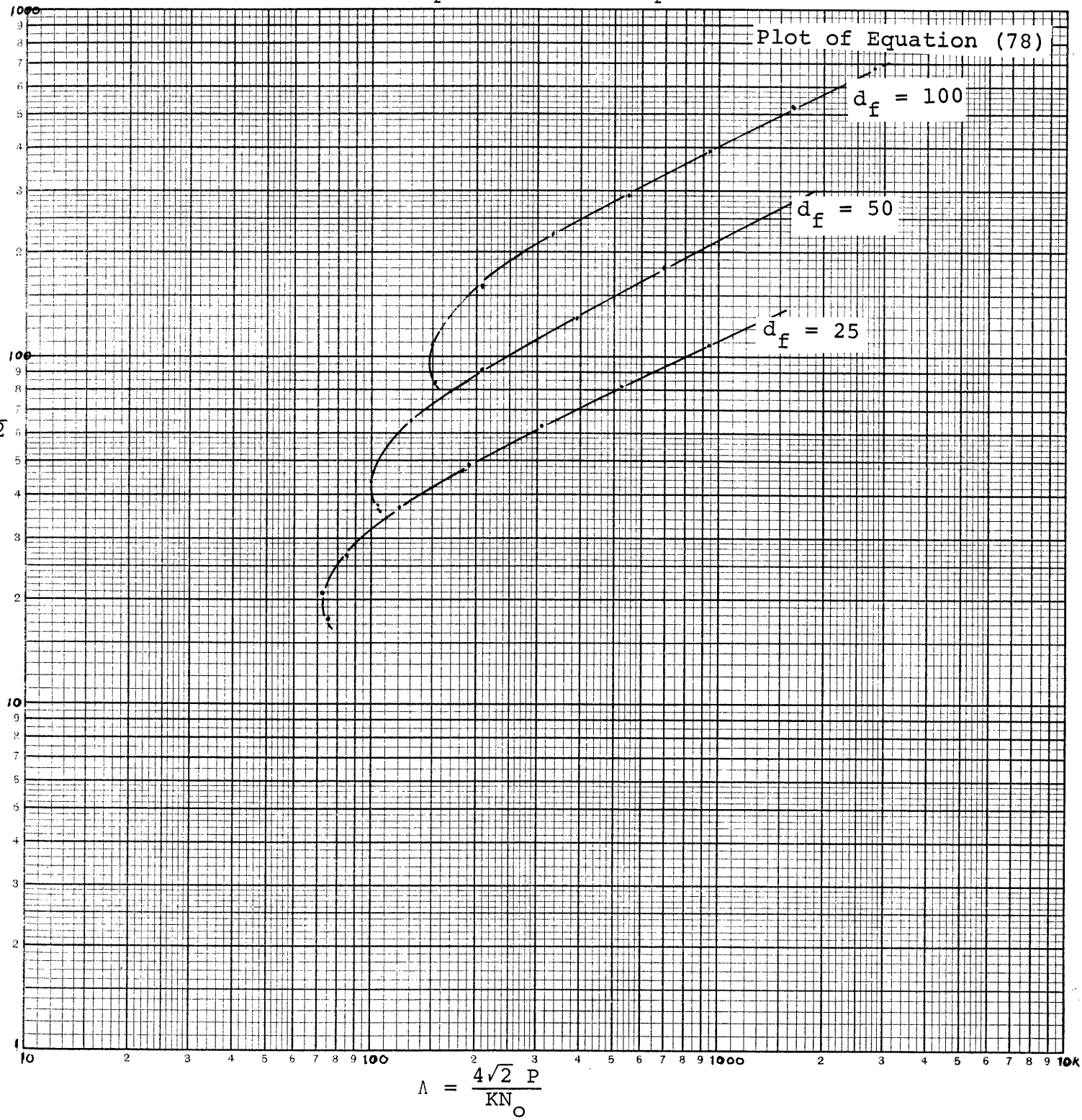

Figure 20

Booton Theoretical Performance for Figure 15

Theoretical Linear Performance for Figure 16

One hole message

Realizable - zero delay mean square error

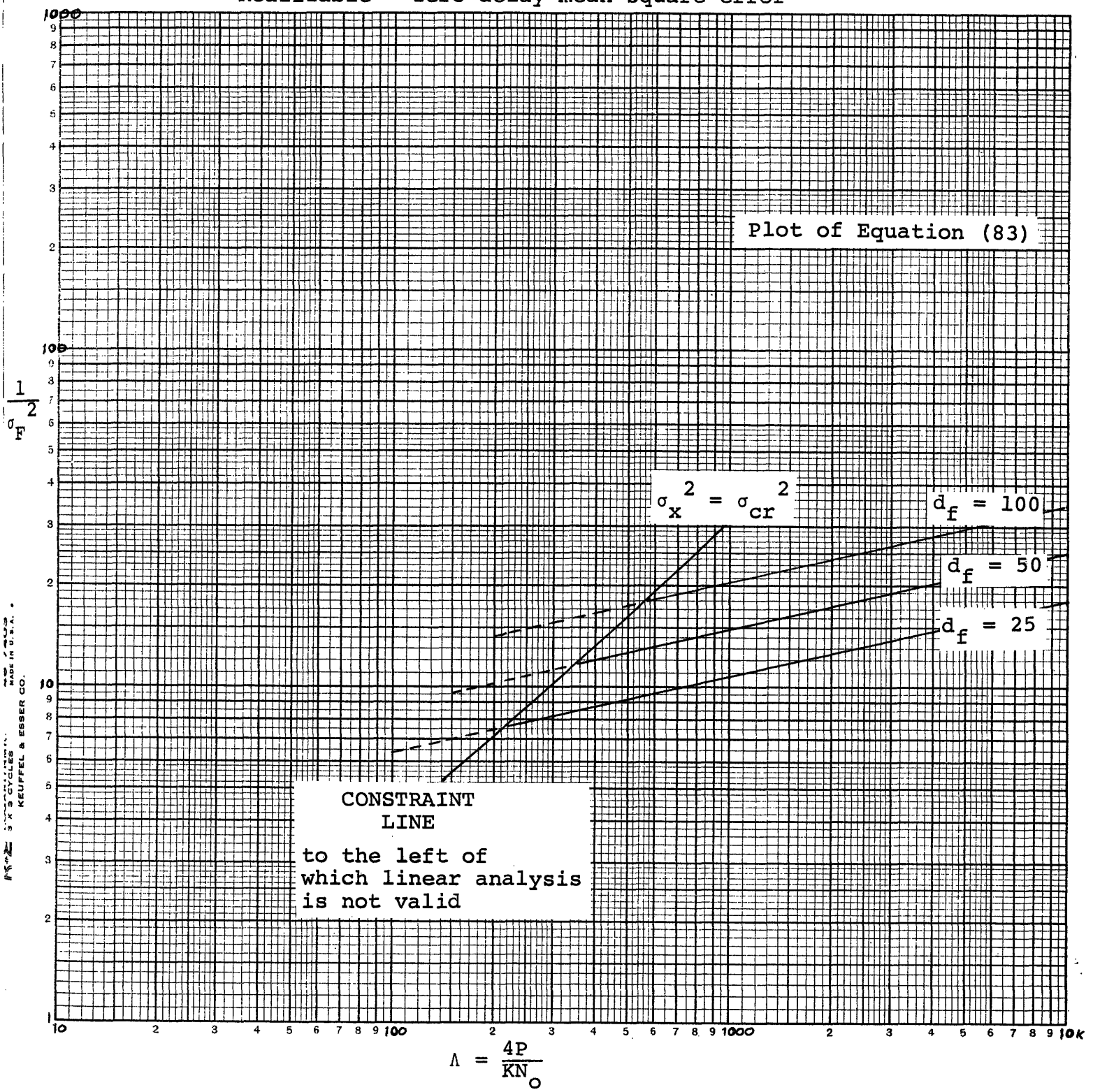

Figure 21

Theoretical Linear Performance for Figure 16

Two pole message

Realizable - zero delay mean square error

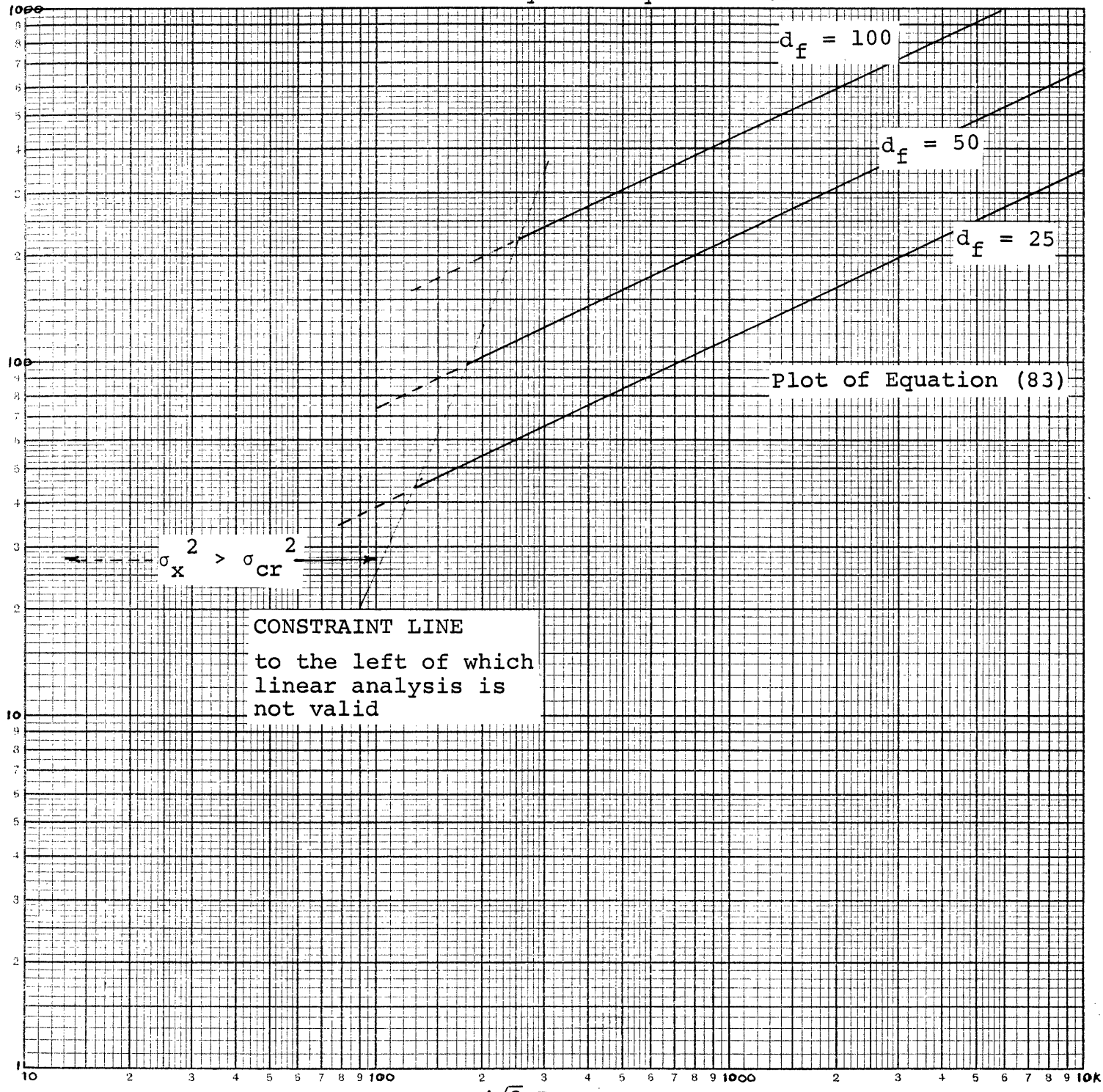

Figure 22

Theoretical Linear Performance for Figure 16

Five pole message

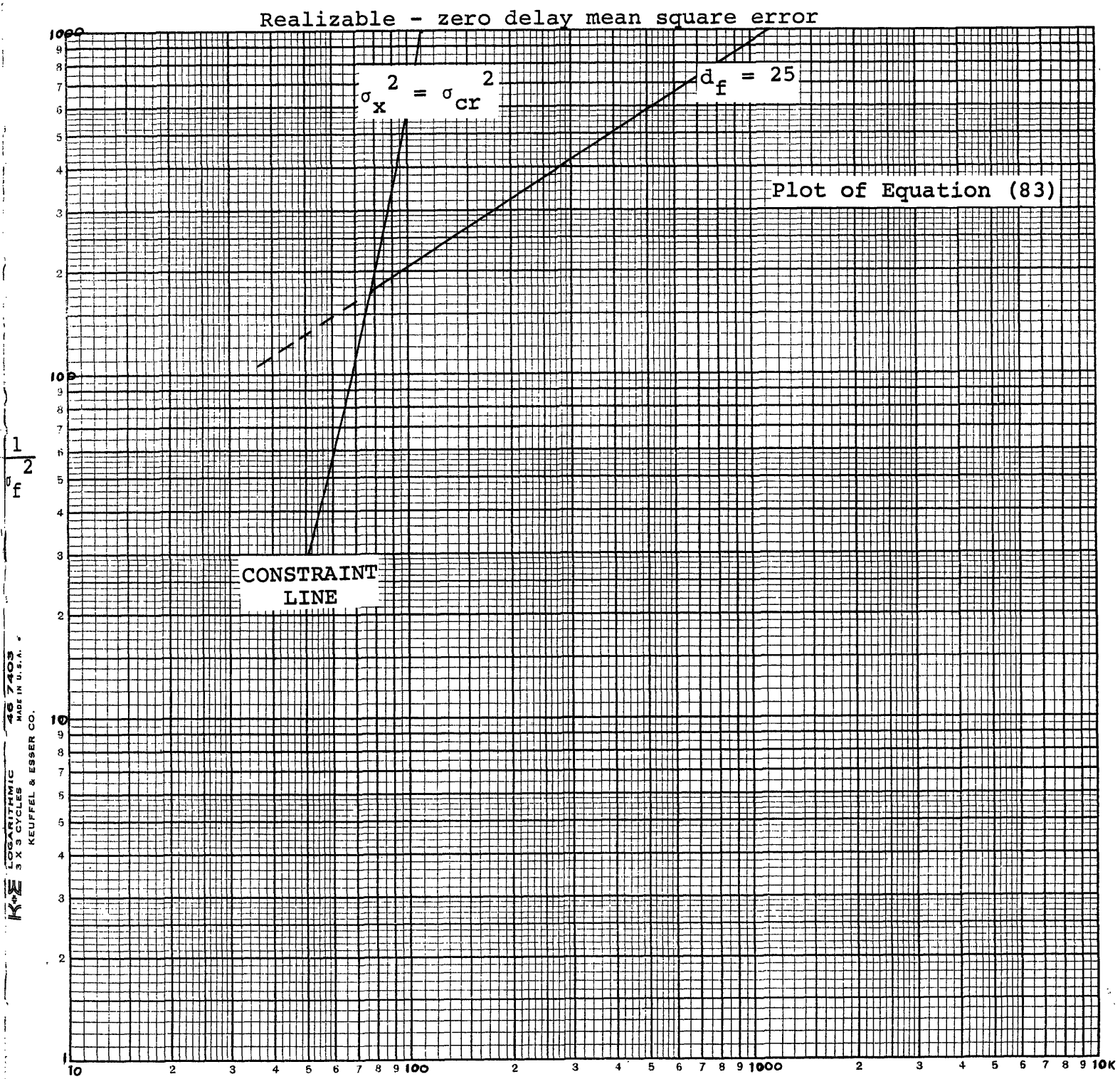

Figure 23

CHAPTER 4

DIGITAL SIMULATION OF OPTIMUM DEMODULATOR

4.0 INTRODUCTION

This chapter will be devoted to the performance analysis of the system in figure 24 by using digital simulation techniques.

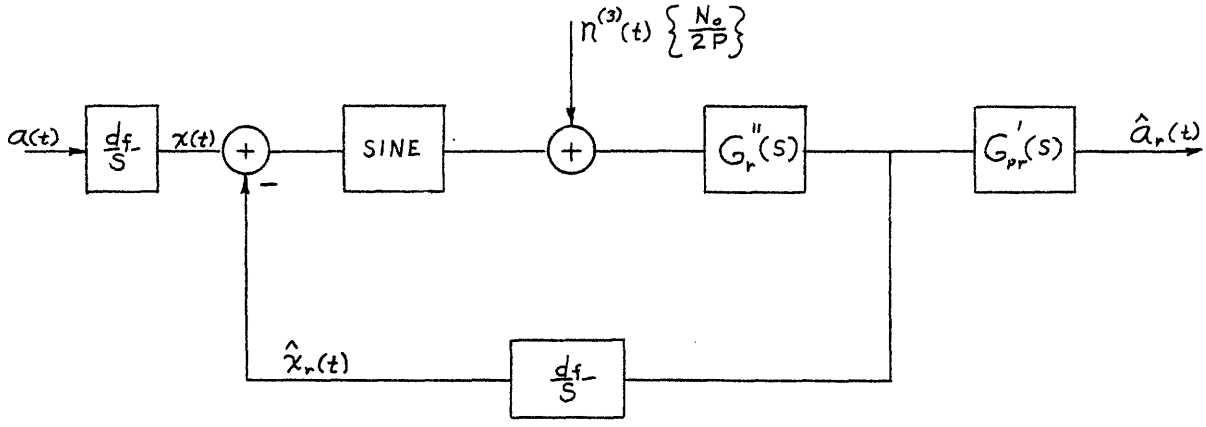

Figure 24

Optimum Receiver

Note that Figure 24 is the optimum receiver that was derived in chapter two. It is redrawn here merely for convenience. The filters used in this model will all be zero delay, optimum Wiener filters.

4.1 DIGITAL MODELING

An obvious difficulty with figure 24, as far as digital simulation is concerned, is that it is an analog system. The message a(t), the noise $n^{(3)}(t)$ and the impulse response $[h_i(t)]$ of the filters are all continuous waveforms. Our problem then is to find an equivalent digital model for these three components. The following three sections will explore the digital modeling of $h_i(t)$, a(t) and $n^{(3)}(t)$, in that order.

4.1.1 SAMPLED DATA MODEL OF CONTINUOUS FILTER

From the process of Wiener filtering we automatically obtain the frequency domain representation for the continuous optimum filter.

In the continuous case the relationship of the input x(t) and the output y(t) of a linear filter is given by the familiar convolution integral (figure 25)

$$y(t)=\int_{-\infty}^{\infty} h(\tau)x(t-\tau)\,d\tau \qquad (85)$$

If x(t) were as shown in figure 26-a then a sampled data version of x(t), call it $x_n(t)$, is shown in figure 26-b. Mathematically

$$x_n(t) = \sum_{0}^{\infty} x(nT)\,u_o(t-nT)$$

Likewise, if h(t) is the impulse response for the continuous filter, then

$$h_n(t) = \sum_0^\infty h(nT)\ u_o(t - nT) \tag{86}$$

is the impulse response of the sampled data filter. The problem then is to find the frequency domain expression for $h_n(t)$. If we consider (86) as being the product of function h(t) and a unit impulse train

$$\delta_T(nT) = \sum_0^\infty u_o(t - nT) \tag{87}$$

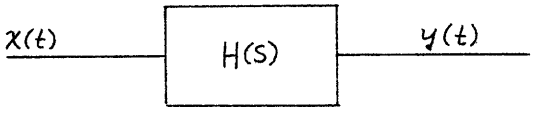

Figure 25

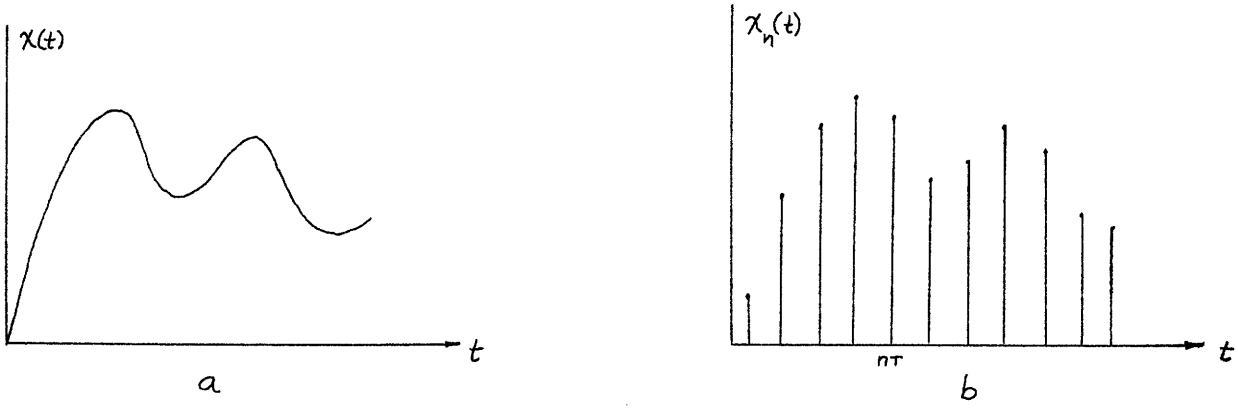

Figure 26

where, $L\{h(t)\} = H(s)$ (Laplace transform)

and

$$L\{\delta_T(nT)\} = L\sum_0^\infty u_o(t - nT) = \frac{1}{1 - e^{-sT}} \tag{88}$$

then

$$h_n(t) = h(t)\ \delta_T(nT) \tag{89}$$

or

$$H_n(s) = H(s) * \frac{1}{1 - e^{-sT}} \tag{90}$$

where the symbol * indicates the complex convolution operation. † Formally,

$$H_n(s) = \frac{1}{2\pi J}\int_{-j\infty}^{j\infty} H(p)\ \frac{1}{1 - e^{-T(s-p)}}\ dp\ . \tag{91}$$

If

$$\lim_{s\to\infty} H(s) = 0 \tag{92}$$

and H(s) has all its poles in the left half s plane, then

---

† Reference 15.

by applying the methods of contour integration where the contour encloses the entire left half plane, then

$$H_n(s) = \sum_{\text{poles of } H(p)} \text{Residues of} \left\{ H(p) \frac{1}{1 - e^{-T(s-p)}} \right\}. \quad (93)$$

If we define

$$z = e^{sT} \quad (94)$$

then we can rewrite (93) as

$$H(z) \equiv \sum_{\text{poles of } H(p)} \text{Residues of} \left\{ H(p) \frac{1}{1 - e^{-pT} z^{-1}} \right\} \quad (95)$$

Example 1

Find H(z) for,

$$H(s) = \frac{1}{s^2 + \sqrt{2}\, s + 1} . \quad (96)$$

Hence

$$H(p) = \frac{1}{(p + p_1)(p + p_2)} , \quad (97)$$

where

$$p_{1,2} = \frac{-\sqrt{2}}{2} [1 \pm J] \quad (98)$$

then

$$\text{RES}\left[H(p)\ \frac{1}{1 - e^{-pT}z^{-1}}\right]_{p=p_1} = \frac{-\frac{1}{\sqrt{2}}}{1 - e^{+\frac{\sqrt{2}}{2}(1+J)T}\ z^{-1}} \tag{99}$$

and

$$\text{RES}\left[H(p)\ \frac{1}{1 - e^{-pT}z^{-1}}\right]_{p=p_2} = \frac{+\frac{1}{\sqrt{2}}}{1 - e^{+\frac{\sqrt{2}}{2}(1-J)T}\ z^{-1}} \tag{100}$$

Summing (99) and (100) and combining the result gives the answer:

$$H(z) = \frac{\sqrt{2}\ e^{-\frac{\sqrt{2}}{2}T}\ \sin[(\sqrt{2}/2)T]\ z^{-1}}{1 - 2e^{-\frac{\sqrt{2}}{2}T}\ \cos[(\sqrt{2}/2)T]z^{-1} + e^{-\sqrt{2}\ T}\ z^{-2}} \tag{101}$$

The problem remains to interpret H(z) so that we may realize it on a digital computer. Consider H(z) to be the transfer function for a digital input X(z) and digital output Y(z),

$$H(z) = \frac{Y(z)}{X(z)} = \frac{P(z)}{Q(z)} \tag{102}$$

Cross multiplying (18) yields

$$Y(z)\ Q(z) = X(z)\ P(z) \quad ^{*} \tag{103}$$

By converting back into the time domain difference equations we can realize the filter on the digital computer. An example will serve well in demonstrating the technique.

Example 2

Using the system function in (101) we obtain

$$H(z) = \frac{Y(z)}{X(z)} = \frac{\sqrt{2}\ e^{-\frac{\sqrt{2}}{2}T} \sin\left[(\sqrt{2}/2)T\right]\ z^{-1}}{1 - 2e^{-\frac{\sqrt{2}}{2}T} \cos\left[(\sqrt{2}/2)T\right]\ z^{-1} + e^{-\sqrt{2}\ T}\ z^{-2}} \tag{104}$$

or

$$Y(z) = \left\{\sqrt{2}\ e^{-\frac{\sqrt{2}}{2}T} \sin\left[(\sqrt{2}/2)T\right]\right\}X(z)\ z^{-1}$$

$$+ \left\{2e^{-\frac{\sqrt{2}}{2}T} \cos\left[(\sqrt{2}/2)T\right]\right\}Y(z)\ z^{-1} - \left[e^{-\sqrt{2}\ T}\right]Y(z)\ z^{-2} \tag{105}$$

---

* Reference 16.

From transform theorems we know that, in general, if we multiply a function in the frequency domain by e^{-as}, then the time domain expression is delayed by "a" seconds. Likewise if

$$F(z) \iff f(t)$$

then

$$F(z)\ z^{\pm n} \iff f(t \pm nT) \tag{106}$$

Applying (106) to (105) yields

$$y(nT) = \{\sqrt{2}\ e^{-\frac{\sqrt{2}}{2}T} \sin [(\sqrt{2}/2)T]\}x(nT - T)$$

$$+ \{2e^{-\frac{\sqrt{2}}{2}T} \cos [(\sqrt{2}/2)T]\}\ y(nT - T) - e^{-\sqrt{2}\ T}\ y(nT - 2T) \tag{107}$$

Rewriting (107) yields

$$y(nT) = b_1x(nT - T) + b_2y(nT - T) - b_3y(nT - 2T) \tag{108}$$

where the b_i are obvious.

Equation (108) is immediately realizable in a block diagram representation that is compatible with the digital computer. See Figure 27.

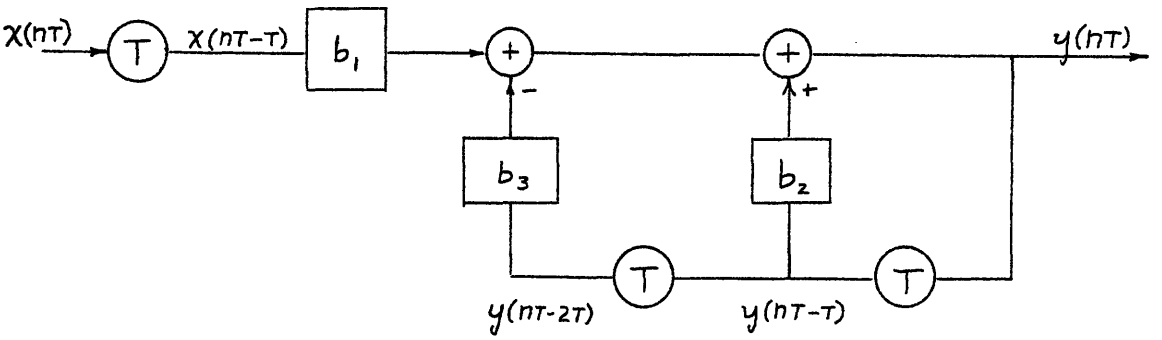

Figure 27

Digital model of H(s)

(Circles indicate a unit delay and squares indicate gains)

As a summary of this section we will outline the method. First, Wiener filtering yields a continuous filter H(s). Second, find the digital equivalent H(z) by using (95). Third, rewrite the transfer function as in equation (103). Finally convert (103) to the time domain and interpret the result as a block diagram. In the appendix we list some filters and their digital equivalents.

4.1.2 SAMPLED DATA MODEL OF MESSAGE a(t)

For our system a (nT) is to be a sample function from a zero mean Gaussian random process. In addition, it is to have a known spectral distribution and unit variance.

We will generate a(t) using the digital computer. In so doing we are automatically taking care of the requirement

that a(t) be converted to a sampled function, a(nT). It remains to give a(nT) the proper statistical and power characteristics.

For our first problem we will make a(nT) a zero mean Gaussian function. The IBM-7094 computer has in its library a random number generator the output of which has a uniform distribution between zero and one.

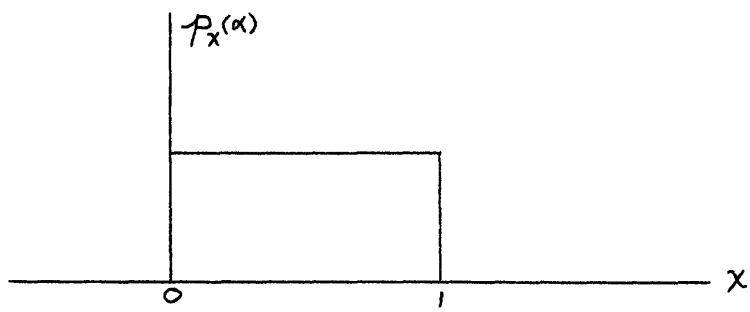

Figure 28

First let x_1 and x_2 be two independent variables from $p_x(x)$ and then define

$$\theta = 2\pi x_1 \tag{109}$$

$$z = \sqrt{-2 \text{ Log}(x_2)} \tag{110}$$

$$q_1 = z \sin \theta \tag{111}$$

$$q_2 = z \cos \theta \tag{112}$$

If the transformation (109) - (112) are correct, then g_1 and g_2 will be independent zero mean Gaussian random variables. To prove this, one needs only to show that, given g_1 and g_2, θ is a uniform distribution and $z = \sqrt{g_1^2 + g_2^2}$ is a Rayleigh distribution. Hence

$$\frac{g_1}{g_2} = \frac{z \sin \theta}{z \cos \theta} = \tan \theta$$

$$\theta = \tan^{-1} \frac{g_1}{g_2} \tag{113}$$

Davenport and Root[17] shows that (113) is a uniform distribution, and

$$z^2 = -2 \text{ Log } (x) \tag{114}$$

$$x = e^{-\frac{z^2}{2}} \tag{115}$$

$$P(z) = \left|\frac{dx}{dz}\right| P(x)\Big|_{x=z^{-1}} \tag{116}$$

Carrying out the indicated operation in (116) we obtain,

$$P(z) = (1)ze^{-\frac{z^2}{2}} . \tag{117}$$

Suppose, g_1 and g_2 were independent N(o,1); then if

$$z = \sqrt{g_1^2 + g_2^2} \quad \text{and} \quad P(g_i) = \frac{1}{\sqrt{2\pi}} e^{-\frac{g_i^2}{2}} \tag{118}$$

and we make a suitable change of variable to polar coordinates, then

$$P(z) = \int_0^{2\pi} z \frac{1}{2\pi} e^{-\frac{z^2}{2}} \, d\theta$$

$$P(z) = ze^{-\frac{z^2}{2}} \tag{119}$$

Since equation (117) and equation (119) are the same, then we can deduce that g_1 and g_2 are in fact independent zero mean Gaussian random variables. The transformations (109) - (112) are easily executed on the computer.

We have made our source Gaussian so the next problem is to mold the spectrum of a(nT) into one of our choice. First we will make a(nT) have a flat spectral distribution and then pass it through a filter of our choice to obtain the final message.

The variables g_1 and g_2 can be represented as in figure 29a. Each rectangle represents an independent Gaussian variable so that we may consider their statistical character easily. The letter T is the sampling rate. Since the variables have zero mean, then their

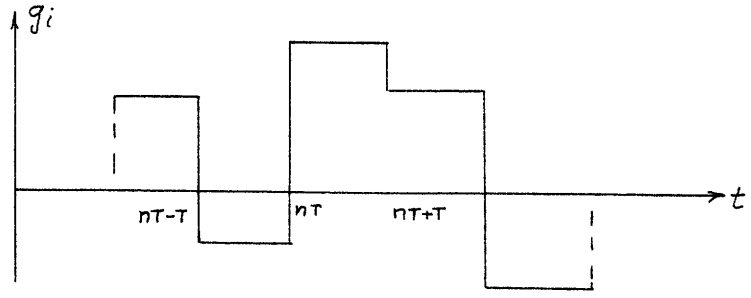

(a)

Independent Generated Variables, Gaussian Distributed

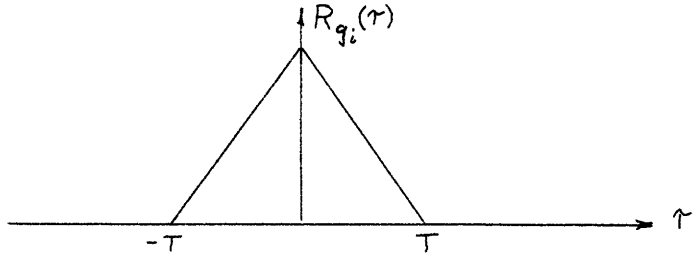

(b)

Correlation function of g_i

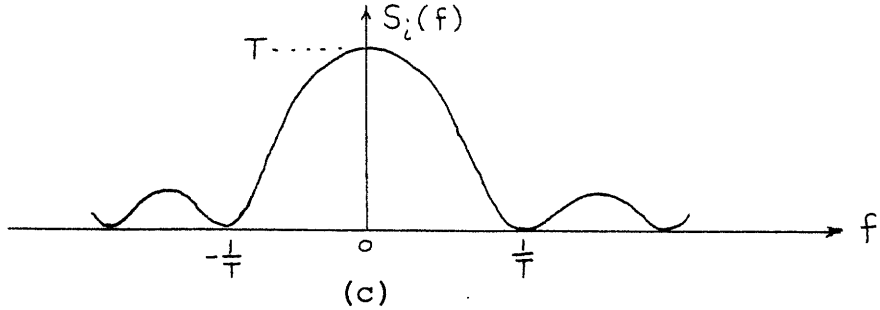

(c)

Power spectral density of g_i

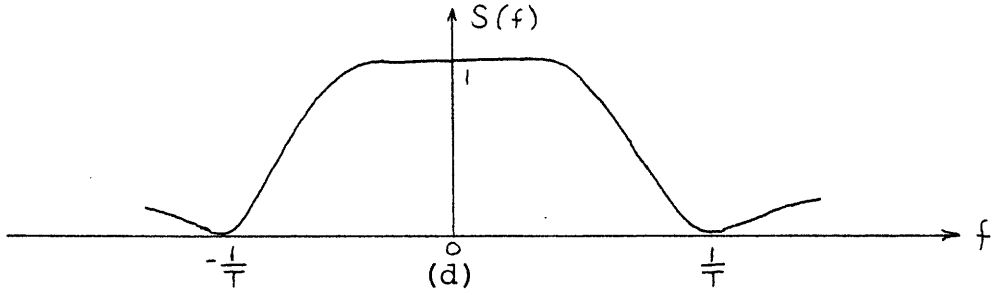

(d)

Normalized power spectrum of g_i

Figure 29

covariance function equals their correlation function. The correlation function for the process in 29a, is shown in 29b. We know that the power spectral density for a stationary random process is given by the Fourier transform of the correlation function. For completeness, by definition

$$S_i(\omega) = \int_{-\infty}^{\infty} R(\tau) e^{-J\omega\tau}\, d\tau, \quad \omega = 2\pi f \tag{120}$$

Carrying out the indicated operations yields

$$S(\omega) = T\,[\frac{\sin\ \omega T}{\omega T}]^2. \tag{121}$$

A sketch of $S_i(\omega)$ is shown in figure 29c. This spectrum still does not appear flat with unit height. If we pass g_i through a gain of $1/\sqrt{T}$ then we obtain the spectrum shown in figure 29d. Note that if we pass $S(\omega)$ through a filter whose highest frequency of interest, f_h, is much less than $f_m = 1/T$, then we can consider $S(\omega)$ flat with unit height. The point here is that the sampling rate T must be sufficiently small so that the approximations

$$f_h << f_m = \frac{1}{T} \tag{122}$$

and

$$S(\omega) = 1 \quad |f| < f_h \tag{123}$$

are valid.

In this thesis we will only consider the Butterworth family of messages given by

$$S_a(\omega:n) = \frac{\frac{2n}{K}\sin\frac{\pi}{2n}}{1 + (\frac{\omega}{K})^{2n}} \tag{124}$$

where K will be taken as unity for simplicity.

The above discussion is best summarized with an example:

Example 3

Suppose we wanted to generate the message

$$S_a(\omega:2) = \frac{2\sqrt{2}}{\omega^4 + 1} \tag{125}$$

$$S_a(\omega:2) = \frac{(\sqrt{2\sqrt{2}})(\sqrt{2\sqrt{2}})}{(-\omega^2 + \sqrt{2}\,j\omega + 1)(-\omega^2 - \sqrt{2}\,j\omega + 1)} \tag{126}$$

From transform theorems and $S(\omega) = 1$

$$S_a(\omega:2) = S(\omega)\,|H(\omega)|^2 \tag{127}$$

$$S_a(\omega:2) = |H(\omega)|^2 \tag{128}$$

$$S_a(\omega:2) = H(\omega)\,H^*(\omega) \tag{129}$$

$$H(\omega) = \frac{S_a(\omega:2)}{H^*(\omega)} = \frac{\sqrt{2\sqrt{2}}}{s^2 + 2s + 1} \tag{130}$$

Hence to generate $S_a(\omega:2)$ we have merely to pass the normalized version of g_1 through the filter given by (130). Naturally the filter $H(\omega)$ will be realized in the sampled data framework.

4.1.3 SAMPLED DATA MODEL OF NOISE n(t)

The last continuous system variable that we need to cast into the digital framework is the additive noise, n(t). In 4.1.2, when we were developing the Gaussian structure of the message, we were dealing with two independent Gaussian random variables. We need only to take the other variable and treat it as the additive, independent, zero mean, white Gaussian channel noise. All of the arguments that went into developing the message also hold for the noise. Instead of going through it all again only the significant results will be presented here.

We want the channel noise to be white with two sided spectral density of $N_o/2$. Hence the normalizing factor for g_2 will be $\sqrt{N_o/2T}$ so we get the result shown in figure 30. Once again the approximation (122) must be maintained to insure

$$S_n(\omega) = \frac{N_o}{2} \quad |f| < f_h \tag{131}$$

where f_h is the highest message frequency of interest.

We will not use a filter on the noise source because the loop filter will take care of the out-of-band noise.

4.2 OPTIMUM F.M. DEMODULATOR, DIGITAL MODEL

By applying the results of section 4.1 to the continuous F.M. system shown in figure 24, we can obtain the equivalent digital model shown in figure 31.

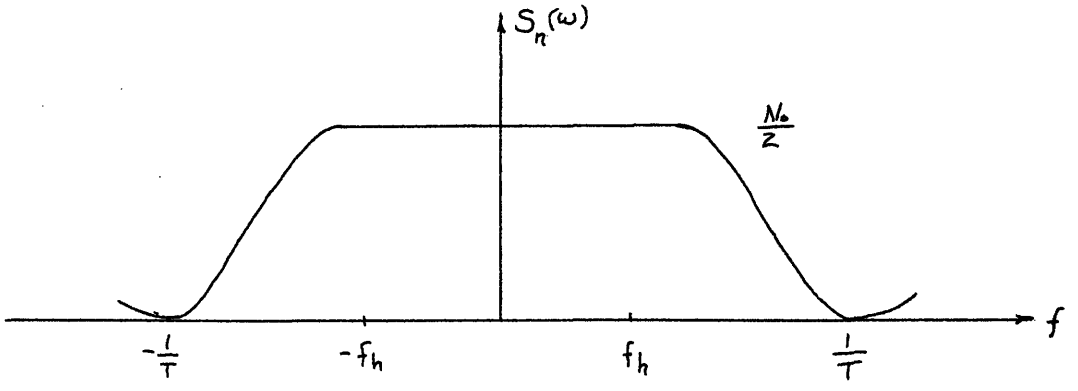

Figure 30

Additive "white" channel noise spectrum

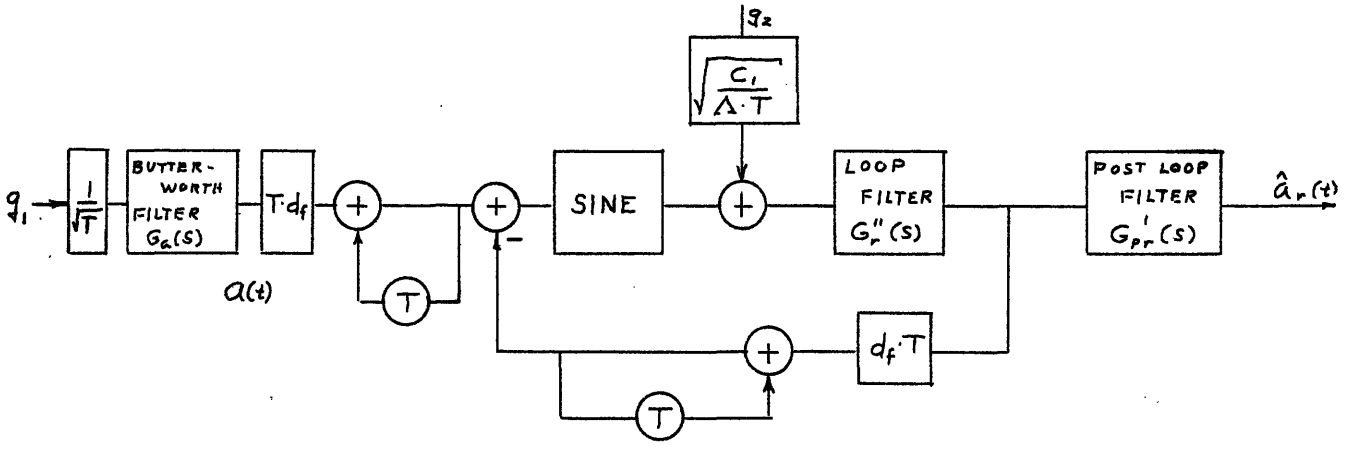

Figure 31

Digital model of F.M. demodulator

Even though the message and the noise are in digital form we will still define them as a(t) and n(t) respectively and leave their digital nature implied. When the three filters are expressed in their appropriate digital form, then figure 31 is the complete digital model of the demodulator. The system is now ready to be simulated on the digital computer.

Let us divert from the complete model for a moment and concentrate on the two integrators in figure 31. Note the presence of the "T" in the gain term for the integrators. Intuitively it is clear that the "T" is necessary. Mathematically the presence of the "T" is difficult to justify but it has been done by Papoulis.[18] The "T" factor must premultiply all filters that are expressible as ratios of polynomials in the frequency domain and whose numerators are at least one degree less than the denominator. For filters with equal powers in the numerator and in the denominator we are required to divide them out so that the numerator is one power less. The "T" term is then to be placed in the remainder term.

Example 4

$$H(s) = \frac{s + 3}{s + 1} = 1 + \frac{2}{s + 1} \quad \text{[see figure 32]} \quad (132)$$

Now we can revert back to the complete digital receiver. In the simulation we compute the phase error

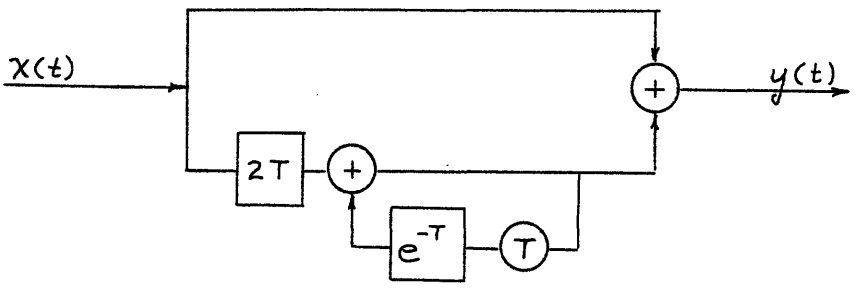

Figure 32

Realization of H(s)

variance and the mean square demodulation variance as it was explained in chapter 3, section 3.1.

$$\sigma_f^2 = \text{VAR}\,[a(t) - \hat{a}(t)] \tag{133}$$

and

$$\sigma_x^2 = \text{VAR}\,[x(t) - \hat{x}(t)] \tag{134}$$

For the sampled data model, (133) and (134) can be written as:

$$\sigma_f^2 = \frac{1}{M} \sum_{i=1}^{M} [a(t) - \hat{a}_r(t)]^2 \tag{135}$$

$$\sigma_x^2 = \frac{1}{M} \sum_{i=1}^{M} [x(t) - \hat{x}_r(t)]^2 \tag{136}$$

where M is the total number of Gaussian random numbers put into the system. Clearly, the greater we made M, the more confidence we have in the resultant. Also, if we make N independent runs with M numbers in each run, then *

$$\sigma_{fN}^2 = \frac{\sigma_f^2}{N} \tag{137}$$

In other words the variance of the mean square error variance, σ_{fN}^2, decreases linearly with the number of runs. Ideally, then for our system we want to make M and N as large as possible. Computer availability precludes this ideal situation so we have to compromise between the length of a run and an acceptable confidence level. After one performs a few simulations he gets a feeling for the length of time it takes for the system to reach a statistical steady state. In the next section, we have an example that demonstrates the length of time that it takes for a typical system to reach steady state.

4.3 SIMULATION RESULTS AND DISCUSSION

Optimum receivers for the first and second order Butterworth messages were simulated on the digital computer. Also, a second order receiver was used to demodulate a fifth order message. For the latter simulation

---

* References 17 and 19.

the system was sub-optimum so that only limited conclusions may be drawn from the results.

Performance curves for the first order case are shown in figures 33 and 34.* Referring to figure 31, the appropriate filters for the first order message are

$$G_a(s) = \frac{2}{s + 1} \tag{138}$$

$$G_r''(s) = \frac{(\gamma - 1)s + \delta}{s(s + 1)} \tag{139}$$

$$G_{pr}'(s) = \frac{\delta - \gamma + 1}{(\gamma - 1)s + \delta} \tag{140}$$

where

$$\delta^2 = d_f{}^2 \Lambda \ , \quad \Lambda = \frac{4P}{KN_o}$$

$$\gamma = \sqrt{2\delta + 1}, \ K = 1$$

In figure 33 we see that the nonlinearity enters into the system performance when the mean square phase error is approximately 0.5 radian^2. Note how nicely the simulation reveals the performance characteristics below threshold. That portion of the curves would be nearly impossible to plot using any other method except the actual laboratory experimental situation. Figure 34 shows how the loop performed in estimating x(t). This plot is made modulo-2π.

* Zaorski[20] did a similar simulation.

Performance curves for the second order case are shown in figures 35 and 36. The Wiener filters for this case are described by

$$G_a(s) = \frac{\sqrt{2\sqrt{2}}}{s^2 + \sqrt{2}\, s + 1} \tag{141}$$

$$G_r''(s) = \frac{M}{d_f} \frac{s^2 + Ls + N}{s^2 + \sqrt{2}\, s + 1} \tag{142}$$

$$G_{pr}'(s) = \frac{1}{M} \frac{\tau_2 s + \tau_3}{s^2 + Ls + N} \tag{143}$$

where

$$M = 2\gamma^{\frac{1}{6}} - \sqrt{2} \qquad \tau_2 = 2\gamma^{\frac{1}{3}} - 2\sqrt{2}\, \gamma^{\frac{1}{6}} + 1$$

$$L = \frac{2\gamma^{\frac{1}{3}} - 1}{M} \qquad \tau_3 = \gamma^{\frac{1}{2}} - 2\gamma^{\frac{1}{6}} + \sqrt{2}$$

$$N = \frac{\gamma^{\frac{1}{2}}}{M} \qquad \gamma = d_f^{\,2}\, \Lambda$$

$$K = 1 \qquad \Lambda = \frac{4\sqrt{2}\, P}{KN_o}$$

Figure 35 shows the mean square demodulation performance. Notice for this case that the linear region performance is about an order of magnitude better than for the one pole case. Also, the threshold for the corresponding curves for a given d_f has measurably improved for the second order case.

For this second order case the threshold occurs very roughly at a phase error variance of 0.2 radians^2. It appears that the σ_x^2 at threshold might be an inverse function of d_f.

The fifth order simulation is shown in figure 37. For this case we put a fifth order message into a second order system. Hence these are sub-optimum performance curves.

For all of the above simulations a sampling rate of .002 seconds was used. This value of T was at least twenty times faster than any of the time constants encountered in the above systems. Also, .002 seconds is about 500 times faster than the message correlation time so that the spectrum input to the message generation filter surely looked flat.

In the last few paragraphs of section 4.3 we considered the characteristics of the variance of the mean square error variance. In the simulation results this parameter manifests itself clearly. Figure 37.1 is an example showing how the mean square error variance varies with the length of the simulation. Observe that the variance settles down after an initial transient condition. This demonstrates clearly that $\sigma_{fN}^2 \to 0$ as $N \to \infty$ (σ_{fN}^2 is the variance of mean square error variance). These

particular data were taken from a system operating below threshold. Much smaller transients occur when the system is above threshold

Often in commercial systems, bandwidth occupancy is an important consideration because of bandwidth constraints put on the system. In the analysis of this chapter we have implicitly assumed that we have sufficient bandwidth in the transmission media to accomodate the frequency modulated signal for all values of d_f. This tacit assumption may have given us biased conclusions in comparing the one pole case and the two pole case. For example, we concluded that the linear region performance of the two pole case was approximately an order of magnitude better than that of the one pole case. We did not, however, investigate the possibility that perhaps the two pole message occupied more bandwidth than the one pole case.

In the sequel we will not consider bandwidth as a system constraint and thus will not pursue this question any further. Hence, our performance criterion will be restricted to unconstrained linear region performance and threshold levels.

The results of this chapter will be further examined in chapter seven when we have all of the analytical and simulating data at our disposal.

Experimental Performance for Figure 24

One Pole Message

First Order Phase-Locked Loop

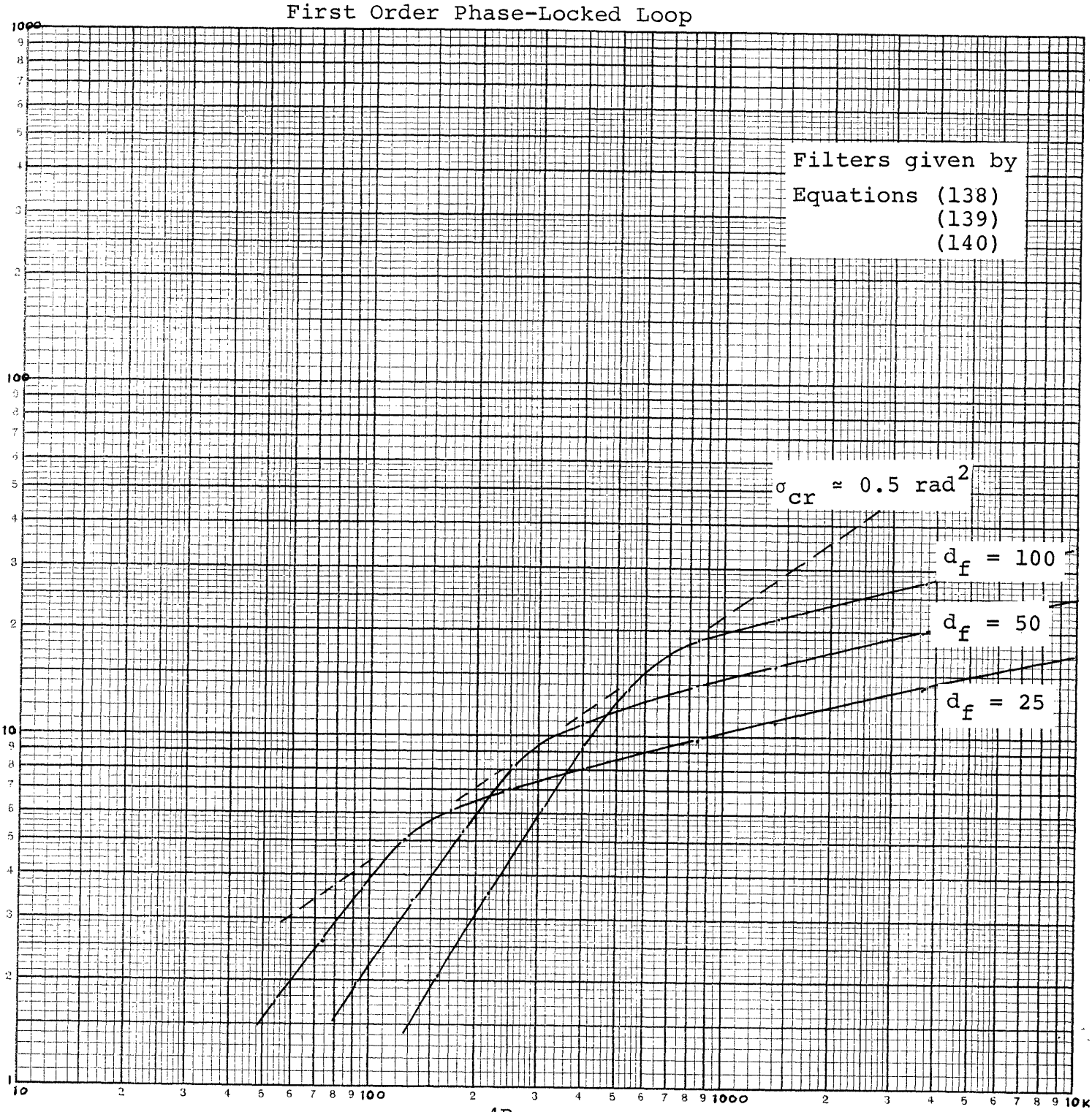

Figure 33

Experimental Performance for Figure 24

One Pole Message

First Order Phase-Locked Loop

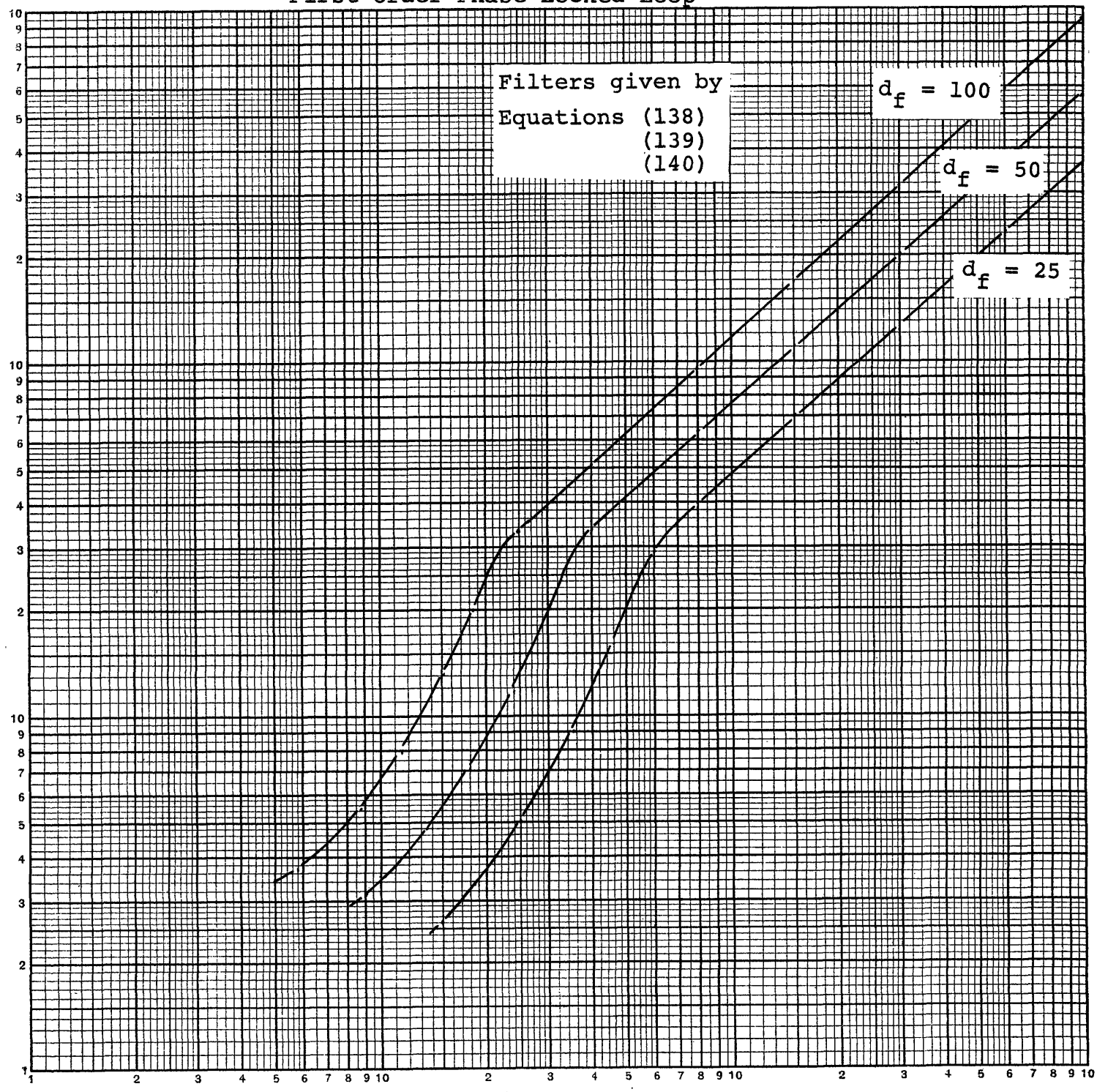

Figure 34

Experimental Performance for Figure 24

Two Pole Message

Second Order Phase-Locked Loop

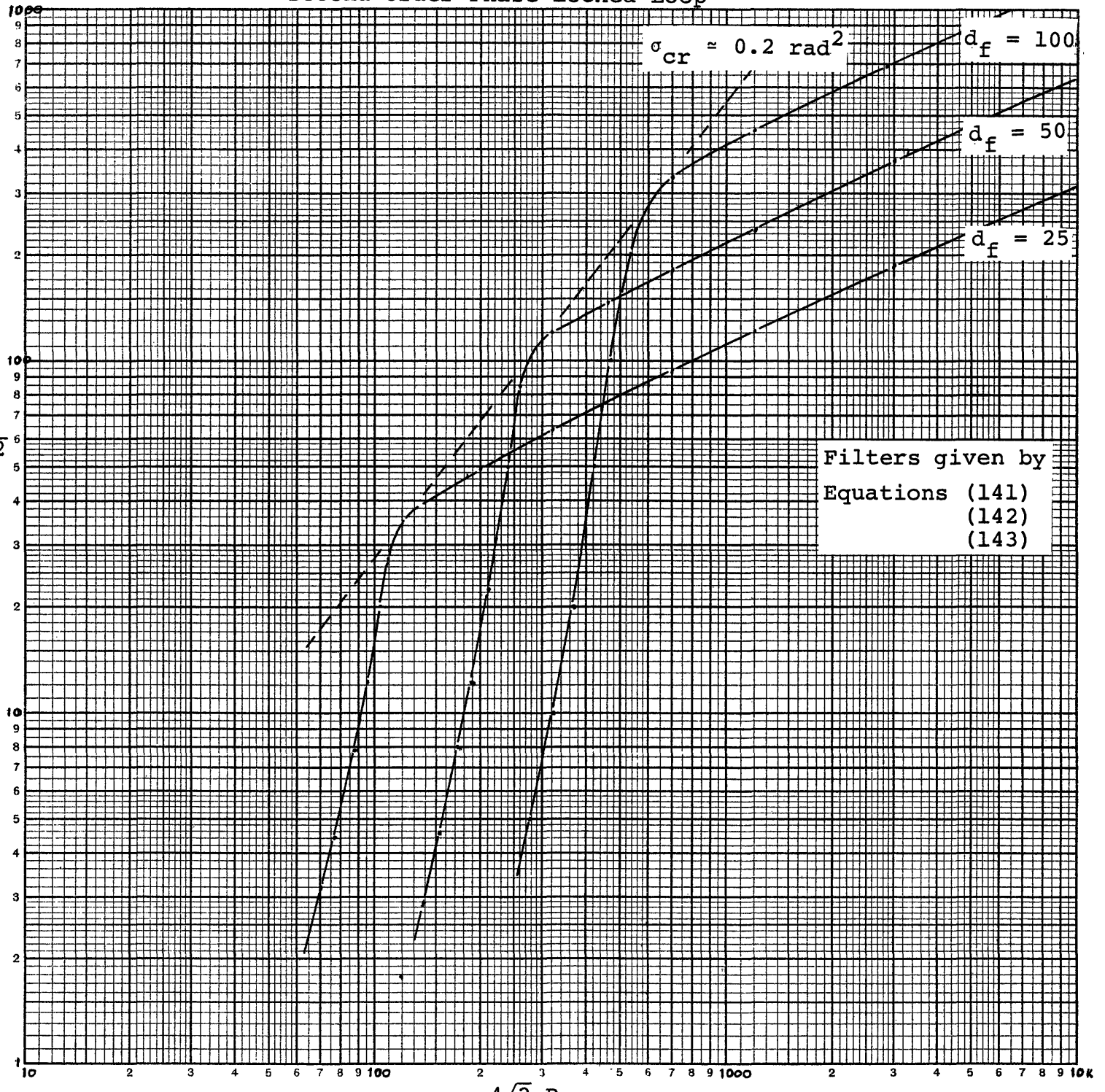

Figure 35

Experimental Performance for Figure 24

Two Pole Message

Second Order Phase-Locked Loop

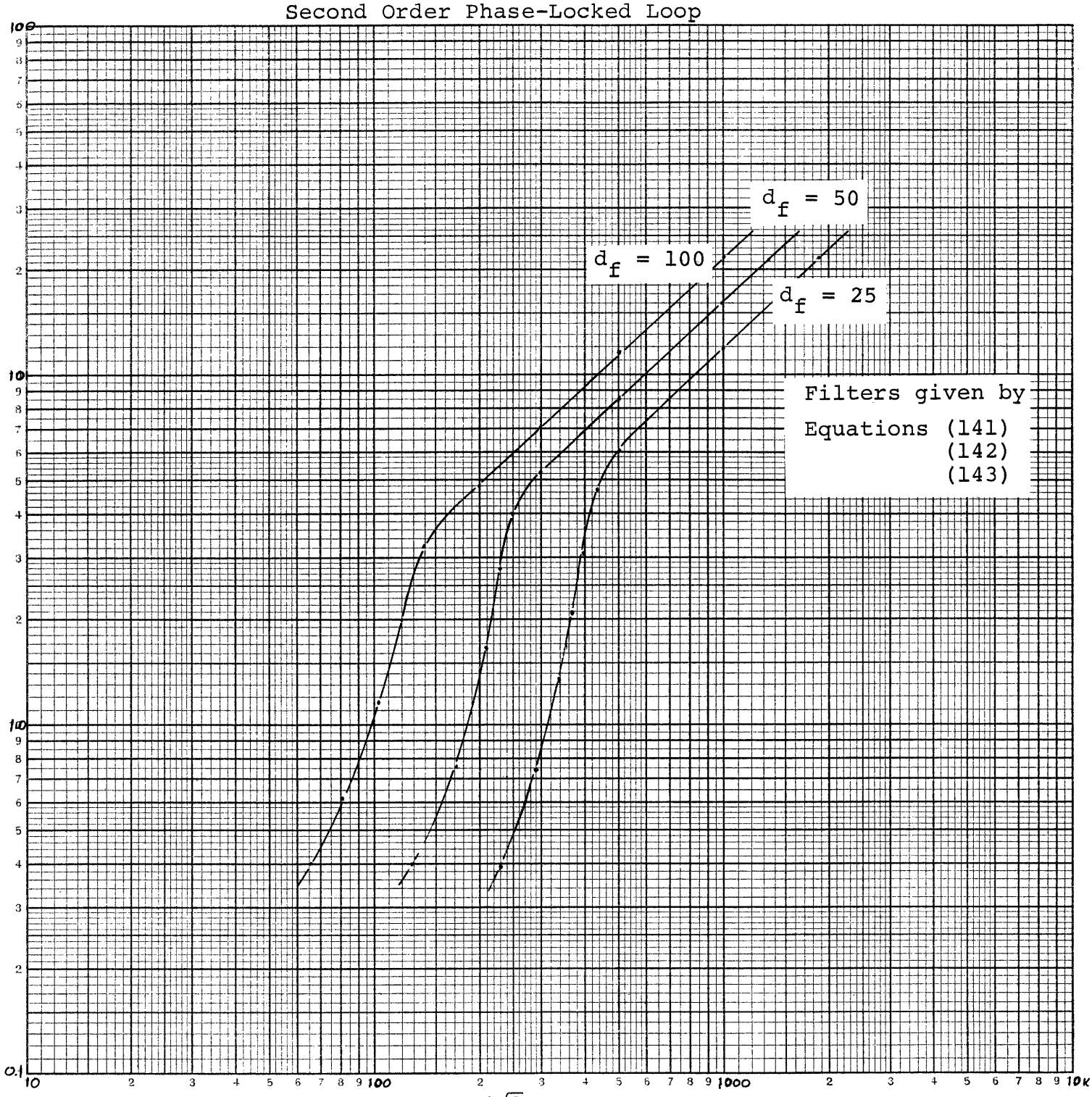

Figure 36

Experimental Performance for Figure 24

Five Pole Message

Second order phase-locked loop

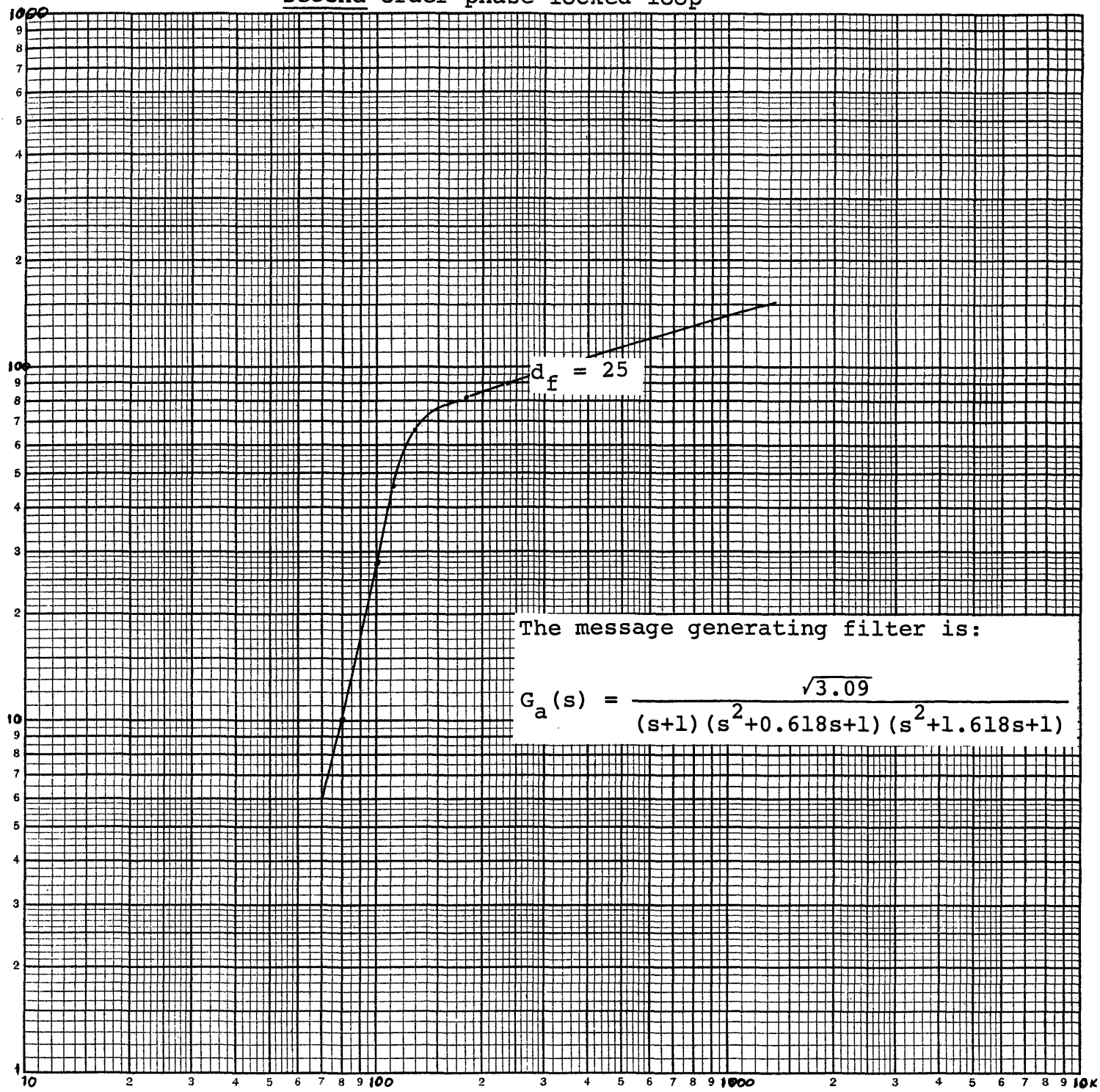

Figure 37

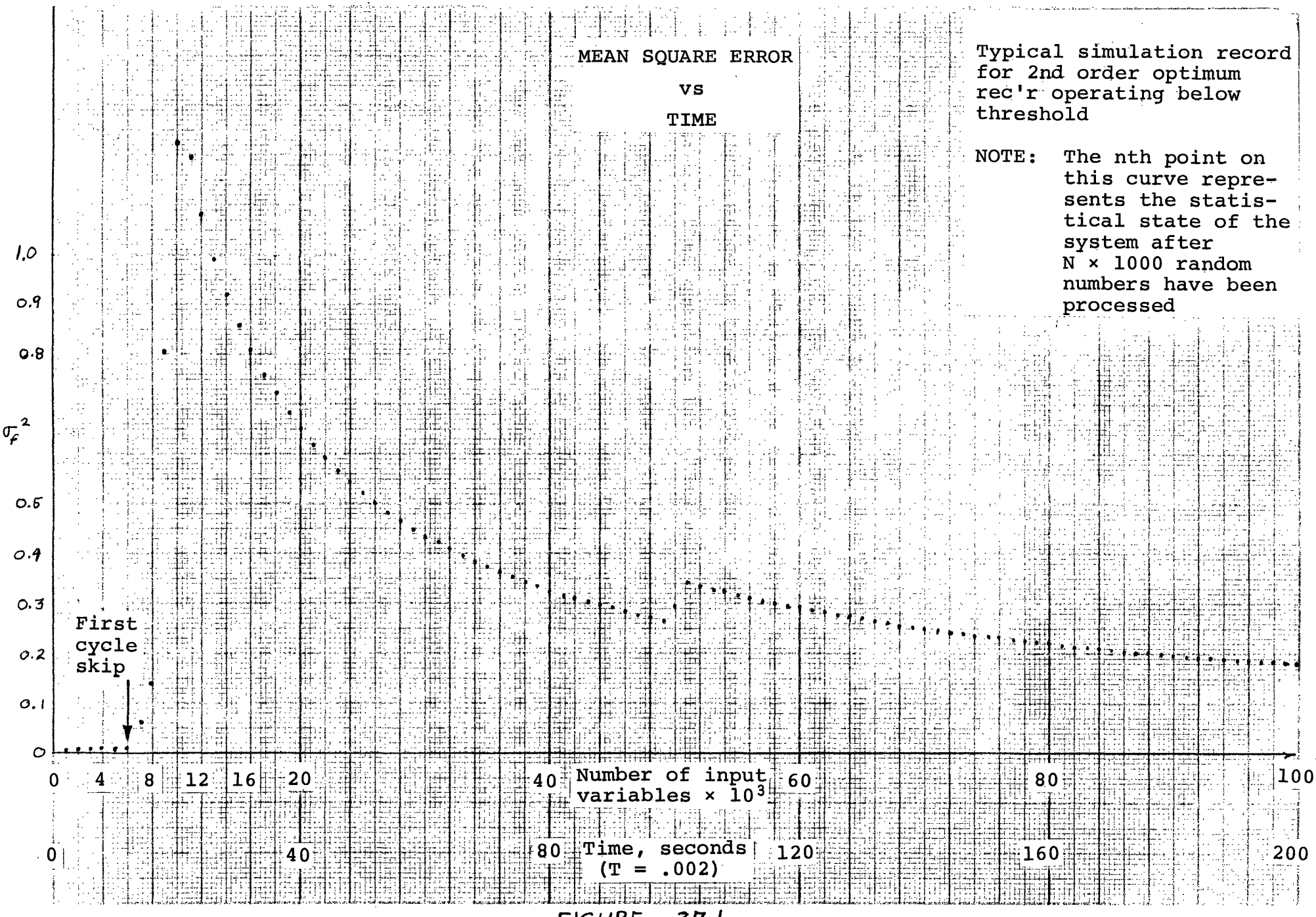
MEAN SQUARE ERROR
vs
TIME
Typical simulation record for 2nd order optimum rec'r operating below threshold
NOTE: The nth point on this curve represents the statistical state of the system after N × 1000 random numbers have been processed
1.0
0.9
0.8
σ_f^2
0.5
0.4
0.3
0.2
0.1
0
First cycle skip
0 4 8 12 16 20 40 60 80 100
Number of input variables × 10^3
0 40 80 120 160 200
Time, seconds (T = .002)

FIGURE 37.1

CHAPTER 5

CONVENTIONAL DEMODULATOR—THEORETICAL ANALYSIS

5.0 INTRODUCTION

It is the stated purpose of this thesis to investigate the performance of the optimum phase locked loop demodulator. In the foregoing chapters we have displayed the optimum system performance in detail but we have left one question unanswered. That question is: "How well does the optimum receiver perform?" To answer this question we must have a frame of reference. We will use the performance of a conventional demodulator as a reference for the performance of the optimum phase locked loop demodulator. Before we plunge into the analysis of the conventional system a brief qualitative description of the system seems appropriate for the sake of completeness.

An idealized conventional receiver is shown in figure 38. The received signal is first passed through a rectangular unit gain filter $H_1(s)$ centered on the transmitter carrier frequency ω_o. The signal is then heterodyned into the intermediate frequency filter $H_2(s)$, which is also rectangular

with unit gain. Both filters $H_1(s)$ and $H_2(s)$ are presumed to have bandwidths wide enough so that they create only a negligible amount of distortion in the transmitted message. The purpose of the filters is to reduce the out of band noise thus keeping the signal to noise ratio at the input to the discriminator as high as possible. Frequency demodulation takes place in the discriminator, which is a non-linear device that responds only to variations in instantaneous frequency. We model the device by saying that whenever the input to the device is

$$x(t) = b(t) \cos [\omega t + \phi(t)] \tag{144}$$

the output is

$$y(t) = \frac{d}{dt} [\phi(t)] \tag{145}$$

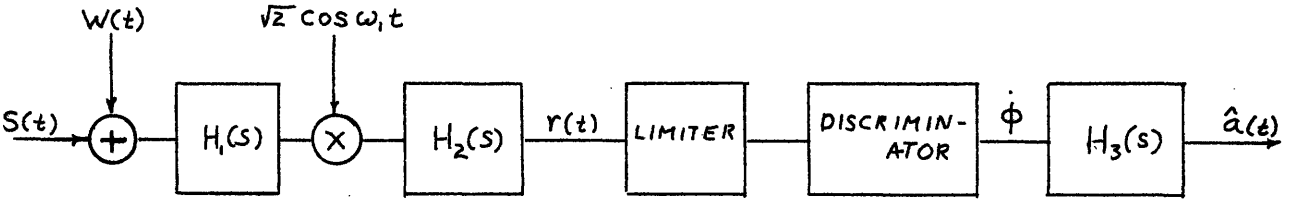

$$S(t) = \sqrt{2P} \cos [\omega_o t + d_f \int_{-\infty}^{t} a(u)du] \tag{146}$$

W(t) = white Gaussian additive channel noise

Figure 38

Idealized Conventional F.M. Receiver

As it turns out in an actual system the discriminator is moderately sensitive to amplitude variations so it is necessary to include a limiter to clip off the amplitude variations.

The final stage in our system is a filter $H_3(s)$ which is designed to eliminate noise outside the message a(t) band. In many physical systems $H_3(s)$ is merely an RC filter. In our system $H_3(s)$ will be the optimum Wiener filter. Since we are ultimately going to compare the phase locked loop with this conventional system, we want this conventional system to be the best one possible so that we don't derive false conclusions about the comparative performance.

In this chapter we will theoretically establish the performance of a conventional receiver. In the next chapter we will verify the validity of these results using simulation techniques.

5.1 CONVENTIONAL F.M. RECEIVER ANALYSIS—THEORETICAL

Consider the received signal r(t) that is shown in figure 38,

$$r(t) = \sqrt{2P} \cos \left[\omega_c t + d_f \int_{-\infty}^{t} a(u)du\right] + n(t). \qquad (147)$$

The amplitude $\sqrt{2P}$ and the carrier frequency are constants and n(t) is a narrow band Gaussian noise whose power spectrum is $N_o/2$. a(t) is the message that we are trying to decipher and for our purpose a(t) will be of the Butterworth family. The noise n(t) is the filtered version of the white channel noise and is independent of the message a(t). We can write n(t) in its in-phase and quadrature components as

$$n(t) = \sqrt{2}n_c(t) \cos \omega_c t - \sqrt{2}n_s(t) \sin \omega_c t \qquad (148)$$

Hence (147) becomes,

$$r(t) = [\sqrt{2P} + \sqrt{2}\, n_c(t)] \cos [\omega_c t + d_f \int_{-\infty}^{t} a(u)du] - \sqrt{2}\, n_s(t) \sin \omega_c t \qquad (149)$$

$$r(t) = R(t) \cos [\omega_c t + d_f \int_{-\infty}^{t} a(u)du + \theta] \qquad (150)$$

where

$$\theta = \tan^{-1} \frac{\sqrt{2}\, n_s(t)}{\sqrt{2P} + \sqrt{2}\, n_c(t)} \qquad (151)$$

when the input carrier to noise power ratio is large, $n_c(t)$ and $n_s(t)$ are much smaller than $\sqrt{2P}$ most of the time, then

$$\theta(t) \simeq \frac{n_s(t)}{\sqrt{P}} \qquad (152)$$

Hence, most of the time

$$r(t) \simeq R(t) \cos \left[\omega_c t + d_f \int_{-\infty}^{t} a(u)du + \frac{n_s(t)}{\sqrt{P}}\right] \tag{153}$$

is the input to the discriminator. The discriminator output, as stated before is the instantaneous frequency of r(t)

$$\dot{\phi}(t) = d_f\, a(t) + \frac{\dot{n}_s(t)}{\sqrt{P}} \tag{154}$$

In the frequency domain the power spectrum of (154) is,

$$\dot{\Phi}(\omega) = d_f{}^2 S_a(\omega) + N_o(\omega) \tag{155}$$

$$\dot{\Phi}(\omega) = d_f{}^2 S_a(\omega) + \omega^2 \frac{N_o}{2P} \tag{156}$$

A graphical description of how the noise enters into our problem is shown in figure 39.

Equation (156) is the power spectrum of the output of the discriminator. This is the spectrum that must be filtered. If we consider the first and second order Butterworth messages, the appropriate zero delay Wiener filters can then be determined. The spectra and the associated filters are given in table 5-1.

$S_a(\omega)$	$H_3(s)$	Constants
$\frac{2}{\omega^2 + 1}$	$\frac{A}{s^2 + \gamma s + \alpha}$	$A = \frac{\alpha^2}{1 + \alpha + \gamma}$ $\alpha^2 = d_f^2 \Lambda$ $\gamma = \sqrt{2\alpha + 1}$ $\Lambda = \frac{4P}{N_o}$
$\frac{2\sqrt{2}}{\omega^4 + 1}$	$\frac{\alpha_1 s + \alpha_2}{[s + \gamma^{\frac{1}{6}}][s^2 + \gamma^{\frac{1}{6}} s + \gamma^{\frac{1}{3}}]}$	$\gamma = d_f^2 \Lambda$ $\alpha_1 = 2\gamma^{\frac{1}{3}} - 2\sqrt{2}\ \gamma^{\frac{1}{6}} + 1$ $\alpha_2 = \gamma^{\frac{1}{2}} - 2\gamma^{\frac{1}{6}} + \sqrt{2}$ $\Lambda = \frac{4\sqrt{2}\ P}{N_o}$

Table 5-1

Post Discriminator Filters

The problem remains to compute the mean square demodulation error,

$$\sigma_f^2 = \text{VAR}\ [a(t) - \hat{a}(t)] \tag{157}$$

where $a(t)$ is the delivered message and $\hat{a}(t)$ is the estimate of the message at the output of the Wiener filter. Again,

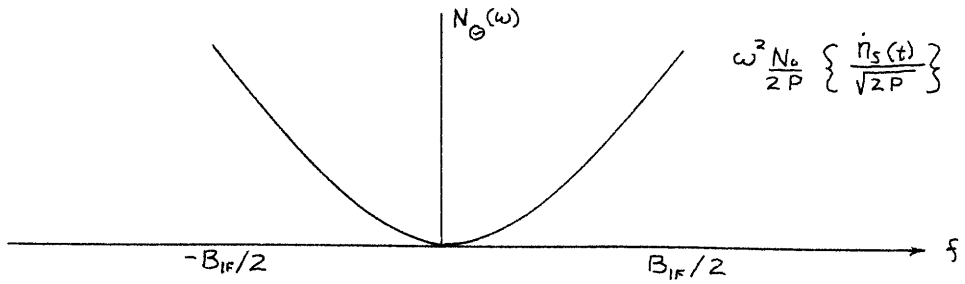

Discriminator output noise spectrum
39-d

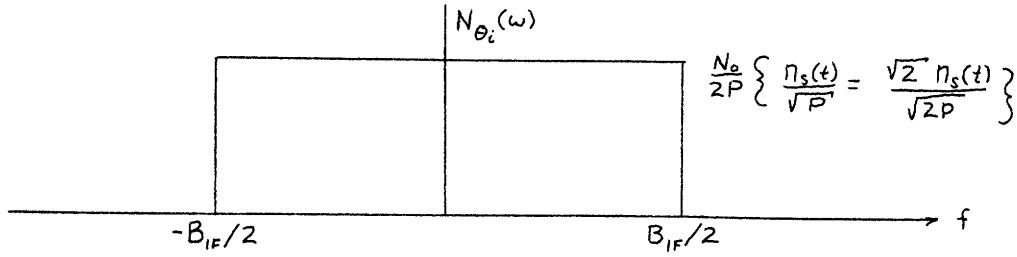

Normalized noise spectrum (input)
39-c

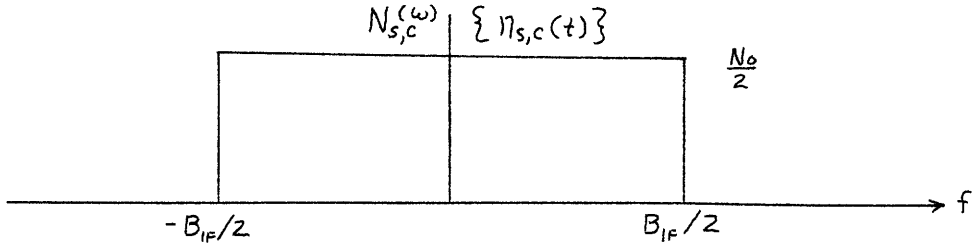

Noise component spectra (input)
39-b

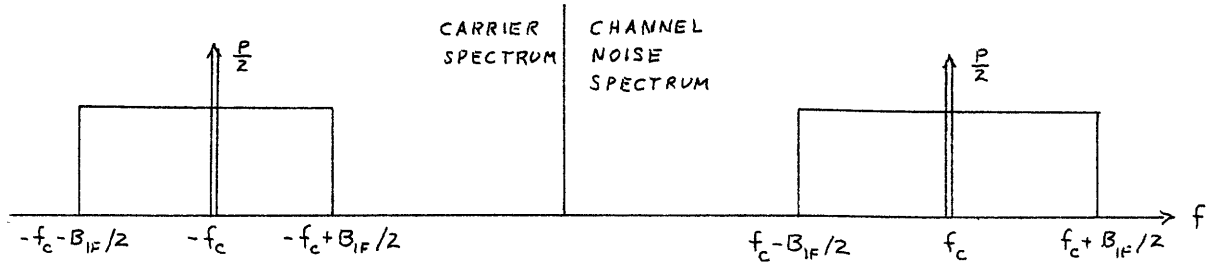

Two sided channel noise of spectral height $\{N_o/2\}n(t)$
39-a

Figure 39

White Noise in Conventional Receiver

$$\sigma_f^2 = \int_{-\infty}^{\infty} \{S_a(\omega)|1 - H_3(\omega)|^2 + N_\theta(\omega)|H_3(\omega)|^2\}\frac{d\omega}{2\pi} \qquad (158)$$

is the appropriate equation for the mean square error. If we proceed to apply (158) to the terms in equation (156) and table 5-1, we will obtain a straight line performance curve. Obviously this could not represent the true performance of a conventional receiver because we know for low SNR the system should become nonlinear and exhibit a threshold. The problem with the above development is that it does not take into account the system nonlinearly. The source of our error is in the approximations (152). There we assumed that the received carrier power was much greater than the received noise power.

Rice[21] conjectured that the discriminator output noise spectrum was not just one term but two terms and is given by

$$N_\theta(\omega) = \{4\pi^2[N_+ + N_-] + \omega^2 \frac{N_o}{2P}\} \qquad (159)$$

Here N_+ and N_- are the expected number of times per second that the discriminator input noise phase increases and decreases by an odd multiple of π radians respectively.

Lawton[22] applied Rice's ideas to the case of a zero mean Gaussian modulating signal. Some of Lawton's results will be presented here. For the Gaussian message,

$$N_+ = \frac{1}{\sqrt{\pi}} \frac{B_{IF}}{\sqrt{12}} \int_{\sqrt{\rho}}^{\infty} e^{-u} \sqrt{1 + 2au^2}\, du \tag{160}$$

where ρ is the carrier to noise power ratios in the IF bandwidth at the discriminator input (see figure 39-a)

$$\rho = \frac{\frac{P}{2} + \frac{P}{2}}{\frac{N_o}{2} B_{IF} + \frac{N_o}{2} B_{IF}} = \frac{P}{N_o B_{IF}} \tag{161}$$

and

$$a = d_f^2 \frac{3[\text{power in } a(t)]}{\pi^2 B_{IF}^2} \tag{162}$$

and

B_{IF} is the IF bandwidth expressed in Hertz.

Carrying out the indicated operations in (160), we obtain,

$$N_+ = \frac{1}{4\pi\sqrt{\pi}} \sqrt{2}\ d_f e^{-\rho} \sqrt{1 + \frac{1}{3} \frac{(\frac{B_{IF}\pi}{\sqrt{2}\, d_f})^2}{\rho}} \tag{163}$$

Since we are dealing with a random process we may assume $N_+ = N_-$ and proceed to find an expression for (159). That is

$$N_\theta(\omega) \simeq \frac{N_o}{2P} \{\psi^2 + \omega^2\} \tag{164}$$

$$\psi^2 = \left(\frac{4P}{N_o}\right)\sqrt{2\pi}\, d_f e^{-\frac{P}{N_o B_{IF}}} \sqrt{1 + \frac{2}{3}\frac{B_{IF}^3 \pi^2}{d_f^2 \left(\frac{4P}{N_o}\right)}} \qquad (165)$$

Note that (165) diminishes rapidly for large $P/N_o B_{IF}$ and thus yields our previous noise term $N_o\omega^2/2P$. Now we can calculate the mean square error for our system with a degree of confidence. Proceeding with (158) * for the one pole Butterworth and using table 5-1 and (164) we obtain,

$$\frac{1}{\sigma_f^2} = \frac{1 + \alpha + \gamma}{1 - \frac{\alpha^2(2\gamma - 1)(\gamma + 1) - (\gamma - 2)\alpha^3}{\gamma(1 + \alpha + \gamma)^2} + \frac{\alpha\psi^2}{(1 + \alpha + \gamma)}} \qquad (166)$$

where in this case

$$\Lambda = \frac{4P}{N_o}$$

and

$$\psi^2 = \Lambda\sqrt{2\pi}\, d_f e^{-\frac{\Lambda}{4B_{IF}}} \sqrt{1 + \frac{2}{3}\frac{B_{IF}^3 \pi^2}{d_f^2 \Lambda}} \qquad (167)$$

For the two pole Butterworth case

$$\frac{1}{\sigma_f^2} = \frac{1}{2\sqrt{2}\, I_5 + \frac{2\sqrt{2}}{\gamma} I_3} \qquad (168)$$

---

* Newton, Gould & Kaiser Integral Tables, Reference 12.

where

a) $$I_3 = \frac{[2\alpha_1^2\gamma^{\frac{5}{6}} + \alpha_2^2\gamma^{\frac{1}{2}}] + \psi^2[\alpha_1^2\gamma^{\frac{1}{2}} + 2\alpha_2^2\gamma^{\frac{1}{6}}]}{6\gamma}$$

b) $$I_5 = \frac{1}{2\Delta_5}\{m_1 + 2\alpha_1 m_2 + [(2\gamma^{\frac{1}{3}} - \alpha_1)^2 - 4\gamma^{\frac{1}{6}}(\gamma^{\frac{1}{2}} - \alpha_2)]m_3 + (\gamma^{\frac{1}{2}} - \alpha_2)^2 m_4\}$$

c) $$\alpha_1 = 2\gamma^{\frac{1}{3}} - 2\sqrt{2}\ \gamma^{\frac{1}{6}} + 1$$

d) $$\alpha_2 = \gamma^{\frac{1}{6}} - 2\gamma^{\frac{1}{6}} + \sqrt{2}$$

e) $$\alpha_3 = 2\gamma^{\frac{1}{6}} + \sqrt{2}$$

f) $$\alpha_4 = 2\gamma^{\frac{1}{3}} + 2\sqrt{2}\ \gamma^{\frac{1}{6}} + 1$$

g) $$\alpha_5 = \gamma^{\frac{1}{2}} + 2\sqrt{2}\ \gamma^{\frac{1}{3}} + 2\gamma^{\frac{1}{6}}$$

h) $$\alpha_6 = \sqrt{2}\ \gamma^{\frac{1}{2}} + 2\gamma^{\frac{1}{2}}$$

i) $$m_1 = -\gamma^{\frac{1}{2}}\alpha_4 + \alpha_5\alpha_6$$

j) $$m_2 = -\gamma^{\frac{1}{2}} + \alpha_3\alpha_6$$

k) $$m_3 = (\alpha_5 m_2 - \alpha_3 m_1)/\gamma^{\frac{1}{2}}$$

l) $$m_4 = (\alpha_5 m_3 - \alpha_3 m_2)/\gamma^{\frac{1}{2}}$$

m) $$\Delta_5 = \gamma^{\frac{1}{2}}(\alpha_6 m_4 - \alpha_4 m_3 + m_2)$$

and,

$$\Lambda = \frac{4\sqrt{2}\ P}{N_o} \tag{169}$$

and

$$\psi^2 = \sqrt{\pi}\ \Lambda d_f e^{-\frac{\Lambda}{4\sqrt{2}\ B_{IF}}} \Big/ \sqrt{1 + \frac{2\sqrt{2}}{3}\frac{B_{IF}^{\ 3}\pi^2}{d_f^{\ 2}\ \Lambda}} \tag{170}$$

The performance curves associated with equations (166) and (168) are plotted in the next section.

5.2 CONVENTIONAL RECEIVER THEORETICAL RESULTS AND DISCUSSION

Figure 40 shows the theoretical performance of the conventional receiver when the first order Butterworth function is the message. These curves do exhibit a threshold and except for location, the general shape seems to be consistent with the theoretical curve-sets for the phase-locked loop case. Notice in the conventional case that in the linear region, the curves conform exactly with the phase-locked loop case. Hence preliminary observations indicate that if the phase-locked loop is to perform better, then it must give improved threshold occurrence (i.e. threshold should occur at lower SNR). These conventional receiver curves were obtained by plotting equation (166).

Figure 41 is the theoretical conventional receiver performance for the second order Butterworth case. For

this case the performance in the linear region is more than an order of magnitude better than the one pole case. Observe, however, that the threshold occurrence has degraded from the one pole case. This is an important difference from the phase-locked loop case where the threshold performance improved for the higher order system. These second order curves were obtained by plotting equation (168).

In the next chapter we simulate the conventional system. In doing so, we are required to use an intermediate frequency filter prior to the discriminator. It was found that the best intermediate filter was one that had a band width of $1.3 \cdot d_f \cdot K$. Now in the foregoing performance analysis we have assumed an ideal intermediate filter. In the actual simulation situation we have no such device. Since we are using a low pass filter of band width $1.3 \cdot d_f \cdot K$ in the simulation, then for our analytical analysis we have used the noise equivalent band width of that low pass filter. For example, if $d_f = 50$ radians per volt, then $B_{IF} = 32.5$ Hertz. A short discussion of equivalent band width is included in the appendix. Since both the first and second order Butterworth messages have the same 3 db point, we have assumed that the same intermediate filter should serve both systems equally as well. The validity of this assumption has not been tested.

The next chapter will describe the simulation of the conventional receiver.

Theoretical Performance for Figure 38

One Pole Message

Conventional Receiver

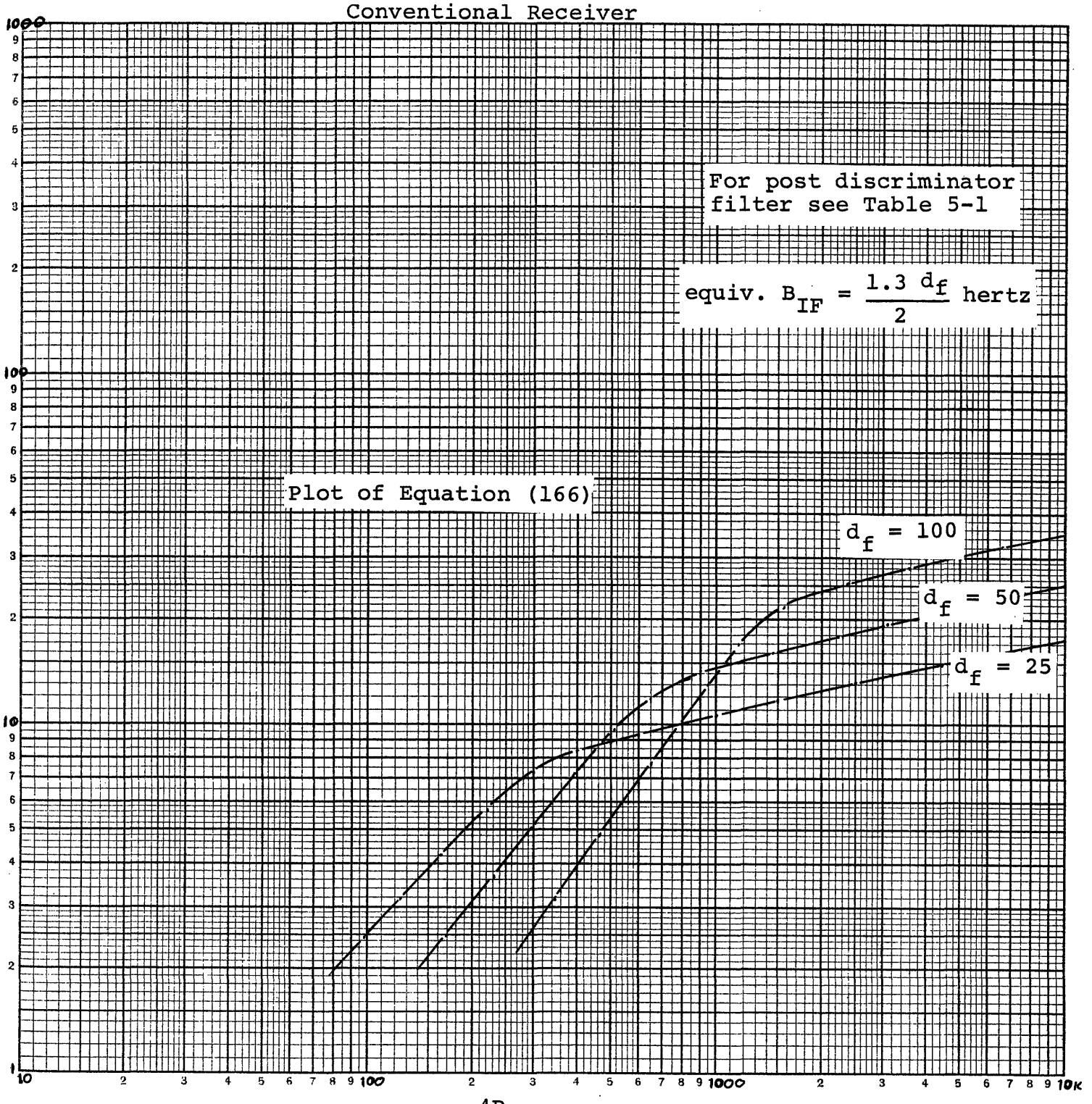

$$\Lambda = \frac{4P}{KN_o}$$

Figure 40

Two Pole Message

Conventional Receiver

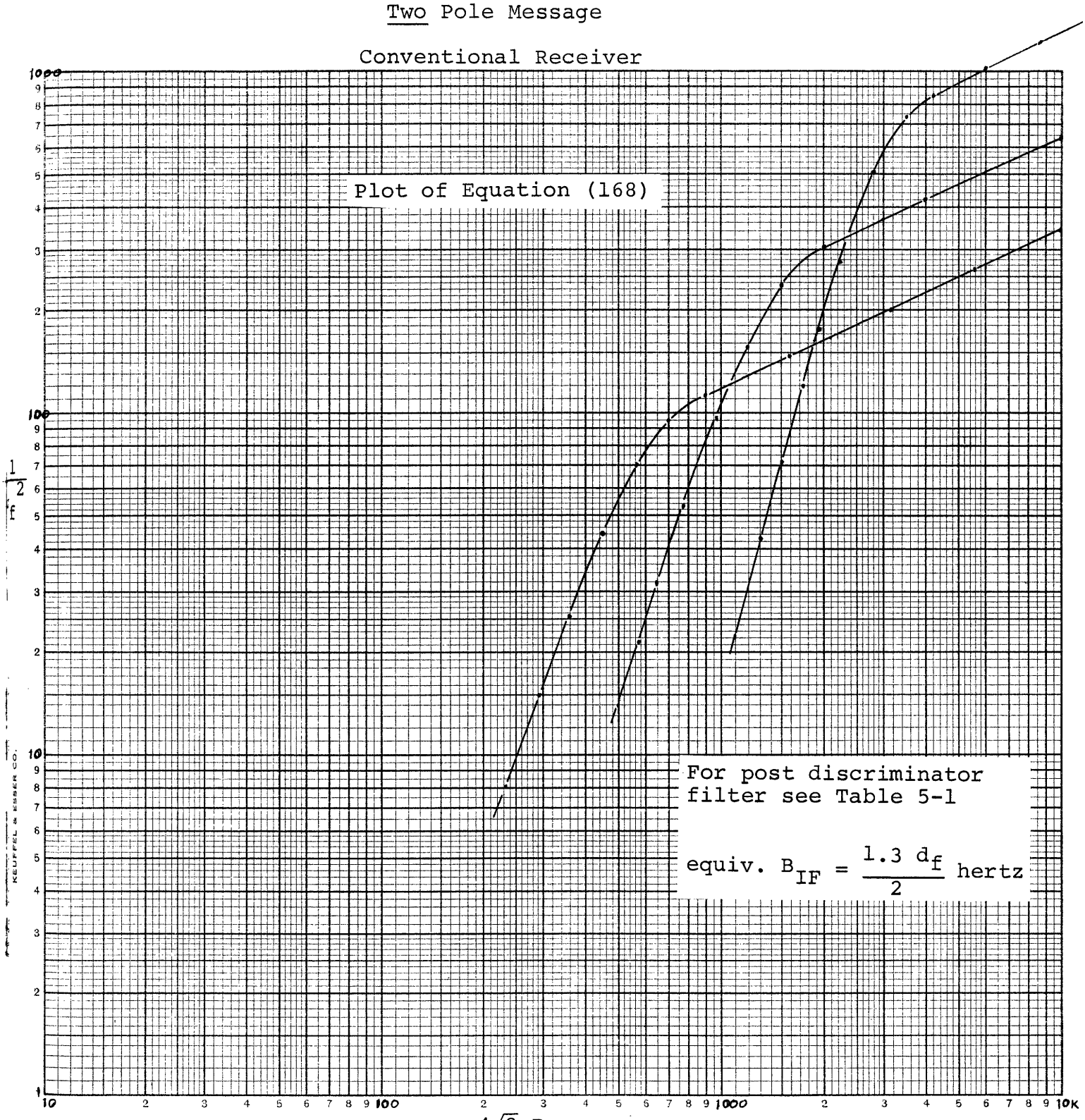

$$\Lambda = \frac{4\sqrt{2}\ P}{KN_o}$$

Figure 41

CHAPTER 6

SIMULATION ANALYSIS OF CONVENTIONAL DEMODULATOR

6.0 INTRODUCTION

In this chapter we will apply the technique of digital simulation to the performance analysis of the conventional demodulator. In general the digital generation of the message and noise will be the same as in chapter four. The filter modeling techniques that were discussed in chapter four also apply. Since the performance of this system will be used as the bases of comparison for the optimum system, then we shall use the same Butterworth family of messages in an effort to establish a meaningful comparison.

6.1 CONVENTIONAL F.M. DIGITAL MODEL

Consider the conventional receiver shown in figure 38 of chapter 5. The input to the limiter-discriminator combination can be written as,

$$r(t) = \sqrt{2P}\cos\left[\omega_c t + \phi(t)\right] + n(t) \qquad (171)$$

where $$\phi(t) = d_f \int_{-\infty}^{t} a(u)\, du \tag{172}$$

and n(t) is narrow-band, zero mean, white Gaussian noise across the intermediate filter bandwidth. As before n(t) can be written as

$$n(t) = \sqrt{2}\,[n_c(t) \cos \omega_c t - n_s(t) \sin \omega_c t], \tag{173}$$

and n(t) is independent of the message a(t).* By expanding (171) and introducing (173)

$$r(t) = [\sqrt{2P} \cos \phi(t) + \sqrt{2}\, n_c(t)]\cos \omega_c t - [\sqrt{2P} \sin \phi(t) + \sqrt{2}\, n_s(t)]\sin \omega_c t. \tag{174}$$

Define, $$X_c(t) = \sqrt{2P} \cos \phi(t) + \sqrt{2}\, n_c(t) \tag{175}$$

$$X_s(t) = \sqrt{2P} \sin \phi(t) + \sqrt{2}\, n_s(t) \tag{176}$$

By standard trigonometric manipulations,

$$r(t) = \sqrt{X_c^2(t) + X_s^2(t)}\, \cos\left[\omega_c t + \tan^{-1} \frac{X_s(t)}{X_c(t)}\right] \tag{177}$$

---

* Reference 17, Chapter 8.

Notice that the magnitude of (177) is not a constant but some random function of time. We assume that the limiter will take care of that problem. Now the output of the discriminator, as we stated before, is the instantaneous value of the phase of the input signal. In this case the phase is explicit in (177):

$$\theta(t) = \tan^{-1} \left[\frac{X_s(t)}{X_c(t)}\right] \tag{178}$$

and the instantaneous value of $\theta(t)$ is merely given by its derivative,

$$\dot{\theta}(t) = \frac{d}{dt} \tan^{-1} \left[\frac{X_s(t)}{X_c(t)}\right] \tag{179}$$

Carrying out the derivative in (179) yields,

$$\dot{\theta}(t) = \frac{X_c(t)\, \dot{X}_s(t) - X_s(t)\, \dot{X}_c(t)}{X_c^2(t) + X_s^2(t)} \tag{180}$$

and we can rewrite (175) and (176) as

$$X_c(t) = \cos \left[d_f \int_{-\infty}^{t} a(u)\, du\right] + \frac{n_c(t)}{\sqrt{P}} \tag{181}$$

$$X_s(t) = \sin \left[d_f \int_{-\infty}^{t} a(u)\, du\right] + \frac{n_s(t)}{\sqrt{P}} \tag{182}$$

where the division by $\sqrt{2P}$ to obtain (181) and (182) has no effect on (180). As before $n_c(t)$ and $n_s(t)$ are also independent zero mean Gaussian random processes with the same spectral density as n(t), namely,

$$S_n(\omega) = S_{n_s}(\omega) = S_{n_c}(\omega) = \frac{N_o}{2} \tag{183}$$

As a check on our result, if we let $n_c(t)$ and $n_s(t)$ be zero in (180) then we obtain

$$\dot{\theta}(t)\Big|_{n(t)\equiv 0} = d_f a(t) \ , \tag{184}$$

which is clearly the desired discriminator output.

The final stage in the conventional receiver is the optimum post discriminator filter. We will derive the optimum filter later because at this point we want to interpret equations (180), (181), and (182) as our conventional receiver. The block diagram representation of equation (181) and (182) is shown in figure 42.

Note here that the quadrature components $X_s(t)$ and $X_c(t)$ have contained in them additive, narrow band, white noise. If the additive noise was not band limited the large amount of noise power would obscure the message and the discriminator would not operate satisfactorily. Keep

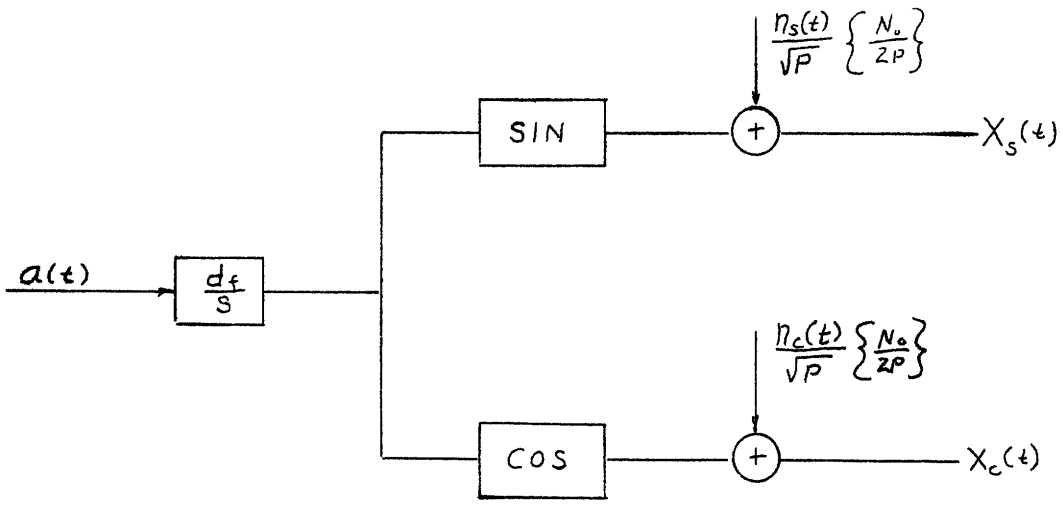

Figure 42

Interpretation of equations (181) and (182)

this fact in mind for it will necessitate the use of another filter in our final digital model.

Equation (180) indicates that we should take the functions $X_{s,c}(t)$ and operate on them as shown in figure 43.

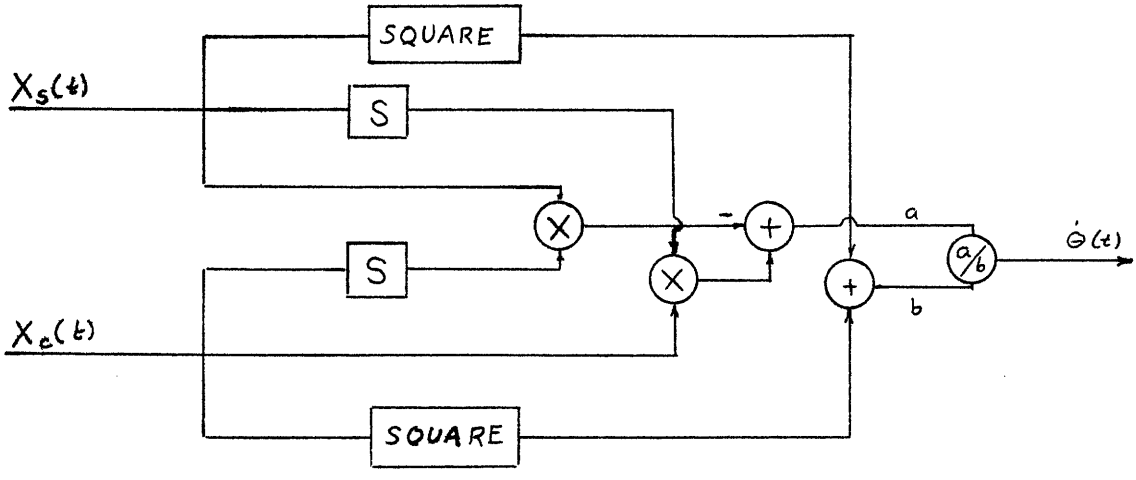

Figure 43

Discriminator Model

The "1/S" term in figure 42 and the "S" term in figure 43 are frequency domain representations for the mathematical operations of integration and differentiation respectively. Digital models of these operators are also given in the appendix.

Now we want to realize the digital equivalent of our entire system using figures 42 and 43 as subsystems. In chapter 5 when we designed the digital model for the additive noise term, we made certain, by choosing an appropriate "T", that it appeared as wide band, white noise well past the message bandwidth. If we take that wide band, white noise and use it in figure 42 our system would not work. Therefore we must, in some way, filter the noise. This new filter will be placed as shown in figure 44, between the two subsystems of figures 42 and 43.

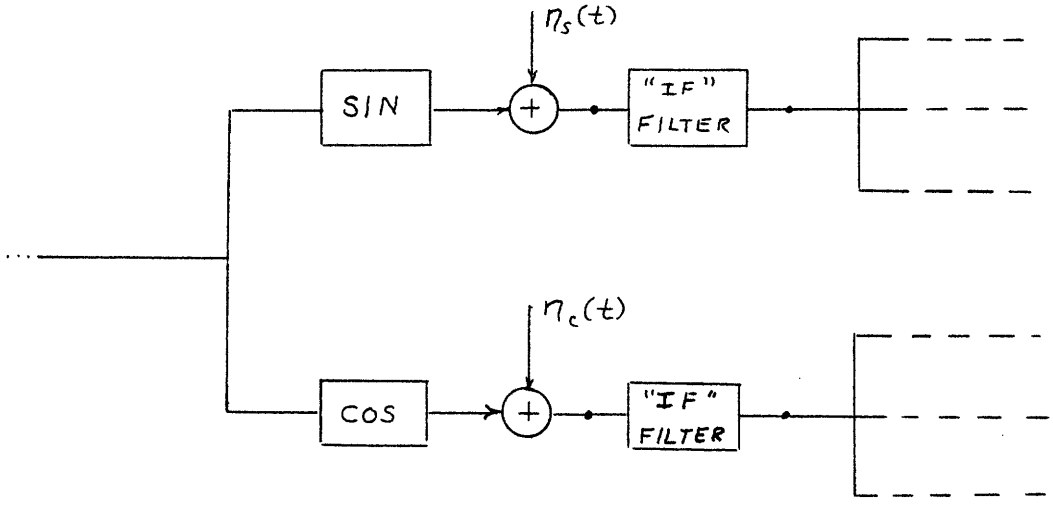

Figure 44

Inclusion of the I.F. Filter

We will call this filter the "I.F." filter for it serves the same purpose as the intermediate filter in the ideal conventional system of figure 38, chapter 5. It will be a unity gain low pass filter in our case because all our signals in this model are at base band. The bandwidth, B_{IF}, of this filter is clearly a dominant factor in the performance of the system. If we make B_{IF} too wide, excessive noise is permitted to enter the discriminator. If we make B_{IF} too narrow then the message will be distorted. Therefore we must make a compromise between the two possibilities. A reasonable compromise would be to find that B_{IF} that gives the best system performance. There are two alternatives for determining the optimum B_{IF}. We can analytically derive it or we may experimentally determine it. To analytically produce the optimum B_{IF} would be a difficult task. This is true because we would have to find the spectrum of

$$\cos\left[d_f \int_{-\infty}^{t} a(u)\, du\right]. \tag{185}$$

We do know the spectrum of a(t) but we do not know the spectrum of (185). Middleton[23] presents a method by which the spectrum of (185) may be determined. Once we have the spectrum one could proceed to analytically find the optimum low pass filter.

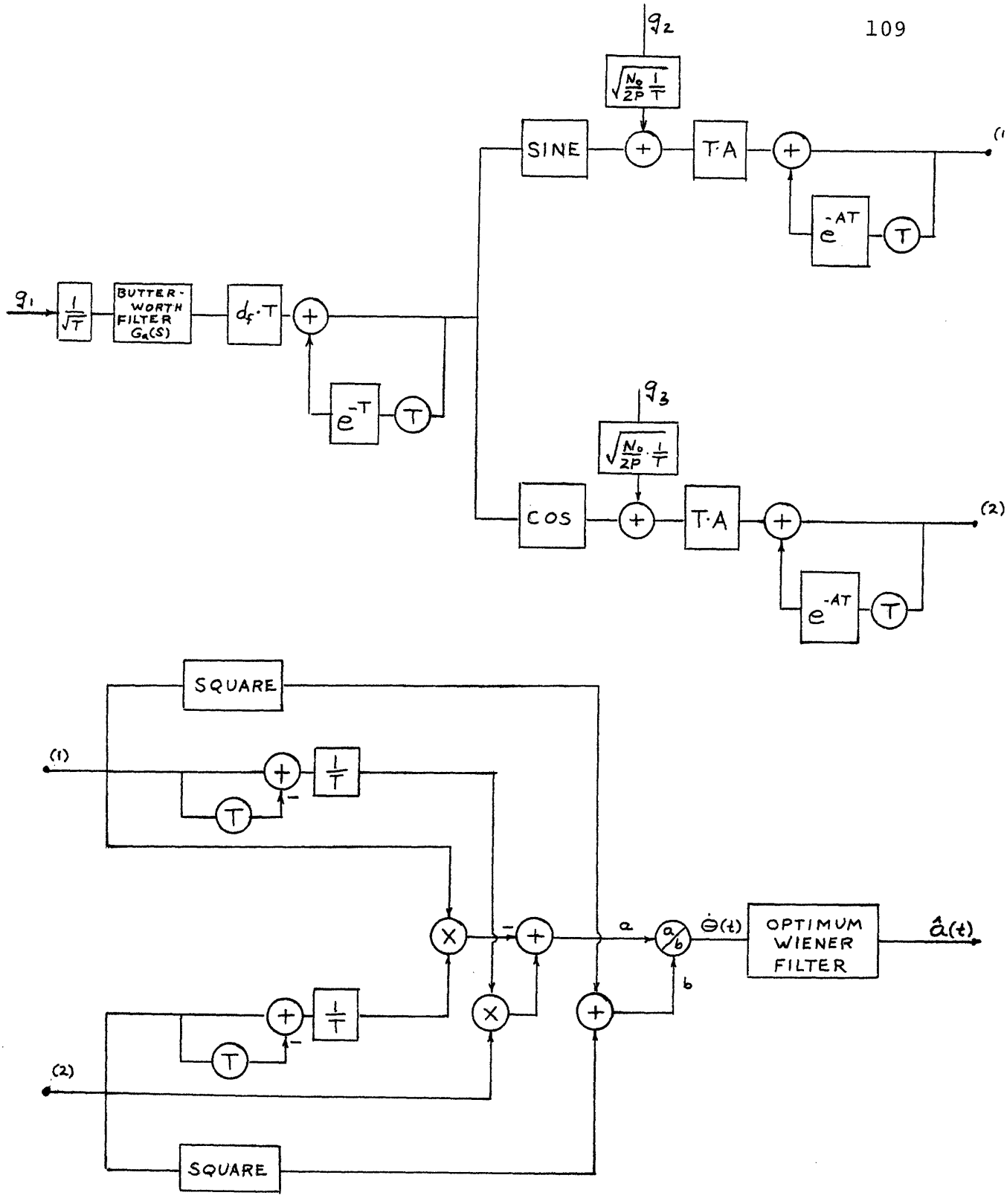

Figure 45

Conventional F.M. System—Digital Model

We will use the other alternative for finding B_{IF} optimum. Therefore the system will be assembled with a variable bandwidth I.F. low pass filter and the B_{IF} that gives the best performance will be chosen as B_{IF} optimum.

The final digital model for our conventional system is given in figure 45.

The next section deals with the derivation of the optimum post discriminator filters, with the determination of B_{IF} and with the simulation results for the Butterworth family of messages.

6.2 CONVENTIONAL F.M. SIMULATION

To calculate the optimum Wiener filter for the output of the discriminator we must know the power density spectrum of the output. In general equation (180) represents the output in the time domain. One would have a difficult time finding the spectrum of (180) so let us explore another possibility. Suppose we consider the weak noise case when the signal to noise ratio at the output of the intermediate filter is high. Then we can write

$$r(t) = \sqrt{2P} \cos \left[\omega_c t + d_f \int_{-\infty}^{t} a(u)\, du\right] + n(t) \qquad (186)$$

where

$$n(t) = \sqrt{2}\, n_c(t) \cos\left[\omega_c t + d_f \int_{-\infty}^{t} a(u)\,du\right] + \sqrt{2}\, n_s(t) \sin\left[\omega_c t + d_f \int_{-\infty}^{t} a(u)\,du\right] \tag{187}$$

Observe here that $n_c(t)$ and $n_s(t)$ are two low pass processes and that they multiply onto a varying frequency sinusoid. Once again we can show

$$N_{c,s}(\omega) = \frac{N_o}{2} \quad , \quad |f| < B_{IF} \tag{188}$$

Combining these results yields

$$r(t) = R(t) \cos\left[\omega_c t + d_f \int_{-\infty}^{t} a(u)\,du + \tan^{-1}\left[\frac{\sqrt{2}\, n_c(t)}{\sqrt{2P} + \sqrt{2}\, n_s(t)}\right]\right] \tag{189}$$

As in chapter 5, page the output of the discriminator is

$$\theta_{WN}(t) = d_f a(t) + \frac{\dot{n}_c(t)}{\sqrt{P}} \quad ,$$

$$|n_s(t)| << \sqrt{P} \tag{190}$$

The problem is now to filter $\theta_{WN}(t)$ optimally where

$$\theta_{WN}(\omega) = \frac{d_f^2 \frac{2n}{K} \sin \frac{\pi}{2n}}{1 + (\frac{\omega}{K})^{2n}} + \omega^2 \frac{N_o}{2P} \tag{191}$$

Here we have assumed that $n_c(t)$ is independent of $a(t)$.

Now that we have the spectrums we can proceed with the usual Wiener filtering problem. The results for the Butterworth family are given in table 6-1.

Message Spectrum	Post Discriminator Filter	Constants
$\frac{2}{\omega^2 + 1}$	$\frac{\alpha^2}{(1 + \alpha + \gamma)} \frac{1}{(s^2 + \gamma s + \alpha)}$	$\alpha^2 = d_f^2 \Lambda$ $\gamma = \sqrt{2\alpha + 1}$ $\Lambda = \frac{4P}{N_o}$
$\frac{2\sqrt{2}}{\omega^4 + 1}$	$\frac{\alpha_1 s + \alpha_2}{(s + \gamma^{\frac{1}{6}})(s^2 + \gamma^{\frac{1}{6}} s + \gamma^{\frac{1}{3}})}$	$\gamma = d_f^2 \Lambda$ $\alpha_1 = 2\gamma^{\frac{1}{3}} - 2\sqrt{2}\ \gamma^{\frac{1}{6}} + 1$ $\alpha_2 = \gamma^{\frac{1}{2}} - 2\gamma^{\frac{1}{6}} + \sqrt{2}$ $\Lambda = \frac{4\sqrt{2}\ P}{N_o}$

Table 6-1

The next problem is to find B_{IF} optimum. A transfer function for the low pass IF filter is

$$H(s) = \frac{R_2 d_f K}{s + R_2 d_f K} \tag{192}$$

The pole of the filter is set at $R_2 d_f K$ because we know that the band width of the input spectrum is at least d_f times the bandwidth of the message spectrum K (we will always use K = 1). An intuitive feeling for this point can be obtained by observing equation (186) above.

Simulations were run for various R_2 in a system using the first order Butterworth message and a $d_f = 50$. The performance results are given in figures 46 and 47. Figure 46 shows the actual performance curves and figure 47 illustrates more clearly how the performance changes as a function of the I.F. bandwidth.

Figure 46 depicts an interesting phenomenon. Notice that the linear region of the curves that exhibit a low threshold, remains slightly below the expected linear performance. However, the curves that have high threshold points do reach the expected linear performance. It is believed that this phenomenon is caused by distortion in the I.F. filter. For large values of R_2, B_{IF} is wide and the linear region performance is high. However, we are allowing excessive noise through the filter and this causes

the threshold to occur early. For small values of R_2, B_{IF} is narrow enough to provide for a good threshold but the rounded corners of the low pass I.F. filter frequency response is clipping off a little of the message spectrum. This droop in the linear region performance will be herein considered as a minor problem and hence the main criteria for the B_{IF} optimum will be a low threshold. Figure 46 shows that the best threshold occurs when the pole of the I.F. filter is at about $1.3 \cdot d_f \cdot K$. This value of R_2 was used throughout the following simulations.

Using the filters shown in table 6-1, figure 45 was hence fully mechanized and the performance results are given in figures 48 and 49.

6.3 CONCLUSIONS

The simulation results for the first and second order receivers are given in figures 48 and 49 respectively. About a 3 db loss in threshold occurred while going from the first order case to the second order case. This is in agreement with the theoretical results in chapter 5.

For both messages the over-all performance curves remain slightly below that of the predicted theoretical curves. The magnitude of the difference is about 0.2 db. This "droop" in performance was predicted on the basis of what we observed in figure 46

Further examination of these curves will be made in the next chapter.

Experimental Determination of Optimum IF Filter

One Pole Message

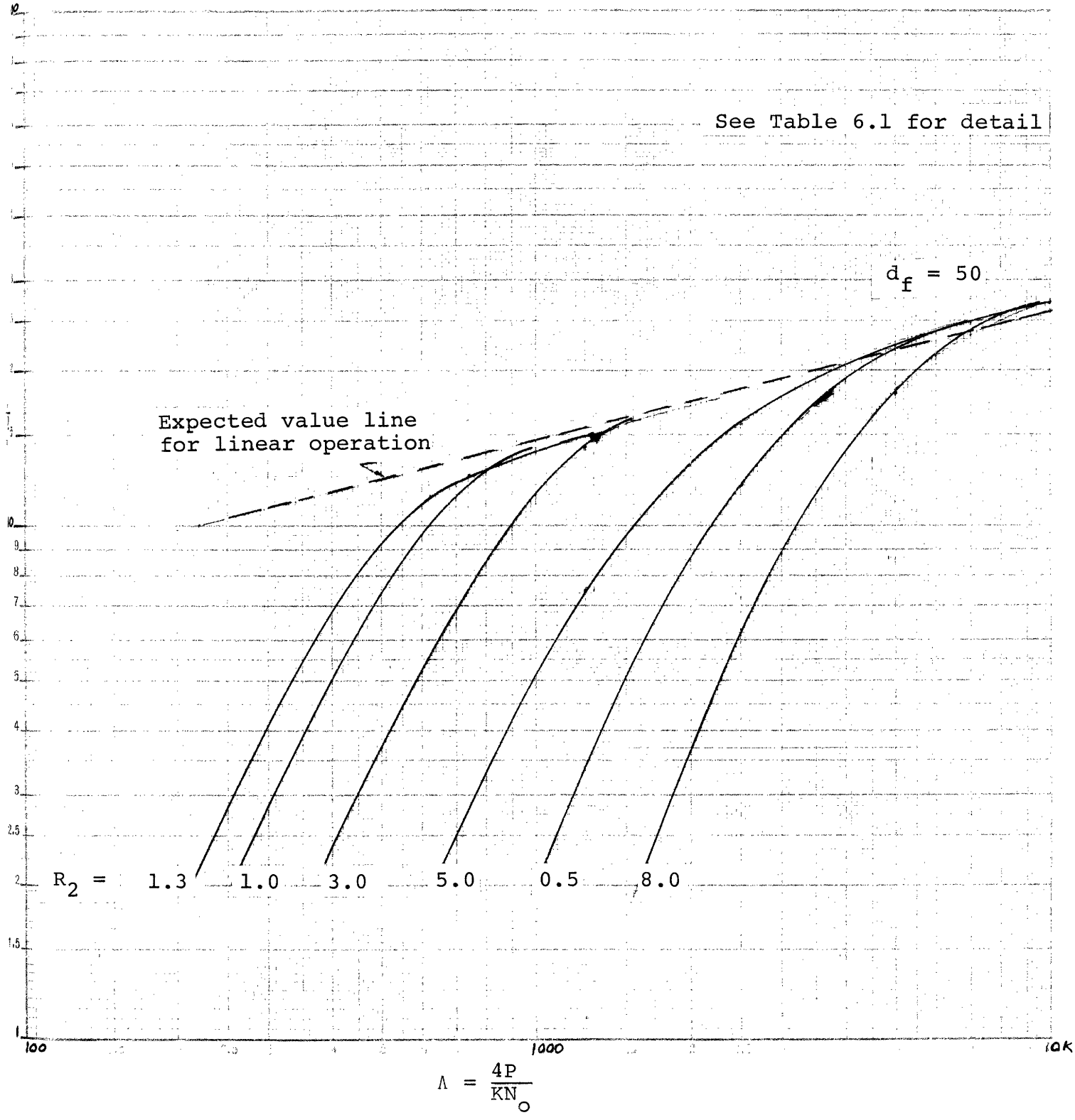

Figure 46

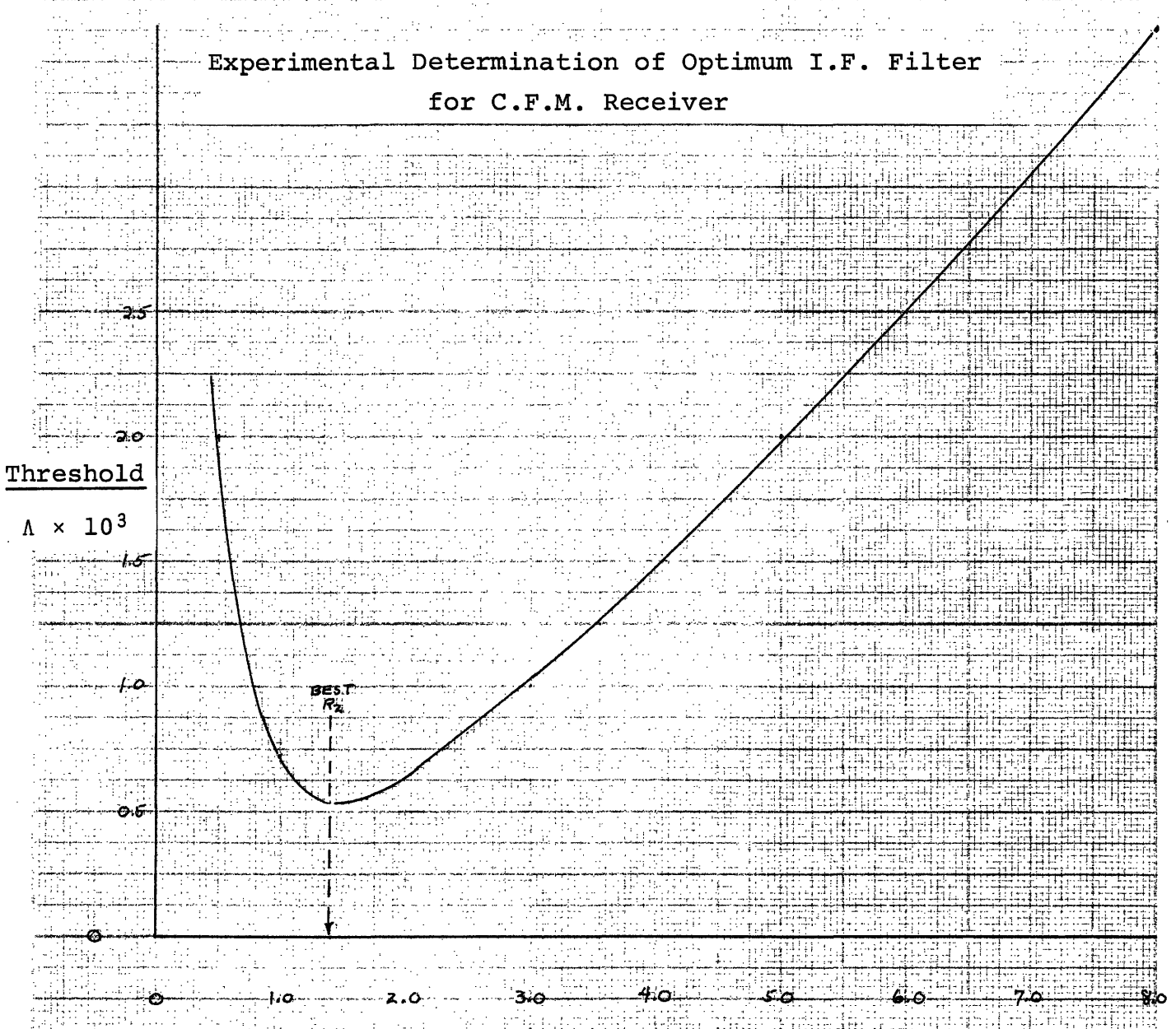
Experimental Determination of Optimum I.F. Filter
for C.F.M. Receiver
Threshold
Λ × 10³
2.5
2.0
1.5
1.0
0.5
0
BEST
R₂
0
1.0
2.0
3.0
4.0
5.0
6.0
7.0
8.0
Multiplying Factor
R₂
proportional to bandwidth of I.F. filter

Figure 47

Experimental Performance for Figure 45

One Pole Message

Conventional Receiver

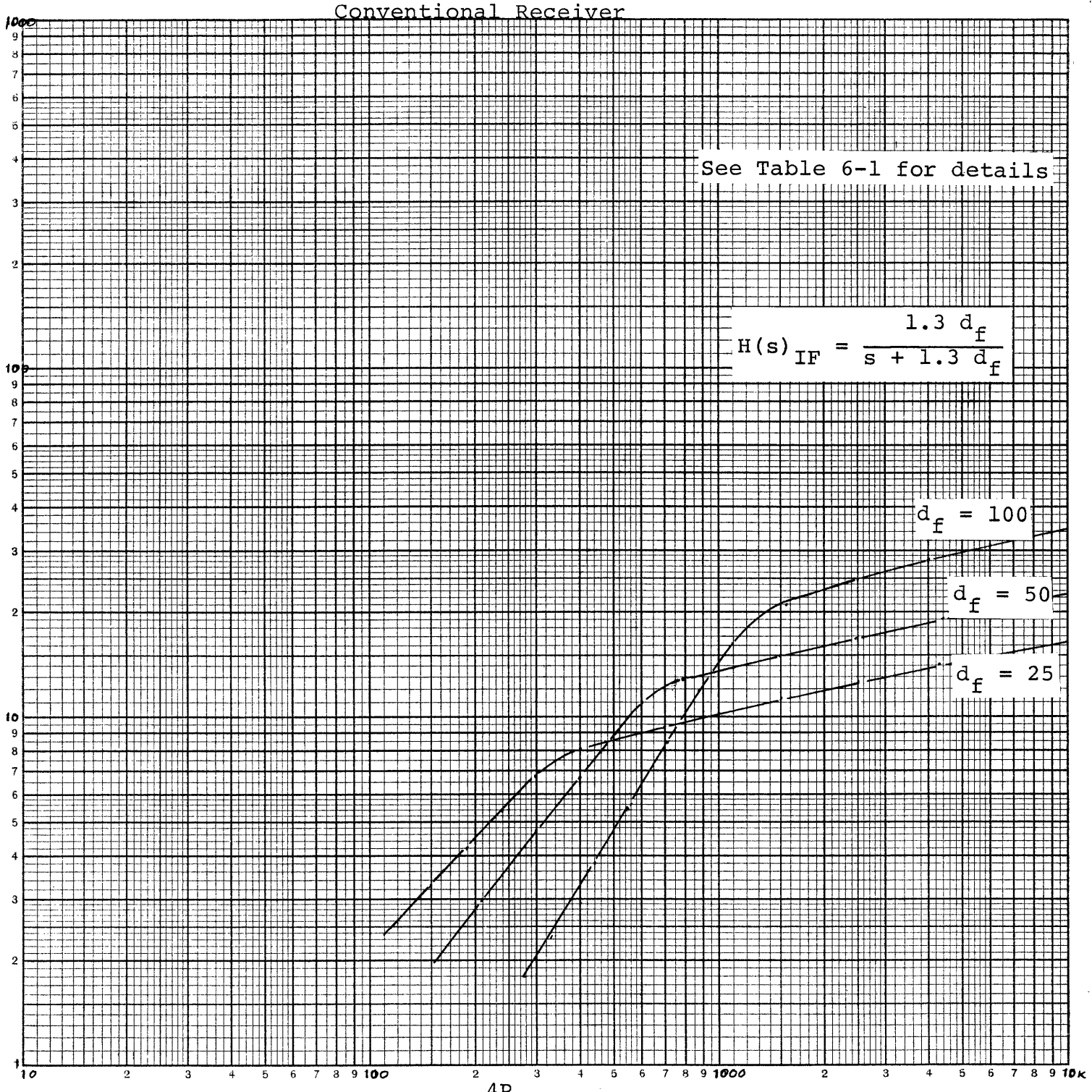

Figure 48

Two Pole Message

Conventional Receiver

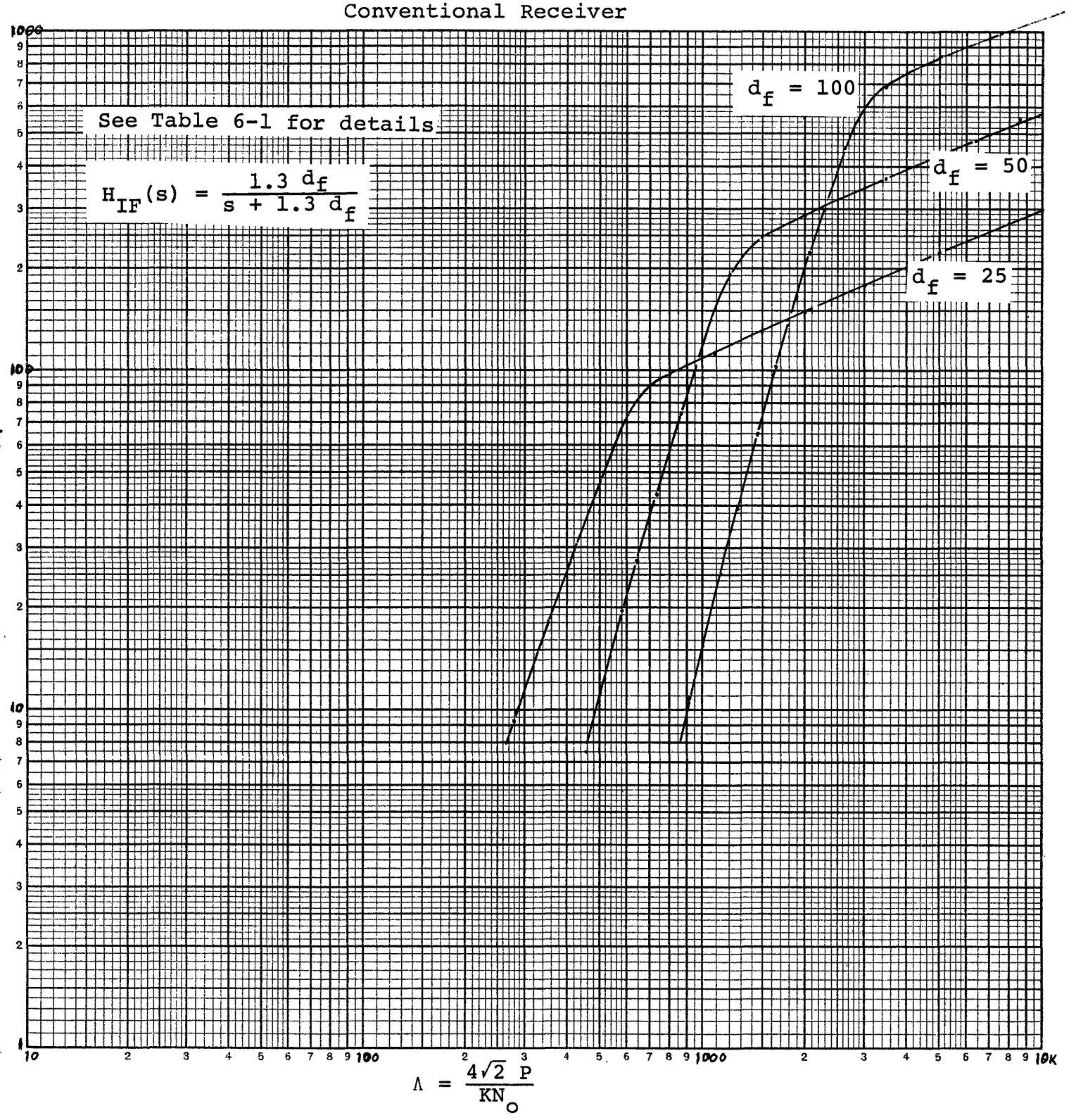

Figure 49

CHAPTER 7

OBSERVATIONS AND CONCLUSIONS

7.0 INTRODUCTION

In this chapter we will compile the results of the foregoing six chapters. It will be done in three sections. The first section will investigate all of the ramifications of the optimum phase-locked loop receiver performance—both the simulated and the theoretical cases. The second section will examine the analytical and simulation results for the conventional receiver. Finally the third section will utilize the observations made on the first and second sections to make reasonable comparisons between the optimum phase-locked loop receiver and the conventional receiver!

7.1 PHASE LOCKED LOOP OBSERVATIONS

In this section we will evaluate solely the performance of the phase-locked loop. There were three methods that we used to investigate the loop. One method was the completely linear analysis, another was the quasi-linear analysis and the last was the simulation analysis. Figure 50 depicts

the relationship of the three methods for the one and two pole cases. For simplicity reasons only the $d_f = 50$ curves are shown here. The quasi-linear analysis gives a fair approximation to the threshold but the simulation analysis spells it out in detail. For the one pole case the quasi-linear technique missed the actual threshold by about 3 db. In the two pole case the error was about 3.5 db. The reason for that large error is not quite clear. For both the one and two pole cases the quasi-linear technique indicated threshold at a mean square phase error of about one radian^2. We know from our simulation results that this is not usually true. In the simulations we saw that the mean square phase error at threshold varied somewhat but that it was usually less than 0.5 radians square.

Now let us consider the two pole message performance versus the one pole message performance. The quasi-linear analysis predicted that the threshold would improve by 1.5 db for the two pole case. In the simulation a 1.0 db improvement was realized thus verifying the prediction of the quasi-linear result.

The quasi-linear technique cannot display the performance below threshold so let us now concentrate on the experimental curves. Observe that, for the one pole case operating below threshold, the performance falls off at

a rate of about 4 db per octave. However, for the two pole case, the performance drops off at 18 db per octave. As a result, the performance curves for the two cases intersect at an SNR of 150 hertz^{-1}. This fact indicates that there is a range of input SNR where the first order receiver gives improved performance over the second order receiver. We can conclude that if our physical system had a low SNR constraint, then, if we had a choice, we would choose to build a first order receiver and transmit a first order message.

Let us now consider the fifth order message simulation of chapter four. In that case a fifth order Butterworth message was used in a system designed optimally for a second order message. Figure 51 compares the results of that simulation with the results for the same system with a second order message input. Interestingly enough, the former case gave <u>improved</u> performance over the latter case. The reason is clear. The higher order Butterworth message has a compressed bandwidth; i.e., more of its power in toward the spectral origin. Thus, <u>less</u> spectral distortion was realized with the fifth order message than with the second order message. Also, since the system was perturbed by the same noise in both cases, the M.S.E. due only to the noise would not change. The overall effect due to less distortion and the same noise interference tends to give a smaller mean

square error. If these observations are typical for a Butterworth message, then we could say that any Butterworth message of order N will give better performance than another Butterworth message of order M < N when they are both considered as inputs to the receiver designed especially for the M^{th} order message. Note that this is an empirical observation and that it has not been proven.

7.2 CONVENTIONAL RECEIVER OBSERVATIONS

In this section we will consider only the conventional receiver. For the conventional receiver we applied three analysis methods similar to those for the phase-locked loop. The linear analysis of chapter three holds for this case as well as for the phase-locked loop because we are considering the same message spectra and the same additive channel noise. For the non-linear theoretical analysis, we used the methods developed by Rice (henceforth called the "Rician" method). The simulation analysis was again used to evaluate the system above, at, and below threshold. Figure 52 shows the combined conventional F.M. results for both the one and the two pole cases. Once again only the $d_f = 50$ curves are shown for simplicity reasons.

First let us consider the theoretical versus the simulated results. The Rician method provided amazingly accurate

predictions about the conventional receiver performance. The graph shows essentially no measurable difference in the threshold. Also below threshold the rate at which the performance decays is almost identical for the theoretical and the corresponding simulated cases. However, notice in figure 52 that the Rician model did not account for everything. In general the simulated curves lie a little below the theoretical curves. The reason for this difference is clear. Rice's model made an assumption that is not actually true. He assumed that the intermediate frequency filter was an "ideal" filter that was wide band enough so as not to cause any distortion in the message. Hence he proceeded to derive his model only on the basis of the noise that was passed by the intermediate filter. In our system not only do we pass noise through the I.F. filter but we also create distortion that manifests itself as reduced receiver performance. It is that extra distortion term that is not included in the theoretical analysis that is the underlying cause for the difference between the corresponding curves.

Now let us consider the two pole message performance versus the one pole message performance. The theoretical curves predict that there should be a 2 db loss in threshold for the two pole case and the simulations confirm this fact. Also, below threshold, the rate of decay for the two pole

case is 11 db/octave and the one pole case decays at about 5 db/octave. An intersection of the curves occurs at about an SNR of 450 hertz^{-1}.

7.3 PHASE-LOCKED LOOP vs. CONVENTIONAL F.M. RECEIVER

Finally we have come to the point where we can make a valid judgement on the performance of our optimum receiver. Observe that in figure 53 we have replotted the simulation curves for $d_f = 50$. Included are both the phase-locked loop simulations and the conventional receiver simulations. Some points are immediately clear. In both the one and two pole cases the phase-locked loop gave superior threshold occurrence. For the one pole message there was a 3 db improvement. For the two pole case there was a 6 db improvement. The 6 db figure arose because two things occurred. When we went from the one pole case to the two pole case, the phase-locked loop model improved its threshold and the conventional model relaxed its threshold.

Notice in the linear regions that the conventional receiver curve lies slightly below the phase locked loop curve. Once again, the I.F. filter problem is showing itself. In the phase-locked loop we do not generally have an IF filter so we are not pestered with that difficulty.

In conclusion we can say that the performance of the realizable, zero-delay, phase-locked loop receiver is superior to that of the best conventional F.M. receiver.

Phase-Locked Loop Results

for Three Methods of Analysis

One and Two Pole Cases

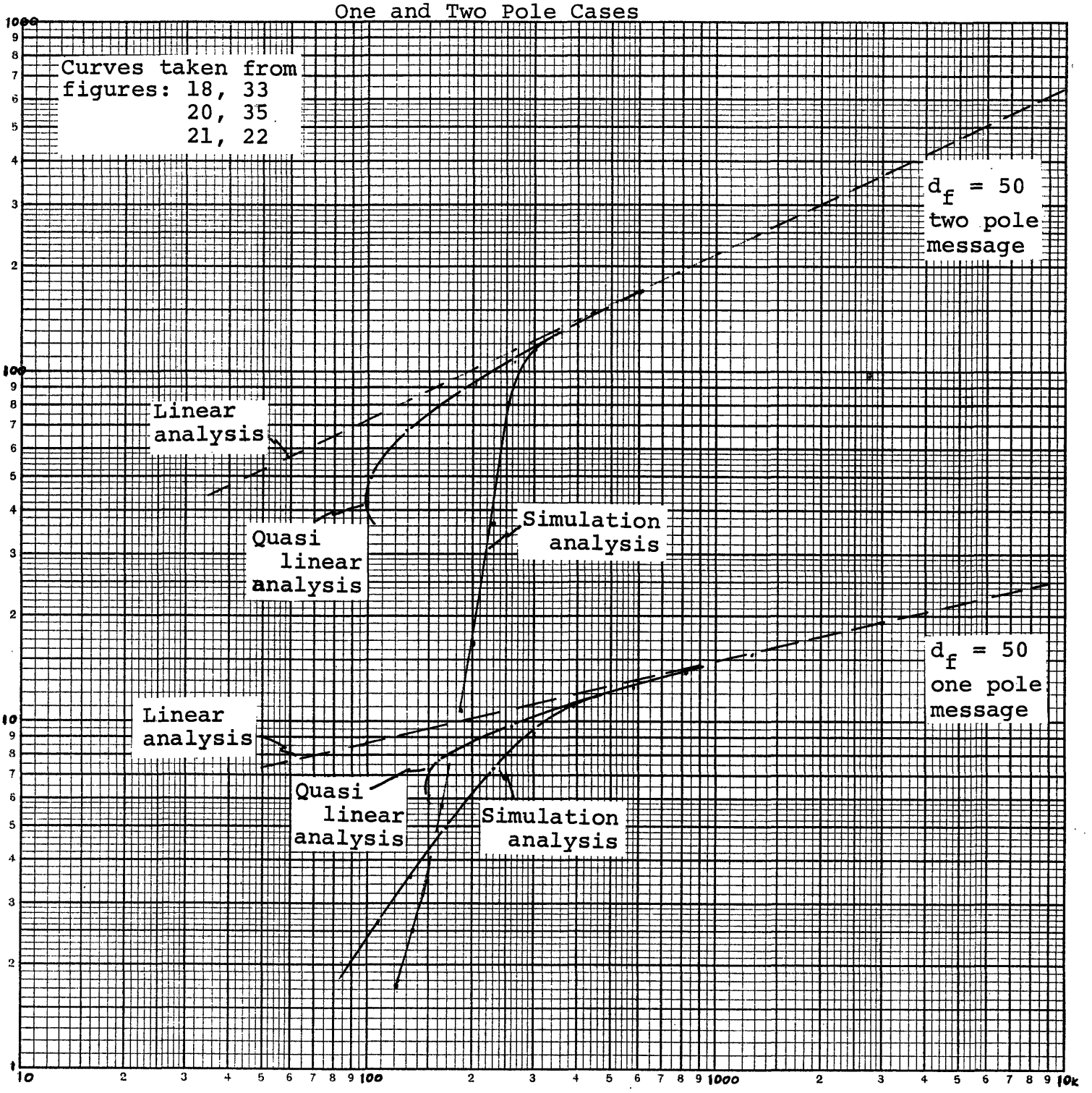

Λ

SNR

Figure 50

Experimental Comparison of Two and Five Order Messages into Second Order Loop

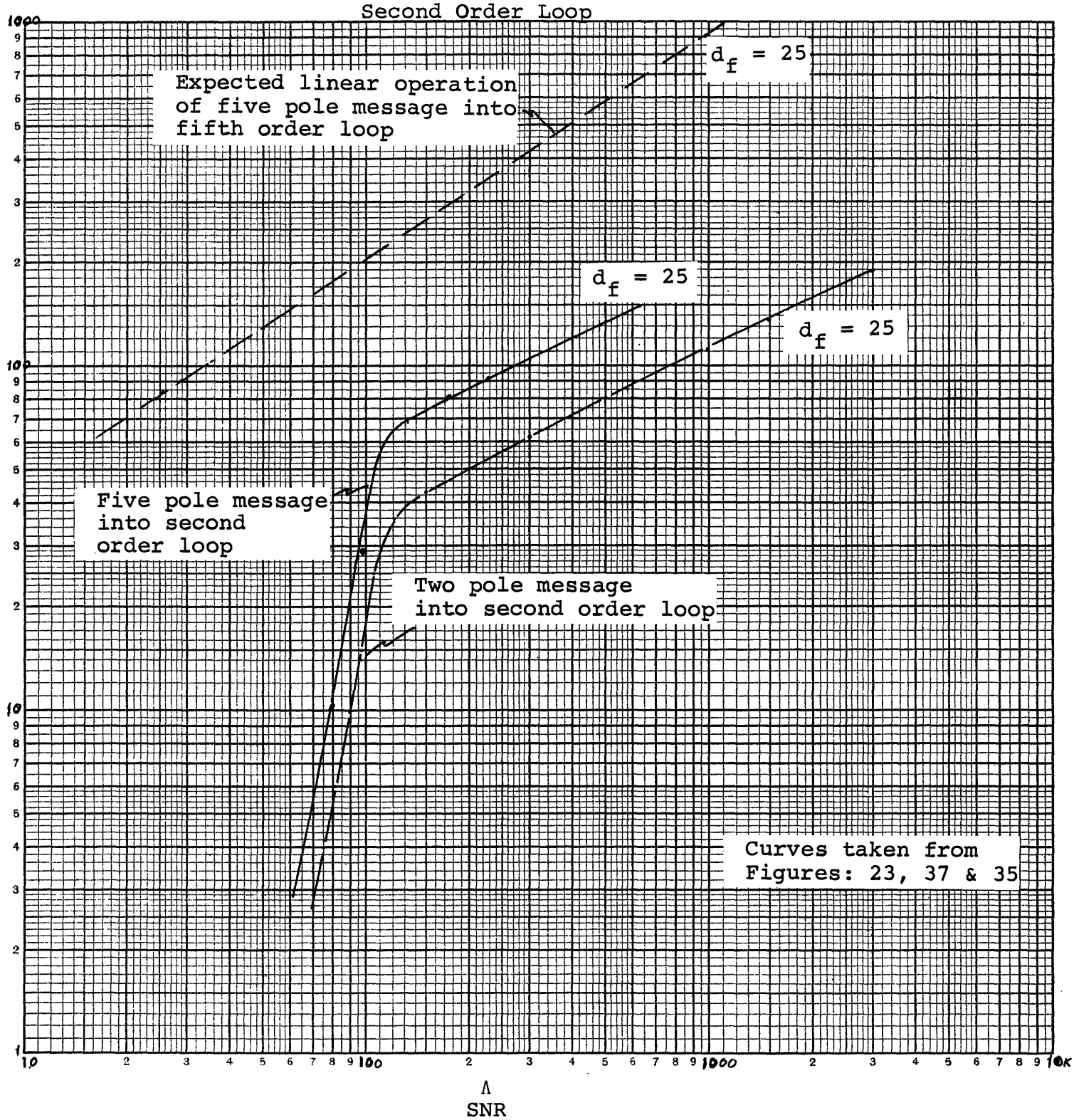

Figure 51

Conventional F.M. Results

for Three Methods of Analysis

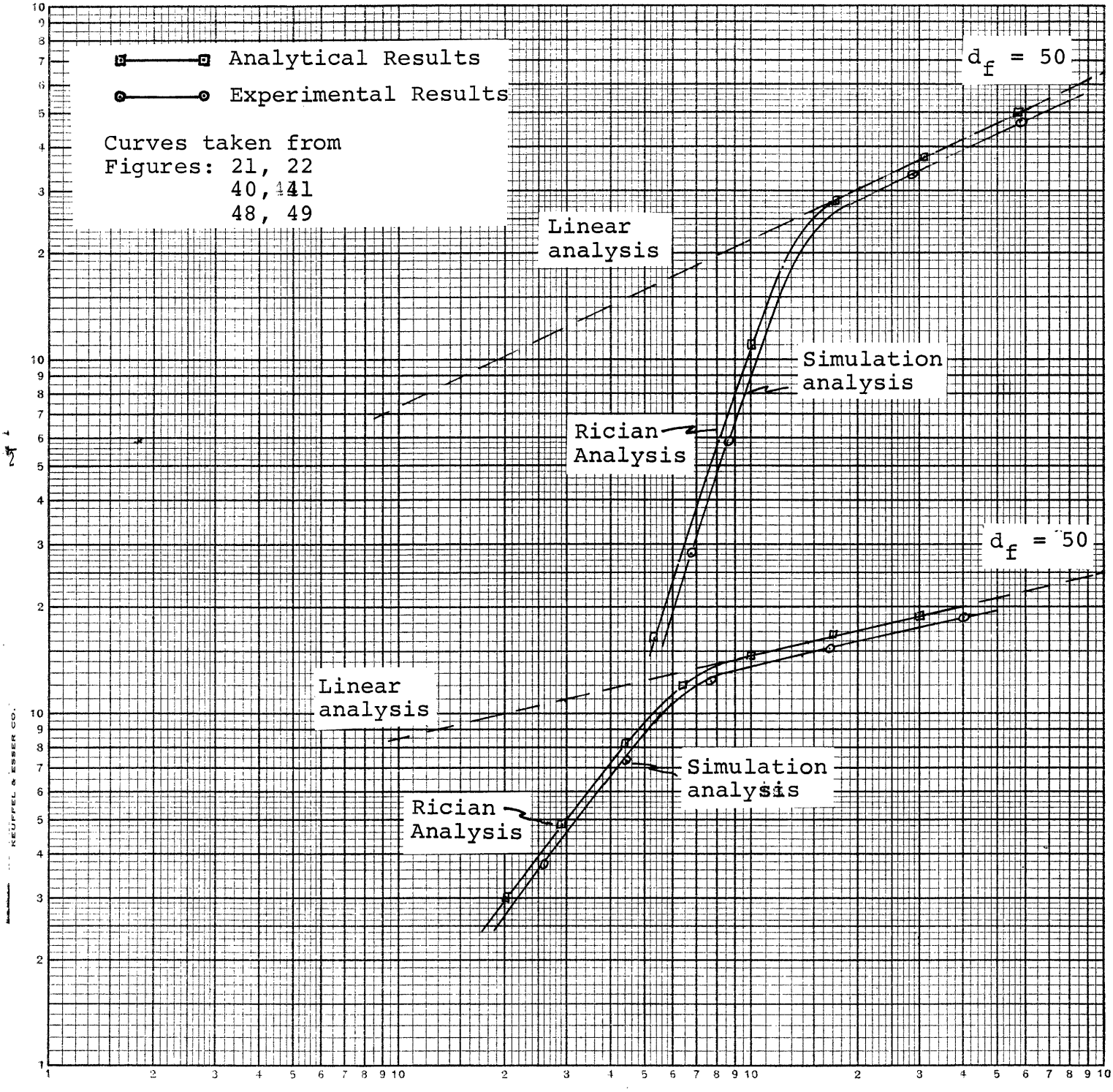

Figure 52

Phase-Locked Loop Rec'r
vs.
Conventional Receiver

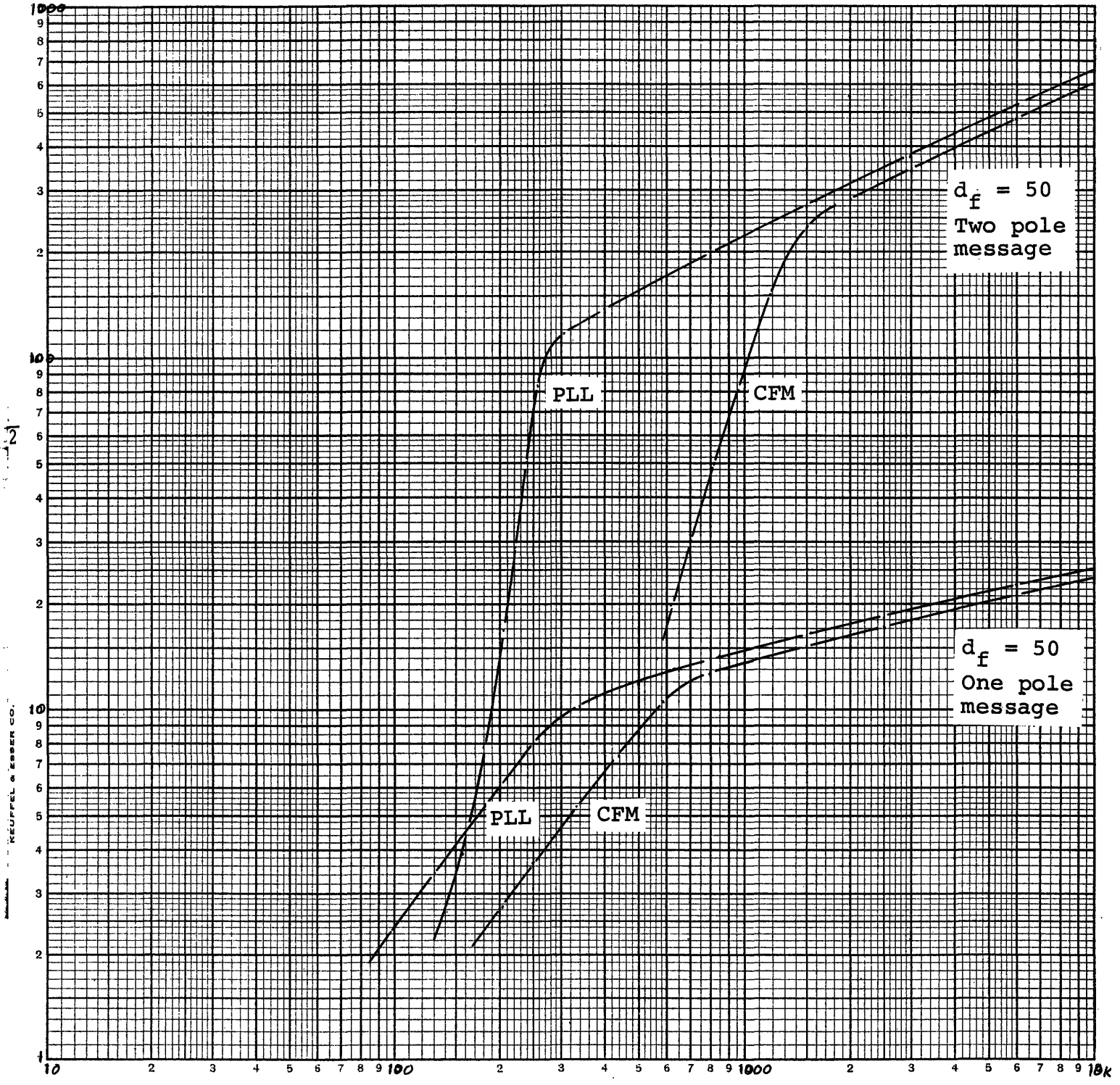

Figure 53

APPENDIX

This appendix will treat those subjects referenced by the text of the thesis. In addition it will explore some additional inroads for applying Booton's quasi-linear analysis technique to the receivers of chapter three.

i) Proof of equation (29)

$$K_{n^{(2)}}(\tau) = K_{n_1}(\tau) = K_{n_2}(\tau) = \frac{N_o}{2} u_o(\tau) \qquad (29)$$

Consider equation (28)

$$n^{(2)}(t) = n_1(t) \sin [\hat{x}(t)] + n_2(t) \cos [\hat{x}(t)] \qquad (28)$$

If W_n is large compared to the bandwidth of sin [x(t)] and cos [x(t)] we can make the approximation

$$K_{n_1}(\tau) = K_{n_2}(\tau) = \frac{N_o}{2} u_o(\tau) \qquad (A1)$$

Using this approximation, it follows that $a(t_1)$ is independent of $n_1(t_1)$ and $n_2(t_1)$. Hence the conditional covariance function

$$K_{n(2)}(t,u)/\hat{x} = K_{n_1}(t,u)/\hat{x} + K_{n_2}(t,u)/\hat{x} \tag{A2}$$

Where

$$K_{n_1}(t,u)/\hat{x} = E\{n_1(t)\ \sin\ [\hat{x}(t)]\ n_1(u)\ \sin\ [\hat{x}(u)]\}$$

$$= \sin^2\ [\hat{x}(u)]\ E[n_1(t)\ n_1(u)]$$

$$= \sin^2\ [\hat{x}(u)]\ \frac{N_o}{2}\ u_o(t-u) \tag{A3}$$

Likewise,

$$K_{n_2}(t,u)/\hat{x} = \cos^2\ [\hat{x}(u)]\ \frac{N_o}{2}\ u_o(t-u) \tag{A4}$$

Thus

$$K_{n(2)}(t,u)/\hat{x} = \sin^2\ [\hat{x}(u)]\ \frac{N_o}{2}\ u_o(t-u)$$

$$+ \cos^2\ [\hat{x}(u)]\ \frac{N_o}{2}\ u_o(t-u)$$

$$K_{n(2)}(t,u) = \frac{N_o}{2}\ u_o(t-u) \tag{A5}$$

Q.E.D.

ii) Digital Filters

a) $H(s) = \frac{d_f}{s}$

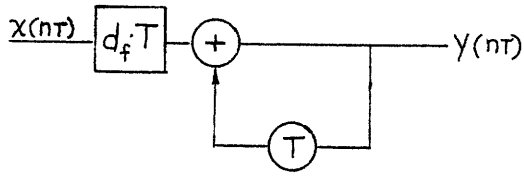

b) $H(s) = s$

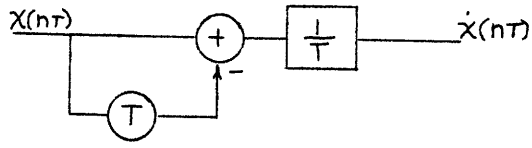

c) $H(s) = \frac{a}{s + b}$

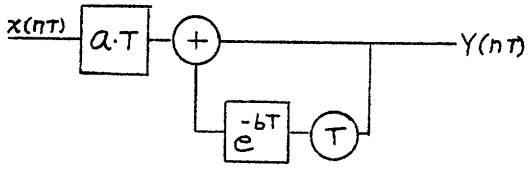

d) $H(s) = \frac{\omega_n\sqrt{1 - c^2}}{s^2 + 2c\omega_n s + \omega_n^2}$

$P_1 = e^{-c\omega_n T} \sin[\omega_n T\sqrt{1-c^2}]$

$P_2 = 2e^{-c\omega_n T} \cos[\omega_n T\sqrt{1-c^2}]$

$P_3 = e^{-2c\omega_n T}$

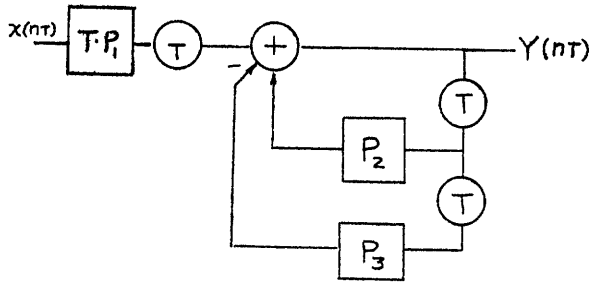

e) $H(s) = A \cdot \frac{s + c\omega_n}{s^2 + 2c\omega_n s + \omega_n^2}$

$P_1 = e^{-c\omega_n T} \cos[\omega_n T\sqrt{1-c^2}]$

$P_2 = 2e^{-c\omega_n T} \cos[\omega_n T\sqrt{1-c^2}]$

$P_3 = e^{-2c\omega_n T}$

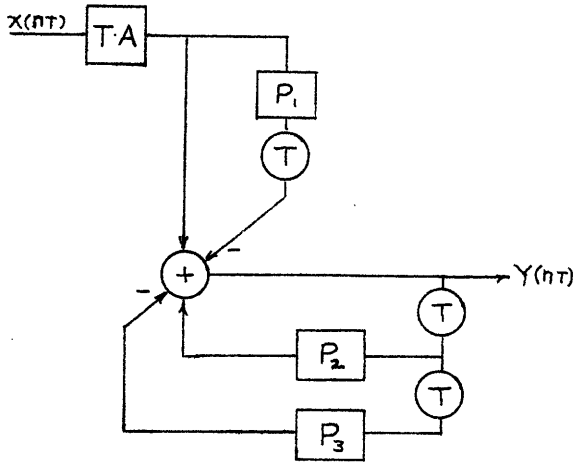

iii) Alternate Receiver Design

Up until now we have used Booton's technique to analyze the optimum receiver as in chapter 3. As shown in figure 15, $G_r''(s)$ is an ordinary zero-delay Wiener filter and the $1/\sqrt{\nu}$ is the gain term advanced by Booton:

$$\frac{1}{\sqrt{\nu}} = e^{-\frac{\sigma_x^2}{2}} \tag{A6}$$

Suppose we consider a different course of development than what we followed in chapter 3. Instead of completely linearizing the system as we did in figure 16, let us find the in-loop filter for figure 15. In other words, we want to find the in-loop Wiener filter that minimized the mean square phase error when

$$S_x(\omega) + \frac{N_o}{2P}\nu \tag{A7}$$

is the input to the loop. For the one pole Butterworth message, this in-loop filter is:

$$g_{\ell o}(s,\sigma_x^2) = \frac{(\gamma - 1)s + \delta}{s(s + 1)} \tag{A8}$$

where $\delta^2 = \frac{\Lambda}{\nu} d_f^2$ $\qquad \gamma = \sqrt{2\delta + 1}$

$\nu = e^{\sigma_x^2}$ $\qquad \Lambda = \frac{4P}{KN_o}$

Now to find the corresponding post loop filter we have to find the overall transfer function that minimizes the mean square demodulation error [i.e., we desire a(t), not x(t) as before] when (A7) is the input. Carrying out this Wiener filter problem yields,

$$H_{opt} = \frac{s[\delta - (\gamma - 1)]}{s^2 - \gamma s + \delta} \tag{A9}$$

and using feed back techniques we can find the post loop filter as

$$g_{po}(s, \sigma_x^2) = \frac{\delta - (\gamma - 1)}{(\gamma - 1)s + \delta} \tag{A10}$$

Now our receiver filters (A8) and (A10) are functions of the mean square phase error. The new nonlinear system is shown in figure A1.

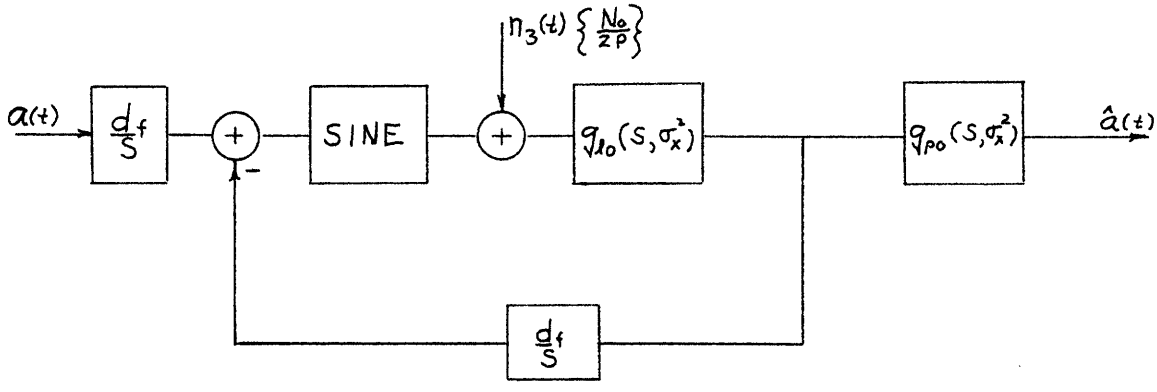

Figure A1

Nonlinear System with Booton-type Filters

Actually to theoretically analyze the system, we do not need to find the filters. Develet[24] proposed a method that will be used here.

For the one pole case, define

$$S_a(\omega) = \frac{2}{\omega^2 + 1} \tag{A11}$$

$$N_a(\omega) = \frac{N_o}{2P} \nu \frac{\omega^2}{d_f^2} \tag{A12}$$

$$N_x(\omega) = \frac{N_o}{2P} \nu \tag{A13}$$

then,

$$1 + \frac{S_a(\omega)}{N_a(\omega)} = \frac{P_\ell(\omega)\ P_R(-\omega)}{Q_\ell(\omega)\ Q_R(-\omega)} \tag{A14}$$

Carrying out (A14) we find

$$P_\ell(s) = s^2 + \sqrt{2\delta + 1}\ s + \delta \tag{A15}$$

$$Q_\ell(s) = s^2 + s \tag{A16}$$

$$s = j\omega$$

If we use Lawton's[10] general result that

$$I_x = \tau_1 - \hat{\tau}_1 \tag{A17}$$

and

$$\sigma_x^2 = N_x I_x \tag{A18}$$

and

$$\sigma_f^2 = \frac{N_x}{d_f^2}\left\{\frac{1}{2}(\tau_1 - \hat{\tau}_1)[(\tau_1 - \hat{\tau}_1)\tau_1 + 2\hat{\tau}_2] - (\tau_3 - \hat{\tau}_3)\right\}$$

where τ_i and $\hat{\tau}_i$ are defined by (A19)

$$P_\ell(s) = s^N + \tau_1 s^{N-1} + \tau_2 s^{N-2} + \ldots \tag{A20}$$

and

$$Q_\ell(s) = s^N + \hat{\tau}_1 s^{N-1} + \hat{\tau}_2 s^{N-2} + \ldots \tag{A21}$$

Then for this low pass case,

$$\tau_1 = \sqrt{2\delta + 1} \qquad \hat{\tau}_1 = 1$$

$$\tau_2 = \delta \qquad \hat{\tau}_2 = 0$$

$$\tau_3 = 0 \qquad \hat{\tau}_3 = 0$$

Hence

$$I_x = \sqrt{2\delta + 1} - 1 \tag{A22}$$

$$\sigma_x^2 = \frac{2d_f^2}{\delta^2} \left[\sqrt{2\delta + 1} - 1\right] \tag{A23}$$

$$\sigma_f^2 = \frac{I_x^2 \left[I_x + 1\right]}{\delta^2} \tag{A24}$$

and

$$\delta = \delta(\sigma_x^2) = d_f\sqrt{\Lambda/\nu}$$

A plot of (A24) for $d_f = 50$ is shown in figure A2. Remember that this plot describes the performance of a receiver that contains Booton-type filters and that Booton's quasi-linear analysis technique was used to analyze it. Figure A3 appropriately shows the arrangement.

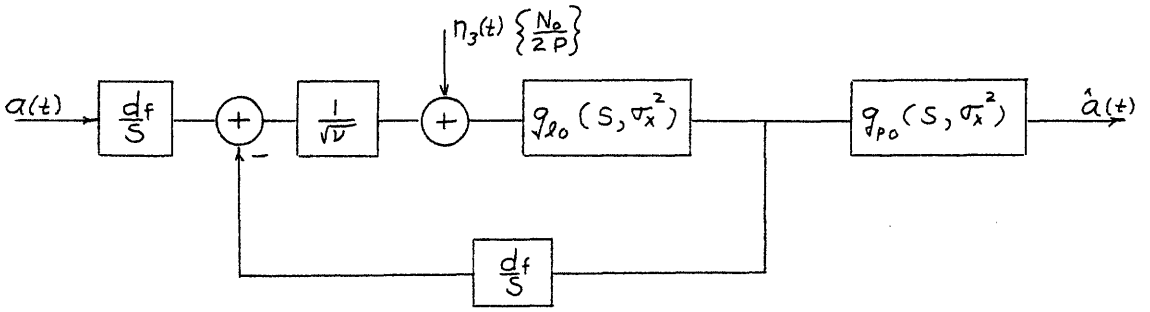

Figure A3

Quasi-Linear Receiver with Booton-type Filters

Also plotted in figure A2 is the corresponding $d_f = 50$ curve for the quasi-linear analysis of a receiver with the usual linear filters (as in chapter 3).

The same sort of analysis as described above was performed for the two pole message. Only the results will be included here.

$$I_x = \tau_1 - \hat{\tau}_1 = 2\rho^{\frac{1}{6}} - \sqrt{2} \tag{A25}$$

$$\sigma_x^2 = \frac{2\sqrt{2}}{\rho} d_f^2 \left[2\rho^{\frac{1}{6}} - \sqrt{2}\right] \tag{A26}$$

$$\sigma_f^2 = \frac{2\sqrt{2}}{\rho} \left[3\rho^{\frac{1}{2}} - 4\sqrt{2}\ \rho^{\frac{1}{3}} + 4\rho^{\frac{1}{6}} - \sqrt{2}\right] \tag{A27}$$

where

$$\rho = \frac{\Lambda d_f^2}{\nu}$$

$$\Lambda = \frac{4\sqrt{2}\ P}{N_o}$$

A plot of (A27) is also shown in figure A2 along with the corresponding curve for the linear filter case.

The system of figure A1 was simulated on the digital computer for the one pole case. We first conducted the simulation for

$$\nu_o = e^{(o)} = 1 \tag{A28}$$

which in effect is exactly the same one pole case that was simulated in chapter four (curve number 1, figure A4). For the next simulation (curve 2) we used those values of mean square phase error that were obtained in the first run

$$\nu_1 = e^{\sigma_{x_o}^2} > 1 \ . \tag{A29}$$

We expected to see an improvement in performance but instead the performance degraded somewhat. Because of the degraded performance shown by curve number 2, we decided that perhaps the σ_x^2 values that were used in run 2 were too large. Subsequently, curve number 3 was run using smaller values of σ_x^2. The specific values are listed on the graph.

Curve number 4 was obtained by using the theoretical values of σ_x^2 for figure A3. These values of σ_x^2 were computed using equation A23.

These results are somewhat surprising because, according to figure A2, the receiver should perform slightly better when the Booton-type filters are used. These results show that the best value for σ_x^2 is zero which reduced the Booton-type filters to those used in chapters three and four.

iv) Equivalent Rectangular Bandwidth

In some texts this concept is referred to as the equivalent noise bandwidth. The idea is best described with an example. Consider the first order Butterworth spectrum $S_a(\omega) = \frac{2K}{\omega^2 + K^2}$ in figure (A5-a):

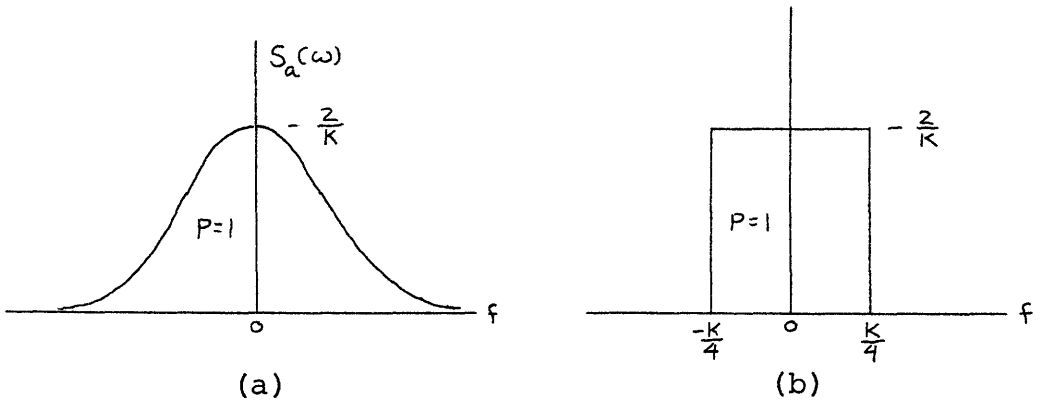

Figure A5

The total power, P, in the message is the area under $S_a(\omega)$. In this case P equals one. Now the E.R.B. is the bandwidth of a rectangle of height $S_a(0)$ and area P. For this case $B_{E.R.B.} = \frac{K}{2}$.

Quasi-Linear Filters vs. Linear Filters

One and Two Pole Cases

Theoretical Quasi-Linear Analysis of P.L.L.

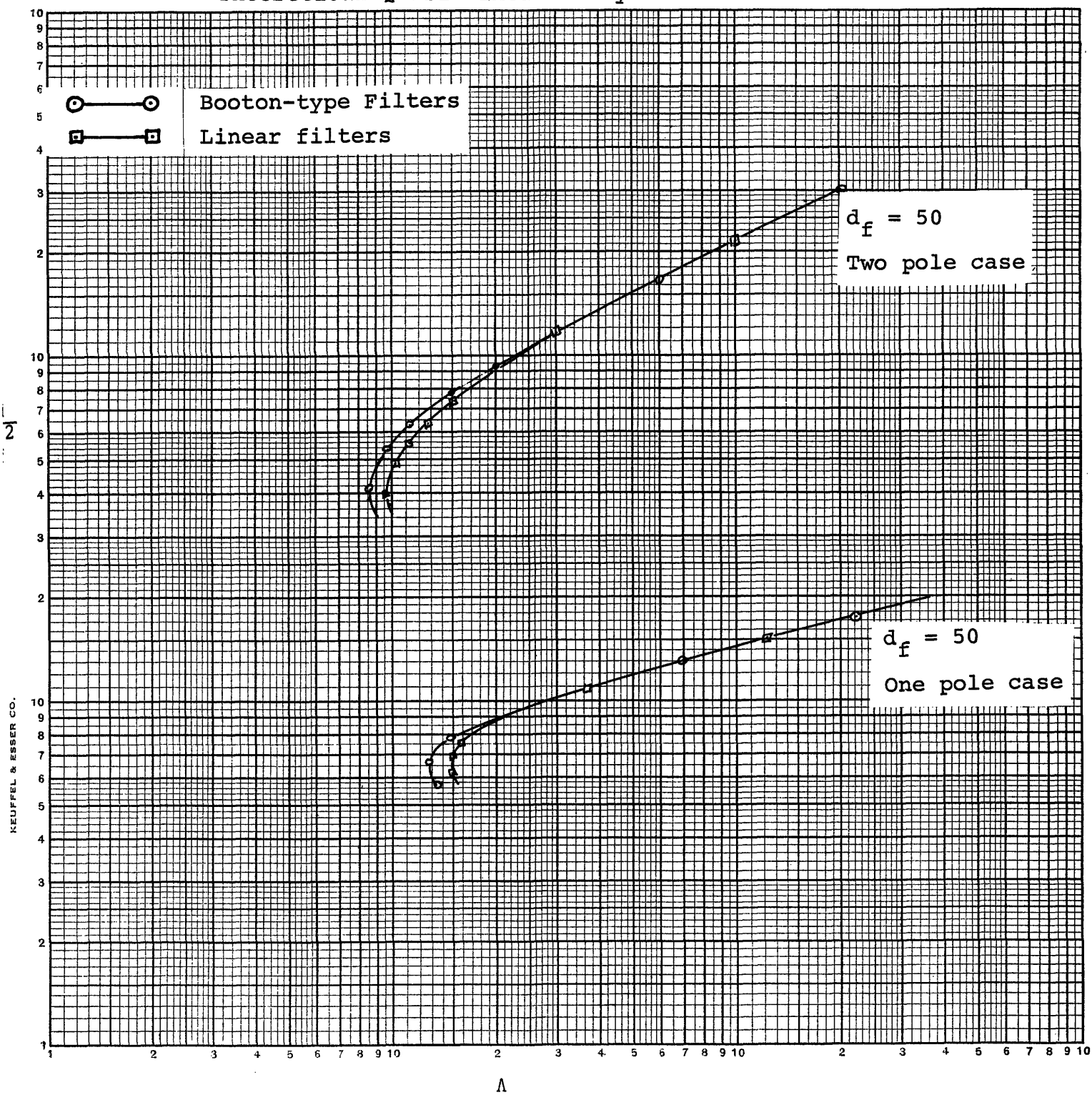

Figure A2

Booton type filters in P.L.L.

$(H(\omega), \sigma_x^2)$

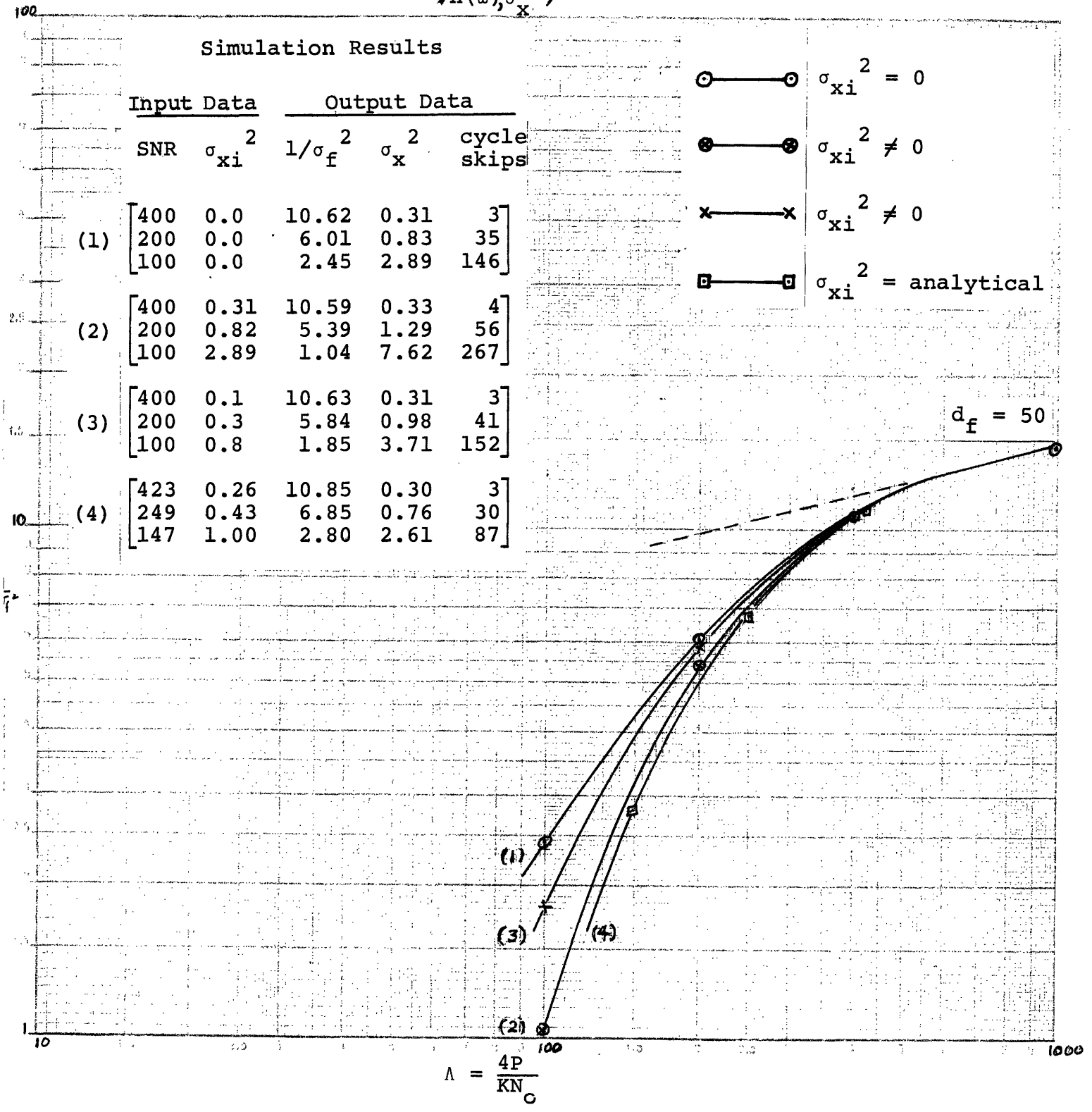

Figure A4

REFERENCES

1. M. Schwartz, "Information Transmission Modulation and Noise," McGraw Hill, N.Y., 1959.

2. H. S. Black, "Modulation Theory," D. van Nostrand, Inc. Princeton, N. J., 1953.

3. E. H. Armstrong, "A method of Reducing Disturbances in Radio Signaling by a System of Frequency Modulation," Proceding IRE, 24, pp. 689-740, 1934.

4. J. G. Chaffee, "The Application of Negative Feedback to Frequency Modulation Systems," BSTJ, Vol. 18, July 1939.

5. D. Richman, "Color Carrier Reference Phase Synchronization Accuracy in NTSC Color T.V."; Proceding IRE 42, 106-133 (1954).

6. D. C. Youla, "The Use of the Method of Maximum Liklihood in Estimating Continuous-Modulated Intelligence which has been Corrupted by Noise," Jet Propulsion Laboratory Report No. DA-04-495-ord 18, Pasadena, California.

7. H. L. Van Trees, "Detection, Estimation and Modulation Theory," (book to be published).

8. A. W. Bode and C. E. Shannon, "A simplified Derivation of Linear Least Square Smoothing and Prediction Theory," Procedings, IRE, Vol. 38, No. 4, pp. 417-425; April, 1950.

9. D. L. Snyder, "The State Variable Approach to Continuous Estimation," Sc.D. Thesis, Mass. Inst. of Tech., Elec. Eng. Dept.; February 1966.

10. H. D. Becker, J. T. Chang and J. G. Lawton, "Investigations of Advanced Analog Communications Techniques," Cornell Aeronautical Laboratory, Inc.: Technical Report No. RADC-TR-65-81; March, 1965.

11. R. C. Booton, Jr., "The Analysis of Nonlinear Control Systems with Random Inputs," Procedings, Symposium on Nonlinear Circuit analysis, New York, N. Y., April 23, 24, 1953.

12. G. C. Newton, Jr., L. A. Gould, J. F. Kaiser, "Analytical Design of Linear Feedback Controls," John Wiley & Sons, Inc.; New York, N. Y.; 1957.

13. M. C. Yovits and J. L. Jackson, "Linear Filter Optimization with Game Theory Considerations," IRE National Convention Record Pt. 4 pp 193-199; 1955.

14. D. L. Snyder, "Optimum Linear Filtering of an Integrated Signal in White Noise," Transactions, IEEE, Vol. AES-2, No. 2, pp. 231-232; March, 1966.

15. B.C. Kuo, "Automatic Control Systems," Prentice-Hall, Inc; 1962.

16. I. M. Horowitz, "Synthesis of Feedback Systems," (Academic Press Inc, New York; 1963).

17. W. B. Davenport, Jr., and William L. Root; "Random Signals and Noise," McGraw-Hill Book Company Inc., New York, 1958.

18. A. Papoulis, "A New Method of Analysis of Sampled-Data Systems," Transactions, IRE, Vol. AC-4, No. 2, pp. 67-73; November, 1959.

19. Y. W. Lee, "Statistical Theory of Communication," John Wiley & Sons, Inc., New York, N. Y., 1960.

20. R. W. Zaorski, "Simulation of Analog Demodulation Systems," M.Sc. E.E. Thesis, Mass. Inst. Tech. Cambridge, Mass.; January, 1965.

21. S. O. Rice, "Noise in F.M. Receivers," in Time Series Analysis, M. Rosenblatt, Ed., John Wiley & Sons, N.Y. 1963.

22. J. G. Lawton, "Investigation of Analog and Digital Communication Systems (Phase 3 Report)," Cornell Aeronautical Laboratory, Inc., Buffalo, N.Y.; Technical Documentary Report RADC-TDR-63-147; May, 1963.

23. D. Middleton, "Statistical Communication Theory," McGraw-Hill Book Company, Inc., N.Y. 1960. Sec. 15.4, 15.5, pp. 655-678.

24. J. A. Develet, Jr., "A Threshold Criterion for Phase-Lock Demodulators," Procedings, IEEE, Vol. 51, pp. 349-356; February, 1963.